UNIVERSITY OF OKLAHOMA

GRADUATE COLLEGE

GROUND STATE ENTANGLEMENT IN 2D STRONGLY INTERACTING BOSE-HUBBARD-TYPE MODELS

A DISSERTATION

SUBMITTED TO THE GRADUATE FACULTY

in partial fulfillment of the requirements for the

Degree of

DOCTOR OF PHILOSOPHY

By

WEI WANG
Norman, Oklahoma
2017

GROUND STATE ENTANGLEMENT IN
2D STRONGLY INTERACTING BOSE-HUBBARD-TYPE MODELS

A DISSERTATION APPROVED FOR THE
HOMER L. DODGE DEPARTMENT OF PHYSICS AND ASTRONOMY

BY

Dr. Bruno Uchoa, Chair

Dr. John Albert

Dr. Deborah Watson

Dr. Kieran Mullen

Dr. Barbara Capogrosso Sansone

DEDICATION

to

My parents, Congzheng and Xiaoming

My children, Elliott and Alexander

My wife, Lihui

Acknowledgements

I would like to thank Barbara Capogrosso-Sansone for her guidance, support, forgivingness and encouragement during my Ph.D. study. This dissertation would not have been possible without reverence to her standard of clear understanding. Thanks to Bruno Uchoa, Kieran Mullen, and Deborah Watson for their advice and encouragement on my academic career in condensed matter physics. Special thanks to Gregory Parker for his generosity which makes me feel at home when studying in our department. I also thank John Albert, Kyung Bai Lee for their lectures in analysis and topology which gave me a taste of the beauty of pure mathematics.

I deeply thank my parents, Congzheng Wang and Xiaoming Wang, for their endless love. I sincerely thank my parents-in-law, Long Liao and Yuqiong Ling, for their selfless support. I also thank my children, Elliott Wang and Alexander Wang, for bringing me true and pure happiness.

Finally and most importantly, I thank my wife, Lihui Liao, for always being with me, through the best and the worst times.

Table of Contents

List of Figures

Abstract

In this dissertation, I present my work on ground state entanglement in Bose-Hubbard-type models. Bose-Hubbard-type models form a wide class of bosonic lattice models and describe systems that can be realized by cold atoms or molecules trapped in optical lattices. By studying ground state entanglement, one can understand quantum phases and phase transitions among them from a microscopic point of view. I will first introduce the two-component Bose-Hubbard model describing Bose-Bose mixtures, and discuss the role played by the interspecies entanglement in the Mott-insulator-to-superfluid phase transition of one component in the presence of a second component. I will show that interspecies entanglement provides a new perspective to understand quantum phases in mixtures. Then I will discuss long-range spatial entanglement in single-species Bose-Hubbard-type models. Specifically, I will build a generic framework for understanding under which conditions these models harbor certain types of topological order. My results provide guidance for future numerical studies which can pave the way for searching experimentally realizable bosonic lattice models harboring nontrivial topological order.

Chapter 1

Introduction

Many-body systems are ubiquitous in nature. They can be man-made such as high-temperature superconductors, or naturally occurring such as biological systems or galaxies. Interesting many-body systems are driven by strong correlations and characterized by their exotic properties resulting from the collective behavior of their constituents. In physics, a thorough understanding of strongly-correlated many-body quantum systems has attracted the interest of scientists for decades due to the astonishing potential technological applications of, e.g., nano-scale materials [3], high-temperature superconductors [4], ultracold atoms and molecules [5].

In a reductionism viewpoint, it was believed that the physics of a many-body system was mainly determined by properties of its individual constituents while the rules stipulating how these constituents behave together played a minor role [6]. However, in the past decades, the study of many-body systems, such as Bose-Einstein condensates [7], high-temperature superconductors [4] and neural networks [8], has revealed that the interactions among constituents, which governs the way the constituents behave together, plays a decisive role in determining the physical properties of many-body systems. The interaction, often of simple nature, e.g., the repulsion among identical electrons caused

by the Pauli exclusion principle, generates great complexity as the number of constituents increases. However, the full complexity of the system is never displayed in a finite-size system, but rather is an emergent phenomenon as the size of the system gets larger and larger up to infinity. The emergent phenomenon is a *macroscopic* property resulting from the microscopic properties of the many-body system. As an example, the robustness of topologically ordered quantum phases in fractional quantum Hall systems [5] is an emergent property determined by the electronic interaction in the presence of magnetic field. Unveiling the relationship between the emergent properties and the microscopic interaction is one of the main challenges in understanding strongly-correlated many-body systems.

Prominent experimentally-realizable many-body models amenable to study collective behavior and emergent phenomena are *Bose-Hubbard-type* models. Their experimental counterparts are ultracold atoms or molecules trapped in optical lattices [9]. These engineered systems are highly-controllable and tunable, and can be used to simulate real condensed matter systems which cannot be probed without affecting the systems themselves. In the past two decades, the study of quantum phase transitions of Bose-Hubbard-type models together with their experimental realization [10, 11, 12, 13, 14, 15] has vastly advanced the understanding of many-body systems, and has revealed promising prospect of systems described by Bose-Hubbard-type models in technological applications such as quantum information processing and physical realizations of quantum computation [16, 17].

Well-known examples of Bose-Hubbard-type models include the prototype single-species Bose-Hubbard model [18, 19], the multi-component Bose-Hubbard model [20, 21, 22] describing bosonic mixtures, the extended Bose-Hubbard model [23, 24] with off-site interaction, e.g., dipolar interaction. A Bose-Hubbard-type model simply consists of an interaction term which tends to localize bosons on lattice sites and a kinetic-energy

term which tends to delocalize bosons. The competition between the interaction and the kinetic energy drives a quantum phase transition between an insulating phase and a superfluid phase. At a given filling factor, depending on the specifics of the interaction, the possible insulating phases can be characterized by *local* order parameter [18, 19] or *nonlocal* topological order [25]. This wealth of insulating phases unfolds the complex relationship between emergent properties of the many-body system and interaction between its constituents, and has been the object of extensive studies in the past decade [23, 24, 26, 27, 28, 22]. Methods like mean-field theory, perturbation theory, renormalization group, and numerical simulations have been successful in studying insulating phases characterized by local order parameters [29]. However, the understanding of exotic quantum phases not described by local order parameters call for new methods and new perspectives.

The best known example of quantum phases characterized by nonlocal order are topologically ordered phases initially studied in the context of fractional quantum Hall effect [30]. Topologically ordered phases are characterized by topological ground state degeneracy and low-energy excitations which can be viewed as quasiparticles called anyons [5, 31]. The braiding properties of anyons are robust against decoherence and can be utilized to perform topological quantum computation which is currently the most promising route to perform quantum computation [32, 5]. The description of these phases is beyond the Ginzburg-Landau symmetry breaking paradigm, and thus challenges the current understanding of collective behavior in certain many-body systems [33]. Recently, it has been realized that the nature of exotic properties in a topologically ordered phase originate from certain nonlocal properties of the system's ground states. These properties are determined by nontrivial ground state entanglement [34]. This perspective encourages the use of concepts borrowed form quantum information theory, especially quantum entanglement, in the study of many-body physics [35]. This perspective also provides

a new angle to understand quantum phases and transitions among them in terms of entanglement associated with ground states. Moreover, it is believed that the study of ground state entanglement in many-body systems can reveal the complex relationship between emergent properties and microscopic interactions in many-body systems [33].

In Bose-Hubbard-type models, insulating ground states characterized by local or non-local order are mainly determined by the dominating interaction which establishes the correlation among the degrees of freedom living on each site of the lattice. The correlation, which is quantum mechanical in nature, reflects the entanglement of the many-body system. Therefore, the ground state entanglement plays a key role in understanding insulating phases. Moreover, a thorough understanding of quantum phases stabilized by Bose-Hubbard-type models in terms of ground state entanglement is crucial in view of potential applications of cold-atom systems trapped in optical lattices in quantum information and quantum computation, in particular topological quantum computation. In this dissertation, I report my work on studying the role played by interspecies entanglement in the Mott-insulator-to-superfluid phase transition in Bose-Bose mixtures trapped in optical lattices. I also report my work on unveiling the relationship between certain type of long-range ground state entanglement and the interaction term in a wide class of two-spatial-dimensional Bose-Hubbard-type models in which the interaction dominates over the kinetic energy.

This dissertation is written based on my work published in References [21], [22] and [25], and is organized as follows.

Chapter 2 briefly introduces Bose-Hubbard-type models and concepts of entanglement. Chapter 3 studies the ground state degeneracy in finite systems and develops a degenerate perturbation theory to study the two-component Bose-Hubbard model in the strong-interaction regime. Results from this chapter are used to study interspecies entanglement. Chapter 4 systematically studies the interspecies entanglement in ground states

of the two-component Bose-Hubbard model, and shows a close relationship between the entanglement and the shift of the Mott-insulator phase boundary of one component in the presence of the other component. Chapter 5 develops a generic framework for the emergence of the $\mathbb{Z}_2$ toric-code topological order and the double-semion topological order in a certain class of Bose-Hubbard-type models. Chapter 6 summerizes my work and discusses my future research plan.

Chapter 2

Bose-Hubbard-type models and ground state entanglement

In this chapter, we introduce Bose-Hubbard-type models and briefly describe the Mott-insulator-to-superfluid quantum phase transition in the single component Bose-Hubbard model. We then review fundamental concepts of interspecies entanglement and long-range spatial entanglement that will be studied in details in Chapter 4 and 5 respectively. We also discuss the concept and basic properties of topological order using the toric code model as an example.

2.1 Bose-Hubbard-type models

A Bose-Hubbard-type model is a many-body model of interacting lattice bosons. This type of model captures the quantum phase transition of different systems ranging from cold atoms trapped in optical lattices [19] through granular films [18]. The prototype of Bose-Hubbard-type models is the single-species Bose-Hubbard model [18, 19]. In the

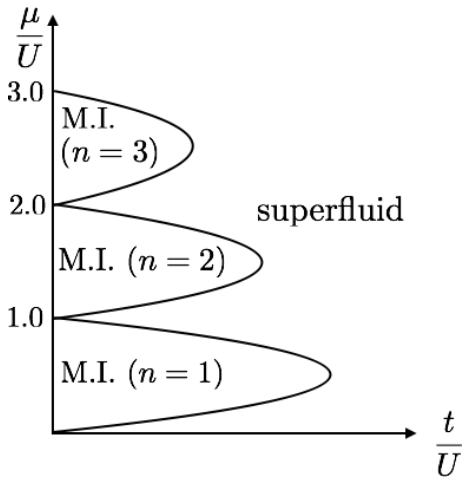

Figure 2.1: Phase diagram of the Bose-Hubbard model. M.I. inside the lobe stands for Mott-insulator phase. The superfluid phase is outside the lobe.

grandcanonical ensemble, it has the following form

$$H = -t \sum_{<i,j>} b_i^+ b_j + \frac{U}{2} \sum_i n_i(n_i - 1) + \sum_i \mu n_i, \tag{2.1}$$

where b_j (b_i^+) is the annihilation (creation) operator corresponding to the site j (i) of the lattice, $n_i = b_i^+ b_i$ is the particle number operator at site i, $< i, j >$ stands for a nearest-neighbor pair of sites, t is the hopping matrix element, U is the onsite interaction, and μ is the chemical potential.

At zero temperature, the Bose-Hubbard model features two quantum phases, the Mott-insulator phase and the superfluid phase [18, 19], as shown in Fig. 2.1, where Mott-insulator phase is inside the lobes while superfluid phase is outside. In the phase diagram, each lobe corresponds to a fixed integer filling factor. At integer filling factor, when the interaction dominates, the system governed by the model is in the Mott-insulator phase, while when the hopping dominates, the system is in the superfluid phase. The Mott-insulator phase is characterized by an excitation energy gap for adding a particle or a hole to the system while the superfluid phase is compressible and gapless. The lobe boundary

can be crossed in two different ways according to the different nature of phase transitions. It can be crossed from the M.I. regime by fixing t/U while increasing (decreasing) μ/U. This phase transition corresponds to adding (removing) a boson to (from) the system. The MI-SF boundary can also be crossed at fixed integer filling factor while increasing t/U. This phase transition corresponds to delocalizing bosons.

The Bose-Hubbard model can be extended to a wide class of bosonic lattice models. For example, there can be more than one bosonic species in the system [20, 21, 22] as will be discussed in Eq. 3.3. One can also set $U = \infty$ (hardcore limit), and add a site-site interaction term to form the *extended* Bose-Hubbard model which can be realized by degenerate gasses, e.g., polar molecules trapped in optical lattices [23, 36]:

$$H = -t \sum_{<i,j>} b_i^+ b_j + \sum_{i,j} V_{ij} n_i n_j, \tag{2.2}$$

where V_{ij} is the site-site interaction amplitude. The interaction in the extended Bose-Hubbard model can be short-ranged, e.g., nearest neighbor interaction, or long-ranged, e.g., dipolar interaction. In principle, the amplitudes t can also be inhomogeneous and dependent on pairs of sites. Furthermore, ring-exchange hopping terms can be present to form a class of models with potential to realize certain topological order as will be discussed in Chapter 5.

In general, the typical form of a Bose-Hubbard-type model consists of the interaction term which tends to localize bosons on lattice sites and the hopping term which tends to delocalize bosons. The competition between the interaction and the hopping drives quantum phase transition between an insulating phase and a superfluid phase. For a given fixed filling factor, the interaction specified by V_{ij} as a function of pairs of sites can give rise to a variety of insulating phases [23, 24, 26, 27, 28, 25], characterized by local order parameter or nonlocal topological order. As a matter of fact, as we will discuss

later in great details, gapped insulating phases are mainly determined by the dominating interaction which establishes the ground state entanglement among the degrees of freedom living on each site of the lattice.

2.2 Entanglement

Entanglement in ground states of many-body system is defined in terms of certain decompositions of the Hilbert space for the whole system into a tensor product of Hilbert spaces of subsystems. There are many possible decompositions corresponding to the different nature of quantum correlations. In this dissertation, we consider two types of decompositions.

2.2.1 Bipartite entanglement

For the two-component Bose-Hubbard model describing, e.g., Bose-Bose mixture of cold atoms trapped in optical lattices, a natural decomposition of the Hilbert space $\mathcal{H}$ of the whole system is in terms of the two components. In other words, $\mathcal{H} = \mathcal{H}^a \otimes \mathcal{H}^b$ where $\mathcal{H}^a$ and $\mathcal{H}^b$ are the Hilbert spaces of the two bosonic species, A and B, respectively. With this decomposition, we study the bipartite entanglement of the ground state and its relationship with the superfluid-to-insulator transition of one of the two components in the presence of the other component. This work is discussed in Chapter 4.

The bipartite entanglement of a pure state, for example the ground state $|\Psi\rangle \in \mathcal{H} = \mathcal{H}^a \otimes \mathcal{H}^b$ of the two-component Bose-Hubbard model, is uniquely characterized by its *Schmidt decomposition* [37]. This means that there exist a basis $\{|\xi_m\rangle\}_{1\leq m\leq M}$ of $\mathcal{H}^a$ and

a basis $\{|\gamma_n\rangle\}_{1\leq n\leq N}$ of $\mathcal{H}^b$ (assuming $M \geq N$) such that

$$|\Psi\rangle = \sum_{n=1}^{N} \sqrt{\epsilon_n}\, |\xi_n\rangle \otimes |\gamma_n\rangle, \tag{2.3}$$

where the set $\{\epsilon_n\}_{1\leq n\leq N}$ is the spectrum of the reduced density operator ρ_a of $\rho = |\Psi\rangle\langle\Psi|$. The amount of bipartite entanglement in $|\Psi\rangle$, as measured by the von Neumann entanglement entropy [37], is

$$-\operatorname{Tr}_a[\rho_a \log \rho_a] = -\sum_{n=1}^{N} \epsilon_n \log \epsilon_n. \tag{2.4}$$

In Chapter 4, by studying the von Neumann entropy of $|\Psi\rangle$, we show a close relationship between the bipartite entanglement of $|\Psi\rangle$ and the superfluid-to-Mott-insulator quantum phase transition.

2.2.2 Spatial entanglement

To avoid ambiguity in the following discussion on spatial entanglement, we clarify vocabulary regarding many-body systems defined on lattices that we will use in the following. A lattice model refers to a generic form of lattice Hamiltonians for many-body systems, e.g., the Bose-Hubbard model as given by Eq. 2.1, without specifying the Hamiltonian parameters, lattice geometry and lattice topology. Lattice geometry refers to the type of lattice, e.g., triangular lattice, square lattice or Kagome lattice. Lattice topology refers to the topology of the manifold in which the lattice is embedded as specified by the boundary conditions. For example, a lattice with periodic boundary conditions is embedded in a torus. A lattice system refers to a lattice model with specified Hamiltonian parameters and lattice geometry, but with unspecified lattice topology. Note that a lattice system can be viewed as a family of lattice Hamiltonians indexed by lattice topology. For example, the

1D Ising model with specified Hamiltonian parameters can be defined on an open string or a closed ring. In the two different lattice topology, the terms entering the Hamiltonians, which involve the boundary of the chain are different in the two lattice topology. When the lattice topology, i.e. boundary conditions, is specified, we say that a lattice system is governed by a specified Hamiltonian. We refer to a lattice system with specified Hamiltonian as a lattice Hamiltonian.

For single-species hardcore bosonic lattice systems governed by a certain Hamiltonian, we consider the following decomposition, $\mathcal{H} = \otimes_{i=1}^{N(\Lambda)} \mathcal{H}_i$, where the index i runs through $N(\Lambda)$, the number of sites in the lattice Λ, and $\mathcal{H}_i = \mathbb{C}^2$ is the Hilbert space of the degrees of freedom on each site. Here $\mathcal{H}_i$ can be viewed as expanded by the occupation number basis $\{|0\rangle, |1\rangle\}$ on the ith site. In terms of this decomposition, the ground state $|\Psi\rangle$ is, in general, multipartite entangled and this type of entanglement is usually called spatial entanglement. The spatial entanglement has a much richer structure than the bipartite entanglement. In the following, we introduce the so called "long-range entanglement" [34] corresponding to topological order of 2D lattice systems, which will be discussed in Chapter 5 for Bose-Hubbard-type models.

2.2.3 Gapped phase and local unitary transformation

The complexity of the spatial entanglement arises from the number of $\mathcal{H}_i$ participating in the decomposition, i.e. the number of lattice sites. The complexity increases with increasing lattice size. A complete measure and characterization of the spatial entanglement in ground states is very challenging. Nonetheless, one can still look at nonlocal properties of the spatial entanglement to describe gapped quantum phases of systems governed by local Hamiltonians [1]. Here, we briefly describe this approach.

[1] A local Hamiltonian is a sum of local operators. Local operators act nontrivially only on a subset of sites which is small compared to the lattice size. A more precise definition is given in Reference [38]

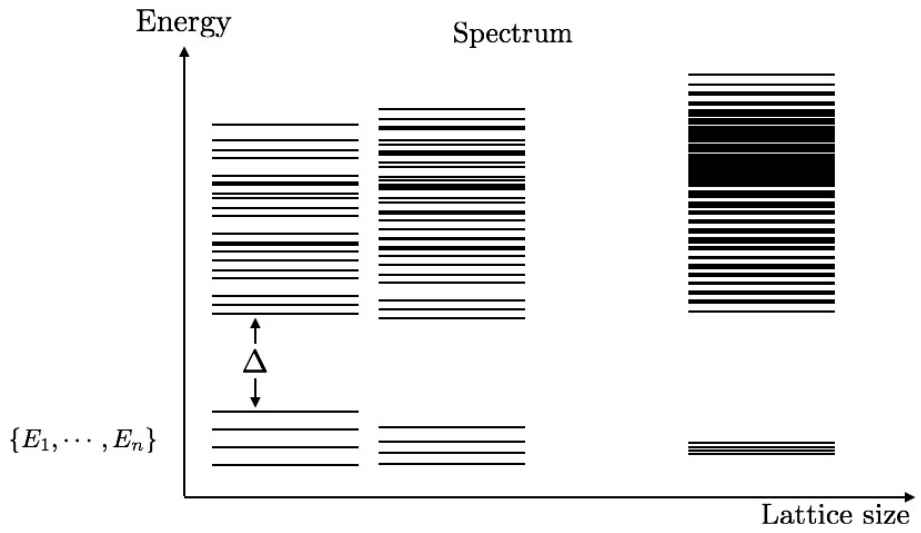

Figure 2.2: Spectrum of a gapped lattice Hamiltonian. Δ separates the lowest eigenvalues from the rest of the spectrum and stays finite in the infinite system size. The spacing between the lowest eigenvalues vanishes as the system size increases.

We start by clarifying the concept of "gapped phase" [33] and then discuss the conditions under which two systems with specified Hamiltonians are in the same quantum phase.

In this dissertation we only consider local lattice Hamiltonians. A lattice Hamiltonian H is said to be gapped if there exists a finite spectral gap Δ separating the lowest eigenvalues $\{E_1, \cdots, E_n\}$, corresponding to the n eigenstates $\{|\Psi_1\rangle, \cdots, |\Psi_n\rangle\}$ of H, from the rest of the spectrum. The gap Δ stays finite when the system size increases to infinity, while the eigenvalue spacing in $\{E_1, \cdots, E_n\}$ vanishes exponentially with increasing lattice size. These properties are illustrated in Figure. 2.2 which shows the change in the spectrum of the system as the system size increases. The eigenstates $\{|\Psi_1\rangle, \cdots, |\Psi_n\rangle\}$, distinguished from other eigenstates with higher energy, span the ground state subspace $\mathcal{E}$ [2], and n is the ground state degeneracy.

Let us now consider two gapped lattice Hamiltonians H_0 and H_1, and with ground

[2]Note that $\{|\Psi_1\rangle, \cdots, |\Psi_n\rangle\}$, $\{E_1, \cdots, E_n\}$ and $\mathcal{E}$ are all system-size-dependent, but n is system-size-independent. For simplicity in notation, we omit the subscript for system size when unnecessary.

state subspaces $\mathcal{E}_0$ and $\mathcal{E}_1$. These two lattice Hamiltonians feature the same quantum phase if they can be adiabatically connected. In other words, there exists a smooth family $H(r)$ of Hamiltonians with $r \in [0,1]$ such that $H(0) = H_0$, $H(1) = H_1$ with the energy gap remaining open when changing r from 0 to 1. It has been shown [34, 38] that the existence of such a $H(r)$ is equivalent to the existence of a *local unitary transformation* $U = Te^{-i\int_0^1 \mathrm{d}rH'(r)}$ [3] such that $\mathcal{E}_1 = U(\mathcal{E}_0)$. Here, a local unitary transformation is simply a unitary operator which is a finite sum of operators of the form $U_{I_1} \otimes \cdots \otimes U_{I_M}$ where $\{I_1, \cdots, I_M\}$ are disjoint subsets of the lattice [4]. Simply speaking, when a local unitary transformation acts on a state, it only changes the local properties of the state while leaving the nonlocal properties unchanged. An example of local unitary transformation is $U = \otimes_{i=1}^{N(\Lambda)} \sigma_i^x$, i.e. the tensor product of the Pauli operators σ_i^x on each site. When it acts on a spin product state $|\uparrow\rangle \otimes |\downarrow\rangle \otimes |\uparrow\rangle \otimes |\downarrow\rangle \cdots$ of eigenstate of the Pauli operators σ_i^z, it results in $|\downarrow\rangle \otimes |\uparrow\rangle \otimes |\downarrow\rangle \otimes |\uparrow\rangle \cdots$. After the action of U, the local state is changed. However, the nonlocal property—$|\uparrow\rangle$ and $|\downarrow\rangle$ are located alternatively—is not changed. Moreover, both $|\uparrow\rangle \otimes |\downarrow\rangle \otimes |\uparrow\rangle \otimes |\downarrow\rangle \cdots$ and $|\downarrow\rangle \otimes |\uparrow\rangle \otimes |\downarrow\rangle \otimes |\uparrow\rangle \cdots$ are not entangled. Indeed, if a state is entangled, then, after the action of a local unitary transformation, the state is still entangled, and vice versa.

In light of the discussion above, we say that two gapped lattice Hamiltonians are in the same quantum phase if and only if their ground states can be connected by a local unitary transformation.

Local unitary transformations can partition gapped lattice Hamiltonians into classes. In each class, lattice Hamiltonians can be connected by local unitary transformations and have the same nonlocal properties in their ground states. Since lattice Hamiltonians in each class are also in the same quantum phase, then, a quantum phase can be viewed as

[3] Here T is the time ordering operator, local Hamiltonian $H'(r)$ is generally not the adiabatic path.

[4] Note that a local unitary transformation is not necessarily a local operator, because it can act nontrivially on the whole lattice.

characterizing a class of gapped lattice Hamiltonians which all possess (or lack) the same nonlocal properties in their ground state entanglement.

2.2.4 Long-range entanglement and topological order

There exist classes of gapped lattice Hamiltonians whose ground states cannot be mapped to product (non-entangled) states by any local unitary transformation. Ground states of lattice Hamiltonians in these classes are called long-range entangled [34]. The long-range entanglement gives a "microscopic" characterizes of topological ordered phase for 2D lattice systems. Moreover, a 2D lattice system possesses topological order if it has long-range entangled ground states when defined with any lattice topology [34, 33].

Topological order can also be defined "macroscopically". A 2D gapped lattice system possesses topological order if the following two conditions are satisfied [31]:

- the ground state degeneracy n depends on the lattice topology only;
- ground states are locally indistinguishable, i.e. for any two ground states, $\left\langle \Psi_\alpha \middle| A \middle| \Psi_\beta \right\rangle \sim C_A \delta_{\alpha\beta}$ in the thermodynamic limit for any local operator A, where C_A is a constant dependent only on A.

These two conditions guarantee that the lattice system can be effectively described by topological quantum field theory in the thermodynamic limit and the low-energy excitations can be described by deconfined anyons. Furthermore, the local indistinguishability of ground states supports the robustness of the topologically ordered lattice systems, that is, a local perturbation cannot break topological nonlocal properties of the lattice system. This robustness to local perturbations makes topologically ordered lattice system one of the best candidate for topological quantum computation. Since Bose-Hubbard-type models can potentially be experimentally realized, it is of great interest to theoretically

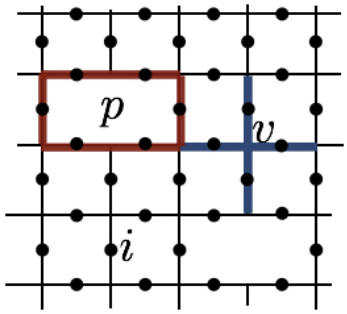

Figure 2.3: This figure shows a square lattice with defects. v stands for a site, i stands for a link, and p stands for a plaquette. Blue links attached to v contributes to A_v. Red links as boundary of p contributes to B_p.

demonstrate the existence of topological order in these models. For this purpose, we develop a generic framework for the emergence of topological order in a certain class of Bose-Hubbard-type models as discussed in detail in Chapter 5.

The best example which illustrates the two conditions specified above is the toric code [39, 1], a lattice system with lattice geometry. The toric code is a spin-$1/2$ lattice system with spins located on the links of the lattice. Alternatively, the system can also be defined with spins located on lattice sites, but for consistency with the literature, we consider the version defined on links. On an arbitrary lattice Λ, the toric code defines the Hamiltonian

$$H^{TC} = -\sum_{v} A_v - \sum_{p} B_p \tag{2.5}$$

where $A_v = \prod_{v\in\partial i} \sigma_i^z$ and $B_p = \prod_{i\in\partial p} \sigma_i^x$. Here, as shown in Fig. 2.3, v stands for a site or vertex, i stands for a link or edge, and p stands for a plaquette or face of the lattice. $v \in \partial i$ means the link i is attached to the vertex v. $i \in \partial p$ means the link i is a part of the boundary of the plaquette p. Examples of ∂i an ∂p are illustrated in Fig. 2.3 where blue links attached to v contribute to A_v and red links as the boundary of p contribute to B_p.

The toric code is exactly solvable since A_v an B_p commute for all v and p. The ground state energy is separated from other excited energy levels by 1 in any system size. The

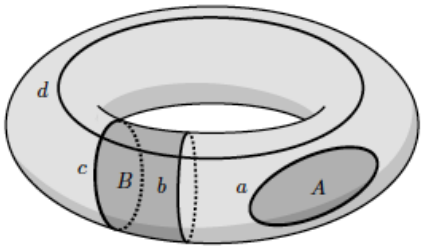

Figure 2.4: This figure is borrowed from Reference [1]. It shows a torus with different type of cycles on it. Contractible cycle a is the boundary of region A. Parallel non-contractible cycles like b and c together form the boundary of region B. Non-contractible cycle d is not the boundary of any region.

ground state degeneracy depends only on the lattice topology and is independent on the lattice geometry. For example, when the lattice is embedded in a sphere, the ground state is unique, while when the lattice is embedded in a torus, the ground state is 4-fold degenerate.

Let us discuss the origin of the ground state degeneracy with the case of torus. On a torus, different cycles, i.e. closed loops, have different topological properties. As shown in Fig. 2.4, contractible cycle a is the boundary of region A, parallel non-contractible cycles like b and c together form the boundary of region B, and single non-contractible cycle d is not the boundary of any region. These different properties determine four types of cycle configurations. A cycle configuration is simply a collection of cycles on the torus. In the first type, a configuration contains contractible cycles and pairs of non-contractible cycles in the same toroidal direction, e.g., cycle a with b and c. In the second and the third type, except for contractible cycles, there is a single non-contractible cycles, e.g., cycle d, in one direction and pairs of non-contractible cycles in the other direction. In the fourth type, there are single non-contractible cycles in both the toroidal directions. These four types of cycle configurations are realized by orthogonal ground states of the toric code and give rise to the 4-fold degeneracy.

The local indistinguishability of ground states is also determined by the topological

properties of cycles. Indeed, any local operator acts only on a local region from where the type of cycle configuration cannot be inferred. Hence, the average of any local operator has no difference in the four ground states. Furthermore, since a local operator cannot change the topological properties of a cycle, e.g., change a to b, it cannot map a type of cycle configuration to another type, and thus cannot induce transitions from one ground state to another.

The locally indistinguishable ground states support anyonic excitations. Here, we briefly discuss anyonic excitations in the toric code. For convenience, we can view $\langle\Psi|-A_v|\Psi\rangle$ indexed by vertex v, and $\langle\Psi|-B_p|\Psi\rangle$ indexed by plaquette p, as energy densities distributed over the lattice in the ground state $|\Psi\rangle$. An anyonic excited state is a low-energy excited state in which the energy densities are locally changed from their values in the ground state. For example, in the ground state $|\Psi\rangle$, $\langle\Psi|-A_v|\Psi\rangle = -1$ and $\langle\Psi|-B_p|\Psi\rangle = -1$ at every vertex and plaquette, while in an anyonic excited state $|\Phi\rangle$, $\langle\Phi|-A_v|\Phi\rangle = 1$ or $\langle\Phi|-B_p|\Phi\rangle = 1$ or both at some finite number of vertices or plaquettes. Vertices v or plaquettes p with $\langle\Phi|-A_v|\Phi\rangle = 1$ or $\langle\Phi|-B_p|\Phi\rangle = 1$ can be viewed as energy "bumps" on the energy landscape. These energy "bumps" represent anyons, quasi-particles.

Anyonic excitations are characterized by statistics, fusion rules and braiding of anyons [5]. The statistics describes the symmetry of anyonic excited states under the interchange of the positions of two identical anyons, and defines the type of anyons. Under the interchange of two identical anyons, the excited state might stay unchanged for bosonic anyons, acquire a minus sign for fermionic anyons, or acquire a phase factor $e^{i\theta}$ for other types of anyons [5]. The fusion rules stipulate how two anyons can be bounded together and behave as another type of anyon. The braiding of anyons characterize how anyonic excited states are changed

[5]Anyons live only in two spatial dimensions. In higher spatial dimensions, states describing identical particle systems must be either symmetric or antisymmetric under the interchange of two identical particles.

under pairwise interchange of the positions of anyons.

In the toric code, the anyon corresponding to $\langle\Phi|-A_v|\Phi\rangle = 1$ and labeled by e is different from the anyon corresponding to $\langle\Phi|-B_p|\Phi\rangle = 1$ and labeled by m. The e (m) anyons always appear in pairs. By applying certain unitary operators to an anyonic excited state, the position of anyons can be moved without changing the excitation energy. When exchanging the positions of two e anyons, the excited state is unchanged, while when exchanging the positions of two m anyons, the excited state is changed from $|\Phi\rangle$ to $-|\Phi\rangle$. It follows that e anyons are bosons while m anyons are fermions. An e anyon and an m anyon can be fused together as a bounded pair which behaves as an fermionic ϵ anyon. By joining two e (m) anyons together at the same vertex (plaquette), they fuse into vacuum of anyons, i.e. the ground state. In an anyonic excited state, interchanging the positions of any pair of anyons only change the state by a phase factor. Because of this braiding property, anyonic excitations of the toric code is called *abelian*. In the case of more complex braiding properties, anyonic excitations are said to be *non-abelian*.

The statistics, fusion and braiding properties of anyonic excitations in a topologically ordered lattice system specify the topological order and give a macroscopic counterpart of long-range entanglement in ground states [33]. Due to the equivalence between the anyonic excitations and the long-range entanglement, in this dissertation, we limit our discussion to properties of the ground state entanglement when studying certain topological order. In particular, we consider the toric-code topological order and the double-semion topological order. A typical ground state of the toric-code topological order is an equal-weight sum of states realizing cycle configurations. Similarly, a typical ground state of the double-semion topological order is a sum of cycle configurations with expansion coefficients dependent on the number of cycles in each configuration. These long-range entangled states will be described more accurately in Chapter 5.

Chapter 3

Analysis and resolution of the ground-state degeneracy of the two-component Bose-Hubbard model

The material presented in the chapter is based on my work published in Reference [21]. In this chapter, we study the degeneracy of the ground-state energy E of the two-component Bose-Hubbard model and of the perturbative correction E_1. We show that the degeneracy properties of E and E_1 are closely related to the connectivity properties of the lattice. We determine general conditions under which E is nondegenerate. This analysis is then extended to investigate the degeneracy of E_1. In this case, in addition to the lattice structure, the degeneracy also depends on the number of particles present in the system. After identifying the cases in which E_1 is degenerate and observing that the standard (degenerate) perturbation theory is not applicable, we develop a method to determine the zeroth-order correction to the ground state by exploiting the symmetry properties of the lattice. This method is used to implement the perturbative approach to the two-component Bose-Hubbard model in the case of degenerate E_1 and is expected to be a valid tool to

perturbatively study the asymmetric character of the Mott-insulator to superfluid transition between the particle and hole side.

3.1 Introduction

Bosonic binary mixtures trapped in optical lattices have attracted considerable attention [40, 41, 42, 43, 44, 20, 45, 46, 47, 48, 49, 50, 2] in the last decade due to theoretic prediction of several new quantum phases originated by the interaction between the two components [20, 45, 46, 47, 48, 49]. The mixture can either consist of two atomic species or the same species in two different internal states, with each component being described within the Bose-Hubbard (BH) picture [19, 18]. The recent experimental realization of bosonic mixtures [41, 42, 43], in addition to their rich phenomenology, has reinforced the interest for this class of systems. The mixture is described by the two-component BH model [20]:

$$H = H^{(a)} + H^{(b)} + U^{(ab)} \sum_{i=1}^{M} n_i^{(a)} n_i^{(b)} \tag{3.1}$$

where $U^{(ab)}$ represents the interspecies interaction, that is, the coupling between the two components $\mathcal{A}$ and $\mathcal{B}$. The local number operators $n_i^{(a)} = a_i^+ a_i$ and $n_i^{(b)} = b_i^+ b_i$ are defined in terms of space-mode bosonic operators a_i and b_i, relevant to species $\mathcal{A}$ and $\mathcal{B}$ respectively, satisfying the standard commutators $[a_r, a_i^+] = [b_r, b_i^+] = \delta_{ri}$ where $i, r \in [1, M]$ and M is the number of lattice sites. $H^{(a)}$ and $H^{(b)}$ are defined by:

$$H^{(c)} = \frac{U^{(c)}}{2} \sum_{i=1}^{M} n_i^{(c)} (n_i^{(c)} - 1) - T^{(c)} \sum_{(i,j)} I_{(i,j)}\, c_j^+ c_i\,, \quad c = a,\, b \tag{3.2}$$

where $U^{(c)}$ is the onsite intraspecies interaction, $T^{(c)}$ is the hopping amplitude describing boson tunneling, $I_{(i,j)}$ are the off-diagonal elements of the symmetric adjacency matrix in

which bond $\{i, j\}$ runs through all pairs of sites with $i \neq j$. For the common case of nearest-neighbor hopping only, one has $I_{(i,j)} = 1$ on bonds $\{i, j\}$ connecting nearest neighboring sites and zero otherwise. The study of mixtures by means of Monte Carlo simulations [50, 2] has greatly contributed to disclose many fundamental properties of the system and provided an accurate, unbiased study of several aspects of the global phase diagram. On the other hand, the perturbation approach still represents a considerably effective tool to obtain a deep insight on the structure of the ground state and the microscopic processes governing the formation of quantum phases. By construction, the analytic character of this method clearly shows how microscopic processes incorporated in the perturbation term of the Hamiltonian along with non trivial entanglement often characterizing mixtures influence the structure of ground states. In particular, entanglement between the two components is already present in the zeroth order correction of the ground state for certain choices of boson numbers $N^{(a)}$ and $N^{(b)}$, non-commensurate to M. In higher dimensions, other analytic techniques such as the Gutzwiller mean-field approach [18, 48] are able to provide significant information for macroscopic states characterized by no or weak entanglement. In some simpler cases, mean-field techniques can be improved by introducing 'local' entanglement between the two components [47, 50].

We are interested in applying the perturbation method to the two-component BH model with the ultimate goal of gaining some insight on the structure of the ground state and the role of entanglement resulting from the interspecies interaction [22]. The application of the perturbation method, though, can be challenging, certainly analytically but also numerically, owing to the remarkably-high degree of degeneracy that often characterizes the ground state of the unperturbed Hamiltonian. In the sequel, we will assume the hopping amplitudes $T^{(a)}$ and $T^{(b)}$ of the two species as the perturbation parameters for the two-component BH model.

To understand the nature of the degeneracy and the challenges of the perturbative

calculation we can consider the following simple example. Let us consider the transition of bosonic component $\mathcal{A}$ from the Mott-insulator (MI) to the superfluid (SF) phase when component $\mathcal{B}$ is SF. This case, studied in Ref. [2, 50] when component $\mathcal{B}$ is dilute, has revealed an evident asymmetric shift of the MI lobe of the (majority) component $\mathcal{A}$ between the particle and hole side of Mott lobe. This effect, in turn, appears to be related to a ground-state structure which features entanglement between $\mathcal{A}$ and $\mathcal{B}$ bosons which is substantially different in the particle and hole-excitation case [22]. The most elementary version of this transition is found in the limit $T^{(a)}, T^{(b)} \to 0$ by considering a SF component $\mathcal{B}$ with $N^{(b)} = k^{(b)}M + 1$ together with a Mott component $\mathcal{A}$ with $N^{(a)} = k^{(a)}M$ (where $k^{(a)}, k^{(b)}$ are nonnegative integers). The corresponding zeroth-order ground state is $|k^{(a)}\rangle \otimes \sum_s (b_s^+/\sqrt{M})\,|k^{(b)}\rangle$, where $|k^{(c)}\rangle$, $c = a, b$ represents a Mott state with filling $k^{(c)}$, and $b_s^+\,|k^{(b)}\rangle$ describes the creation of a solitary boson at site s causing the SF character of species $\mathcal{B}$. In the grand-canonical ensemble, when the energy cost for adding a boson to component $\mathcal{A}$ is zero, the transition to zeroth-order ground state of the form $\sum_{ik} F_{ik} a_i^+ b_k^+\,|k^{(a)}\rangle \otimes |k^{(b)}\rangle$ corresponding to $\mathcal{A}$ and $\mathcal{B}$ both superfluid occurs. In order to minimize the contribution of the interspecies-interaction term to the ground-state energy E_0, the diagonal elements of the $M \times M$ matrix F must be zero. In general, the high degree of degeneracy (represented by the arbitrariness of F_{ik}) is removed by imposing the minimization of the first-order perturbative correction E_1 with respect to the undetermined parameters F_{ik}. This solution scheme, however, is viable only if E_1 is not degenerate, a condition whose validity can be shown to depend on the number of particles, the lattice properties, and possibly on model parameters.

While this simple case can be solved analytically [51], for situations with $N^{(a)} = k^{(a)}M + p^{(a)}$ and $N^{(b)} = k^{(b)}M + p^{(b)}$, where $p^{(a)}$ and $p^{(b)}$ are arbitrary integers $p^{(a)}, p^{(b)} \in [1, M-1]$, the determination of the zeroth-order ground-state amplitudes (e.g matrix elements F_{ik} in the example illustrated above) cannot be done analytically and can easily

become numerically costly. For this reason, determining general conditions for which the ground-state energy E of model H and the first-order correction E_1 are nondegenerate (without resorting to complicated either analytical or numerical calculations) represents a precious, essential information for implementing the perturbation method.

In this chapter we show that both the ground-state energy E of H and the lowest eigenvalue of the perturbation term formed by the $T^{(a)}$ and $T^{(b)}$-dependent terms in H are nondegenerate if the simple condition to have a *connected lattice* Λ is satisfied. Then, after observing that if the unperturbed ground-state energy E_0 is degenerate this degeneracy can be eliminated if the first-order correction E_1 is nondegenerate, we explore the conditions for which first-order correction E_1 is nondegenerate for different choices of $p^{(a)}$ and $p^{(b)}$.

This chapter is organized as follows. Section 3.2 is devoted to give some useful definitions and to recast the model interaction/hopping parameters into a form more advantageous for our perturbation approach. In Section 3.3, we define the connectedness between states of the Fock basis and give the sufficient and necessary condition that links the lattice connectivity to the state connectedness. This allows us to apply the Perron-Frobenius theorem [52] to study the degeneracy properties of the ground-state energy. Concerning the definition of states' connectedness assumed in this chapter, it should be noted that similar definitions, followed by the application of Perron-Frobenius theorem, are used in Katsura and Tasaki's recent work [53] in the proof of the degeneracy of the spin-1 Bose-Hubbard model and previously in Ref. [54, 55, 56] devoted to the study of ferromagnetism of the Hubbard model. Our method differs from previous studies in the fact that we define the connectedness in a different way in order to give an equivalence relation. This allows us to conveniently study the degeneracy of the gorund state energy and its first order correction.

In Section 3.4 we discuss the degeneracy of E_1 in two cases: (1) one of the two species is a MI while the other is SF; (2) there are $k^{(a)}M+1$ (or $k^{(a)}M-1$) species-$\mathcal{A}$ bosons while

species $\mathcal{B}$ is SF with a generic number of bosons. In Section 3.5, we extend our discussion to generic cases with the only requirement, $p^{(a)} + p^{(b)} < M - 1$ or $p^{(a)} + p^{(b)} > M + 1$. Our analysis shows that E_1 is nondegenerate if one assumes certain sufficient conditions on the connectivity of the lattice. These conditions are satisfied by most lattices.

Finally, in Section 3.6 we show that when $p^{(a)} + p^{(b)} = M$, E_1 is degenerate independently on the connectivity of the lattice. We therefore discuss the determination of the unperturbed ground state in terms of symmetry properties of the lattice for $N^{(a)}$ and $N^{(b)}$ such that $p^{(a)} = 1$, $p^{(b)} = M - 1$ or $p^{(a)} = M - 1$, $p^{(b)} = 1$.

3.2 The two-component model in the strongly-interacting regime

We intend to study the two-component Bose-Hubbard model in the strongly-interacting regime where $T^{(a)}, T^{(b)} \ll U^{(a)}, U^{(b)}, U^{(ab)}$. We assume that $T^{(a)} \approx T^{(b)}$, stating that the mobility of the bosons of the two components is essentially the same, and $0 \leq I_{(i,j)} \leq 1$. To avoid phase separation we also assume (repulsive) onsite interactions such that $U^{(ab)} < U^{(a)}, U^{(b)}$. Although in the following we will explicitly consider the case of soft-core bosons, i.e. $U^{(a)}, U^{(b)} < \infty$, the results presented are also valid for the case of hard-core bosons [57]. The application of the perturbation method suggests the definition of new interaction/hopping parameters

$$T^{(a)} = T\,t^{(a)}, \quad T^{(b)} = T\,t^{(b)}, \quad U^{(a)} = U\,u^{(a)}, \quad U^{(b)} = U\,u^{(b)},$$

entailing that model Hamiltonian H takes the form

$$H = U\left[\frac{u^{(a)}}{2}\sum_{i=1}^{M} n_i^{(a)}(n_i^{(a)}-1) + \frac{u^{(b)}}{2}\sum_{i=1}^{M} n_i^{(b)}(n_i^{(b)}-1) + \frac{U^{(ab)}}{U}\sum_{i=1}^{M} n_i^{(a)} n_i^{(b)}\right] + T\Big[-t^{(a)}\sum_{(i,j)} I_{(i,j)}\; a_i^{+}\, a_j - t^{(b)}\sum_{(i,j)} I_{(i,j)}\; b_i^{+}\, b_j\Big], \quad (3.3)$$

in which we call H_0 the U-dependent diagonal part of the Hamiltonian (first, second and third terms in Eq. 3.3) and TW represents the T-dependent kinetic energy part of H (fourth and fifth terms in Eq. 3.3 with W representing the square bracket). Then TW/U represents the perturbation and $\epsilon = T/U$ naturally identifies with the perturbation parameter.

The sites of the optical lattice and the set of all bonds $\{i, j\}$ with weight $I_{(i,j)} \neq 0$ define an edge-weighted graph $\Lambda = (\mathcal{V}(\Lambda), \mathcal{E}(\Lambda))$, where $\mathcal{V}(\Lambda)$ is the set of vertices, i.e. sites, $\mathcal{E}(\Lambda)$ is the set of edges, i.e. bonds (not necessarily nearest neighbors), and $I_{(i,j)}$ is the weight on bond $\{i, j\}$

In the following we will work in a finite-dimensional Hilbert space $\mathcal{H}$ corresponding to fixed particle numbers $N^{(a)} = k^{(a)}M + p^{(a)}$ and $N^{(b)} = k^{(b)}M + p^{(b)}$ for the two components respectively [1]. Here, $k^{(a)}$, $k^{(b)}$, $p^{(a)}$ and $p^{(b)}$ are nonnegative integers with $0 \leq p^{(a)} < M$, $0 \leq p^{(b)} < M$. The space $\mathcal{H}$ is spanned by an orthonormal basis of Fock states $|\mathbf{n}\rangle \otimes |\mathbf{m}\rangle$:

$$|\mathbf{n}\rangle \otimes |\mathbf{m}\rangle = \frac{\prod_{l=1}^{M} a_l^{+\mathbf{n}_l} \prod_{m=1}^{M} b_m^{+\mathbf{m}_m}\,|0\rangle}{\sqrt{\prod_{l=1}^{M}\mathbf{n}_l!\prod_{m=1}^{M}\mathbf{m}_m!}}, \quad (3.4)$$

where $|0\rangle$ is the vacuum states, i.e. every site in the lattice is empty, and $\mathbf{n}$, $\mathbf{m}$ are integers such that $\sum_{l=1}^{M}\mathbf{n}_l = k^{(a)}M + p^{(a)}$, $\sum_{m=1}^{M}\mathbf{m}_m = k^{(b)}M + p^{(b)}$.

To simplify our notation we use $|\mathbf{n}, \mathbf{m}\rangle$ to denote $|\mathbf{n}\rangle \otimes |\mathbf{m}\rangle$. The ground state(s) of H_0 are labelled by $|\bar{\mathbf{n}}, \bar{\mathbf{m}}\rangle$. We call O the set of states $|\mathbf{n}, \mathbf{m}\rangle$s, and $\bar{O}$ the set of the states $|\bar{\mathbf{n}}, \bar{\mathbf{m}}\rangle$s. The operator W confined in the subspace spanned by $|\bar{\mathbf{n}}, \bar{\mathbf{m}}\rangle$'s is denoted by $\bar{W}$.

[1] Particle number operators commute with both H_0 and H.

The matrix representation of W in terms of the basis $|\mathbf{n},\mathbf{m}\rangle$'s is denoted by $\mathbf{W}$ and the matrix representation of $\bar{W}$ in terms of $|\bar{\mathbf{n}},\bar{\mathbf{m}}\rangle$'s is denoted by $\bar{\mathbf{W}}$.

The explicit expression of matrix elements of $\mathbf{W}$ is given by:

$$\begin{aligned}\langle \mathbf{n},\mathbf{m}|W|\mathbf{n}',\mathbf{m}'\rangle = -t^a\,\delta_{\mathbf{m},\mathbf{m}'}\sum_{(i,j)}\Big[I_{(i,j)}\sqrt{\mathbf{n}_j+1}\sqrt{\mathbf{n}'_i+1}\delta_{\mathbf{n}_j+1,\mathbf{n}'_j}\delta_{\mathbf{n}_i,\mathbf{n}'_i+1}\prod_{l\neq i,j}^{M}\delta_{\mathbf{n}_l\mathbf{n}'_l}\Big]\\ -t^b\,\delta_{\mathbf{n},\mathbf{n}'}\sum_{(i,j)}\Big[I_{(i,j)}\sqrt{\mathbf{m}_j+1}\sqrt{\mathbf{m}'_i+1}\delta_{\mathbf{m}_j+1,\mathbf{m}'_j}\delta_{\mathbf{m}_i,\mathbf{m}'_i+1}\prod_{m\neq i,j}^{M}\delta_{\mathbf{m}_m,\mathbf{m}'_m}\Big].\end{aligned}\tag{3.5}$$

It is obvious that the matrix elements are nonpositive. Moreover, a matrix element is nonzero if and only if $\mathbf{n}'_i=\mathbf{n}_i+1$, $\mathbf{n}'_j+1=\mathbf{n}_j$ on bond $\{i,j\}$ while all other $\mathbf{n}'_l=\mathbf{n}_l$, and $\mathbf{m}=\mathbf{m}'$; or $\mathbf{m}'_i=\mathbf{m}_i+1$, $\mathbf{m}'_j+1=\mathbf{m}_j$ on bond $\{i,j\}$ while all other $\mathbf{m}'_l=\mathbf{m}_l$, and $\mathbf{n}=\mathbf{n}'$. This property of matrix elements will be used below.

After recalling that in the strongly-interacting regime we treat the term ϵW as a perturbation with $\epsilon = T/U$, the ground-state energy E of $H = U(H_0+\epsilon W)$ and its eigenvector(s) $|\Psi_l\rangle$ ($l=1,\cdots,f_E$, where f_E is the degeneracy of E) can be expanded via the perturbative series $E=E_0+\sum_{n=1}^{\infty}\epsilon^n E_n$ and $|\Psi_l\rangle = |\psi_l^0\rangle+\sum_{n=1}^{\infty}\epsilon^n|\psi_l^n\rangle$. Note that if $p^{(a)}+p^{(b)}>0$, then H_0 has a degenerate ground-state energy E_0 with degeneracy f_{E_0}. If $f_{E_0}=f_E$, one can apply perturbation theory starting from any ground state of H_0. If $f_{E_0}>f_E$ and W fully lifts the extra degeneracy of E_0, then E_1 and $|\psi_l^0\rangle$ can be uniquely determined by solving the matrix eigenvalue problem (degenerate perturbation theory):

$$\sum_{\bar{\mathbf{n}}',\bar{\mathbf{m}}'}\langle\bar{\mathbf{n}},\bar{\mathbf{m}}|W|\bar{\mathbf{n}}',\bar{\mathbf{m}}'\rangle\langle\psi_l^0|\bar{\mathbf{n}}',\bar{\mathbf{m}}'\rangle = E_1\langle\psi_l^0|\bar{\mathbf{n}},\bar{\mathbf{m}}\rangle\tag{3.6}$$

On the other hand, if neither of the previous scenarios are true, then $|\psi_l^0\rangle$'s are not uniquely determined by solving Eq. 3.6. From this discussion, it becomes apparent that one needs to study the degeneracy of both E and E_1, and, in the case Eq. 3.6 is not applicable, find

an alternative method to determine $|\psi^0\rangle$.

As we will show in the following, the issue of degeneracy is closely related to the connectivity of the lattice.

3.3 Degeneracy of the ground-state energy, connectivity of lattice and connectedness between states

In this section, we discuss the degeneracy of the ground-state energy of H by utilizing the notion of "connectedness" on the states of the basis and the Perron-Frobenius theorem (PFT). This theorem states that if $\mathbf{X}$ is a real symmetric matrix such that (i) off-diagonal elements are all nonpositive, (ii) for any two different indices p and q there exists an N such that $(\mathbf{X}^N)_{p,q} \neq 0$, then its lowest eigenvalue is nondegenerate and the corresponding eigenvector is positive [52]. In the following we will apply PFT theorem for the case of matrix $\mathbf{W}$ and $\mathbf{H}$.

To begin with, we define the "connectedness" on states via a symmetric linear operator X [2] (its corresponding matrix is denoted by $\mathbf{X}$).

Hence, we say that $|\mathbf{n}, \mathbf{m}\rangle$ and $|\mathbf{n}', \mathbf{m}'\rangle$ are connected by a symmetric linear operator X if there exists a finite sequence $\{|\alpha_1, \beta_1\rangle, |\alpha_2, \beta_2\rangle, \cdots, |\alpha_N, \beta_N\rangle\}$ with $|\alpha_1, \beta_1\rangle = |\mathbf{n}, \mathbf{m}\rangle$ and $|\alpha_N, \beta_N\rangle = |\mathbf{n}', \mathbf{m}'\rangle$ in the set O such that for any $1 \leq i < N$, $\langle \alpha_i, \beta_i | X | \alpha_{i+1}, \beta_{i+1}\rangle \neq 0$ or $|\alpha_i, \beta_i\rangle = |\alpha_{i+1}, \beta_{i+1}\rangle$. This definition includes the trivial case $|\mathbf{n}, \mathbf{m}\rangle = |\mathbf{n}', \mathbf{m}'\rangle$. The kinetic energy operator W and the Hamiltonian H are indeed symmetric linear operators. The connectedness associated with X defines an equivalence relation [3] $\Re_X$ on O such that

[2] A linear operator X is symmetric if, for arbitrary states $|\phi\rangle$ and $|\psi\rangle$, $\langle \phi | X | \psi \rangle = \langle \psi | X | \phi \rangle$.

[3] A relation $\Re_X$ on a set O is a collection of ordered pairs $(|\mathbf{n}, \mathbf{m}\rangle, |\mathbf{n}', \mathbf{m}'\rangle)$ in O. If $(|\mathbf{n}, \mathbf{m}\rangle, |\mathbf{n}', \mathbf{m}'\rangle) \in O$, we say $|\mathbf{n}, \mathbf{m}\rangle \, \Re_X \, |\mathbf{n}', \mathbf{m}'\rangle$. $\Re_X$ is an equivalence relation on a set O if it satisfies

(i) reflexivity, i.e. $|\mathbf{n}, \mathbf{m}\rangle \, \Re_X \, |\mathbf{n}, \mathbf{m}\rangle$, (ii) symmetry, i.e. $|\mathbf{n}, \mathbf{m}\rangle \, \Re_X \, |\mathbf{n}', \mathbf{m}'\rangle$ implies $|\mathbf{n}', \mathbf{m}'\rangle \, \Re_X \, |\mathbf{n}, \mathbf{m}\rangle$, (iii) transitivity, i.e. $|\mathbf{n}, \mathbf{m}\rangle \, \Re_X \, |\mathbf{n}', \mathbf{m}'\rangle$ plus $|\mathbf{n}', \mathbf{m}'\rangle \, \Re_X \, |\mathbf{n}'', \mathbf{m}''\rangle$ imply $|\mathbf{n}, \mathbf{m}\rangle \, \Re_X \, |\mathbf{n}'', \mathbf{m}''\rangle$.

For a given relation $\Re_X$, $|\mathbf{n}, \mathbf{m}\rangle / \Re_X$ denotes the set of all $|\mathbf{n}', \mathbf{m}'\rangle$ related to $|\mathbf{n}, \mathbf{m}\rangle$, and $O/\Re_X$ denotes the

$|\mathbf{n}, \mathbf{m}\rangle \, \Re_X \, |\mathbf{n}', \mathbf{m}'\rangle$ if and only if the two states are connected by X. Given this equivalence relation, we can prove that:

Proposition 1. *The following three conditions are equivalent: (a)* $\mathbf{X}$ *is irreducible* [4]*, (b) any* $|\mathbf{n}, \mathbf{m}\rangle$ *and* $|\mathbf{n}', \mathbf{m}'\rangle$ *are connected by X, (c) property-(ii) in PFT is satisfied.*

The proof is given in the Section 3.8.1.

3.3.1 Connectivity of Λ and the nondegeneracy of E

We want to prove that the ground state of H is nondegenerate by making use of PFT. Hence, we need to show that $\mathbf{H}$ satisfies the hypothesis of the theorem. We first notice that both H and W are symmetric linear operators. Moreover, $\langle \mathbf{n}, \mathbf{m}|(H_0 + \epsilon W)|\mathbf{n}', \mathbf{m}'\rangle = \langle \mathbf{n}, \mathbf{m}|H_0|\mathbf{n}', \mathbf{m}'\rangle + \epsilon \langle \mathbf{n}, \mathbf{m}|W|\mathbf{n}', \mathbf{m}'\rangle = \epsilon \langle \mathbf{n}, \mathbf{m}|W|\mathbf{n}', \mathbf{m}'\rangle \leq 0$ for any $|\mathbf{n}, \mathbf{m}\rangle \neq |\mathbf{n}', \mathbf{m}'\rangle$, and hence $\mathbf{H}$ and $\mathbf{W}$ are both real matrices with nonpositive off-diagonal elements, as requested by condition (i) of the PFT. Moreover, $|\mathbf{n}, \mathbf{m}\rangle$ and $|\mathbf{n}', \mathbf{m}'\rangle$ are connected by H if and only if they are connected by W. Next step is to show that condition (ii) is also satisfied. In view of Proposition 1, it is sufficient to show that any $|\mathbf{n}, \mathbf{m}\rangle$ and $|\mathbf{n}', \mathbf{m}'\rangle$ are connected by W. From here on, we will assume that Λ is connected [5] (note that, the connectivity of Λ is different from the connectedness on the basis). We can show that:

Proposition 2. *Any* $|\mathbf{n}, \mathbf{m}\rangle$ *and* $|\mathbf{n}', \mathbf{m}'\rangle$ *are connected by W if and only if* Λ *is connected.*

We first prove the sufficient condition. The general idea of the proof is to connect both states $|\mathbf{n}, \mathbf{m}\rangle$ and $|\mathbf{n}', \mathbf{m}'\rangle$ to a state such that all particles are sitting on the same lattice site

collection of all $|\mathbf{n}, \mathbf{m}\rangle$ /$\Re_X$'s. An important property of equivalence relations is that $O/\Re_X$ is a partition of O [58]. It's easy to check that $\Re_X$ is well-defined here.

[4] A symmetric matrix is irreducible if and only if it cannot be block-diagonalized by permuting the indices.

[5] Λ is connected if any two sites can be linked by a path. Two sites i and j are linked if there exists a path $\{i, \cdots, k_l, \cdots, j\}$ in which every neighboring pair in the sequence forms a bond.

k, and then apply the transitivity property. Let us fix a site k. Then, any other site is linked to k by a path. Since $|\mathbf{n}'', \mathbf{m}''\rangle = c_i c_j^+ |\mathbf{n}, \mathbf{m}\rangle / \| c_i c_j^+ |\mathbf{n}, \mathbf{m}\rangle \|$, $c = a, b$, is connected to $|\mathbf{n}, \mathbf{m}\rangle$ if $\{i, j\}$ is a bond (see Eq. 3.5), we can apply $a_i a_j^+$ or $b_i b_j^+$ subsequently on the appropriate bonds $\{i, j\}$ in order to construct the special state $|\mathbf{n}''', \mathbf{m}'''\rangle$ connected to $|\mathbf{n}, \mathbf{m}\rangle$. $|\mathbf{n}''', \mathbf{m}'''\rangle$ is such that all bosons are sitting on site k. Next, we perform a similar operation on $|\mathbf{n}', \mathbf{m}'\rangle$ to connect it to $|\mathbf{n}''', \mathbf{m}'''\rangle$. By transitivity of connectedness we have that $|\mathbf{n}, \mathbf{m}\rangle$ and $|\mathbf{n}', \mathbf{m}'\rangle$ are connected to each other. A similar construction of intermediate states is also used in [53].

Here, we prove the necessary condition by contradiction. Let us assume that the lattice is not connected. Then, there exists at least two sites k and l not linked by any path. Let K be the set of sites linked to k. Then the complement of K in $\mathcal{V}(\Lambda)$ is nonempty and is not linked to K [6]. Since there always exists states $|\mathbf{n}, \mathbf{m}\rangle$ and $|\mathbf{n}', \mathbf{m}'\rangle$ with different total number of particles on the sites belonging to K, then, these two states are obviously not connected. We get contradiction.

We are now ready to apply PFT to conclude:

Theorem 1. *If Λ is connected, then the ground-state energy of H is nondegenerate and it has a positive [7] ground state.*

Corollary 1. *If Λ is connected, then ϵW has a negative nondegenerate ground-state energy with a positive ground state.*

Another interesting result can be derived by setting the hopping amplitude of one of the components to zero, e. g. $T^{(b)} = 0$. Then, from Eq. 3.5, it is obvious that for any $|\mathbf{n}, \mathbf{m}\rangle$, $|\mathbf{n}', \mathbf{m}'\rangle$ with $|\mathbf{m}\rangle \neq |\mathbf{m}'\rangle$, the two states are not connected by W. One can show the following result (the proof is given in Section 3.8.2):

[6] Every site in K is not linked to any site in its complement.

[7] A vector is positive (in terms of the basis) if its expansion coefficients are all positive.

Corollary 2. *If* Λ *is connected and* $T^{(a)} = 0, T^{(b)} \neq 0$ *(or* $T^{(b)} = 0, T^{(a)} \neq 0$*), the degeneracy of the ground-state energy of* W *is* $M^{N^{(b)}}$ *(*$M^{N^{(a)}}$*).*

It is worth noting that the results presented in this Section are quite general. They hold for the case of nearest-neighbor or longer-ranged hopping. Moreover, they are valid in both the weakly and strongly correlated regime and for both repulsive or attractive interspecies interaction. The only requirement is for the lattice to be connected and $T^{(a,b)}$, $I_{(i,j)}$ to be nonnegative. Finally, we would like to mention that the results presented in this Section are also valid for the case of hard-core bosons although the specifics of the proofs and the degeneracy in Corollary 2 are different [57]. Likewise, the results presented in the following hold for hard-core bosons as well since they are based on the results of Section. 3.3.

3.4 Degenerate perturbation theory

Theorem 1 states that the ground-state energy E of model 3.3 is nondegenerate. In the general case where at least one of the two component is doped away from integer filling, the ground state corresponding to E_0 is degenerate. Then, the first order correction E_1 can either be nondegenerate (i.e. W completely lifts the degeneracy of E_0), in which case $|\psi^0\rangle$ is uniquely determined, or degenerate, in which case $|\psi^0\rangle$ is not uniquely determined. In this section, we discuss degeneracy properties of E_1 in terms of graph theoretical properties of Λ. In the case when E_1 is degenerate, we provide a method to determine $|\psi^0\rangle$ according to symmetry properties of Λ, hence providing a rigorous solution to the degenerate perturbation theory Eq. 3.6. This case is discussed in Section 3.6.

3.4.1 Representing $|\bar{\mathbf{n}}, \bar{\mathbf{m}}\rangle$'s pictorially

At commensurate filling, i.e. $N^{(a)} = k^{(a)}M$ and $N^{(b)} = k^{(b)}M$, the potential energy is minimized when, on each site, there are $k^{(a)}$ $\mathcal{A}$ bosons and $k^{(b)}$ $\mathcal{B}$ bosons (recall we are considering $U^{(ab)} < U^{(a)}, U^{(b)}$). When one or both components are doped away from integer filling factor, the extra particles arrange themselves in order to minimize the interspecies-interaction term in H. In particular, a given site will accommodate at most $k^{(a)} + 1$ species-$\mathcal{A}$ bosons and $k^{(b)} + 1$ species-$\mathcal{B}$ bosons. Hence, we can specify an arbitrary ground-state $|\bar{\mathbf{n}}, \bar{\mathbf{m}}\rangle$ of H_0 in terms of the sites which accommodate extra particles.

More specifically, when $p^{(a)} + p^{(b)} \leq M$, there are no sites with both an extra $\mathcal{A}$ and an extra $\mathcal{B}$ boson. Thus, the set of sites with an extra $\mathcal{A}$ boson has $p^{(a)}$ elements, and the set of sites with an extra $\mathcal{B}$ boson has $p^{(b)}$ elements. Such sets have an empty intersection. On the other hand, when $p^{(a)} + p^{(b)} > M$, there are $p^{(a)} + p^{(b)} - M$ sites with both an extra $\mathcal{A}$ and an extra $\mathcal{B}$ boson. In this case, the relevant sets have a nonempty intersection containing $p^{(a)} + p^{(b)} - M$ sites.

We can therefore identify an arbitrary ground-state $|\bar{\mathbf{n}}, \bar{\mathbf{m}}\rangle$ in terms of the sets $\bar{\mathbf{n}}$ and $\bar{\mathbf{m}}$ corresponding to $p^{(a)}$ sites with an extra $\mathcal{A}$ boson and $p^{(b)}$ sites with an extra $\mathcal{B}$ boson, respectively. The set of ground-states $\bar{O}$ is therefore represented by a collection of pairs of sets $(\bar{\mathbf{n}}, \bar{\mathbf{m}})$s. In the following, for the sake of simplicity but without loss of rigor, we represent states $|\bar{\mathbf{n}}, \bar{\mathbf{m}}\rangle$ pictorially by coloring sites belonging to $\bar{\mathbf{n}}$ in (dark) blue, sites belonging to $\bar{\mathbf{m}}$ in (light) red, and sites belonging to the intersection between $\bar{\mathbf{n}}$ and $\bar{\mathbf{m}}$ in purple (circled in black). Site with neither extra $\mathcal{A}$ nor extra $\mathcal{B}$ bosons are colored in white (circled in grey). Examples of the mapping from $|\bar{\mathbf{n}}, \bar{\mathbf{m}}\rangle$ to $(\bar{\mathbf{n}}, \bar{\mathbf{m}})$ are shown in Fig. 4.2, where states 3.1(a), 3.1(c) and 3.1(e) are represented by 3.1(b), 3.1(d) and 3.1(f) respectively.

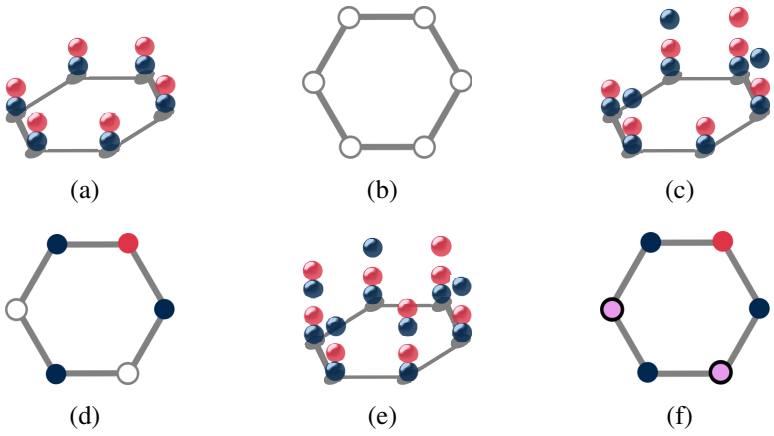

Figure 3.1: 3.1(a), 3.1(c) and 3.1(e) are an example of states in $|\bar{\mathbf{n}}, \bar{\mathbf{m}}\rangle$s for the case of a one-dimensional lattice with periodic boundary condition and M=6. These states correspond to $(k^{(a)} = 1, k^{(b)} = 1, p^{(a)} = 0, p^{(b)} = 0)$, $(k^{(a)} = 1, k^{(b)} = 1, p^{(a)} = 3, p^{(b)} = 1)$, and $(k^{(a)} = 1, k^{(b)} = 1, p^{(a)} = 5, p^{(b)} = 3)$ respectively. The color (dark) blue refers to $\mathcal{A}$ bosons and (light) red to $\mathcal{B}$ bosons. They are represented pictorially by 3.1(b), 3.1(d) and 3.1(f), where (dark) blue sites form the set $\bar{\mathbf{n}}$, (light) red sites form the set $\bar{\mathbf{m}}$, purple (circled in black) sites form the intersection of $\bar{\mathbf{n}}$ and $\bar{\mathbf{m}}$, and white (circled in grey) sites form the set of sites with neither extra $\mathcal{A}$ nor extra $\mathcal{B}$ bosons.

$\bar{W}$ is a symmetric linear operator in the subspace spanned by $|\bar{\mathbf{n}}, \bar{\mathbf{m}}\rangle$s, therefore we can define the connectedness between states $|\bar{\mathbf{n}}, \bar{\mathbf{m}}\rangle$s by $\bar{W}$. From here on, we will describe connectedness by using the representation in terms of color of sites. For example, according to Eq. 3.5, when $p^{(a)} + p^{(b)} < M$, $\langle \bar{\mathbf{n}}, \bar{\mathbf{m}} | \bar{W} | \bar{\mathbf{n}}', \bar{\mathbf{m}}' \rangle$ is nonzero if and only if one white site exchanges color with a blue or red site on a bond while all other colors remain unchanged. When $p^{(a)} = M - 1, p^{(b)} > 1$, $\langle \bar{\mathbf{n}}, \bar{\mathbf{m}} | \bar{W} | \bar{\mathbf{n}}', \bar{\mathbf{m}}' \rangle$ is nonzero if and only if one purple site exchanges color with a blue or red site on a bond while all other colors remain unchanged [8].

It should now be apparent that purple sites behave in the same way as white sites. Using this language, the rules to generate a connected state are as follows: (i) change the color of a white (or purple) site with a red or blue site on a bond; (ii) "exchange" the

[8]These rules can also be stated formally: $\langle \bar{\mathbf{n}}, \bar{\mathbf{m}} | \bar{W} | \bar{\mathbf{n}}', \bar{\mathbf{m}}' \rangle$ is nonzero if and only if either set $\bar{\mathbf{m}} = \bar{\mathbf{m}}'$ while sets $\bar{\mathbf{n}}$, $\bar{\mathbf{n}}'$ only differ by sites i and j belonging to the bond $\{i, j\}$, or set $\bar{\mathbf{n}} = \bar{\mathbf{n}}'$ while sets $\bar{\mathbf{m}}$, $\bar{\mathbf{m}}'$ only differ by sites k and l belonging to the bond $\{k, l\}$.

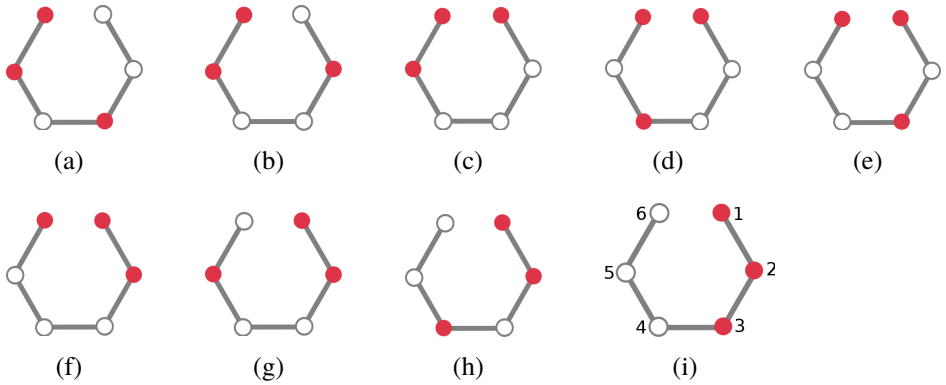

Figure 3.2: 3.2(a) through 3.2(i) represent a sequence of states in $\bar{O}$ with $k^a = k^b = p^{(a)} = 0$ and $p^{(b)} = 3$ for the case of a connected one-dimensional lattice. The sequence connects states 3.2(a) and 3.2(i).

color of two sites with the same color on a bond (this operation is trivial and results from the definition of connectedness where two neighboring states in the connecting sequence can be identical). This second rule is introduced just for the sake of convenience in the remainder of our discussion.

In terms of the pictorial representation that we have described above, a sequence $\{|\bar{\mathbf{n}}, \bar{\mathbf{m}}\rangle, \cdots, |\chi_l, \theta_l\rangle, \cdots, |\bar{\mathbf{n}}', \bar{\mathbf{m}}'\rangle\}$ in $\bar{O}$ connecting $|\bar{\mathbf{n}}, \bar{\mathbf{m}}\rangle$ to $|\bar{\mathbf{n}}', \bar{\mathbf{m}}'\rangle$ can be represented by a sequence of pictures [9]. For example, Fig. 3.2(a) through Fig. 3.2(i) shows a sequence connecting states Fig. 3.2(a) and Fig. 3.2(i), with matrix elements of $\bar{\mathbf{W}}$ between any two adjacent pictures being nonzero.

Next step is the study of the degeneracy of E_1. Since Proposition 1 and the PFT theorem also apply to $\bar{W}$, it is sufficient to check for the existence of a sequence $\{|\bar{\mathbf{n}}, \bar{\mathbf{m}}\rangle, \cdots, |\chi_l, \theta_l\rangle, \cdots, |\bar{\mathbf{n}}', \bar{\mathbf{m}}'\rangle\}$ for any arbitrary $|\bar{\mathbf{n}}, \bar{\mathbf{m}}\rangle$ and $|\bar{\mathbf{n}}', \bar{\mathbf{m}}'\rangle$. In the following, we will study under which conditions arbitrary $|\bar{\mathbf{n}}, \bar{\mathbf{m}}\rangle$ and $|\bar{\mathbf{n}}', \bar{\mathbf{m}}'\rangle$ are connected. These conditions will differ depending on the values of $p^{(a)}$ and $p^{(b)}$.

[9] Formally, it's a sequence of pairs of sets $\{(\bar{\mathbf{n}}, \bar{\mathbf{m}}), \cdots, (\chi_l, \theta_l), \cdots, (\bar{\mathbf{n}}', \bar{\mathbf{m}}')\}$.

3.4.2 One of the species has commensurate filling factor, i. e., $p^{(a)} = 0$ or $p^{(b)} = 0$

It is obvious that when both species have commensurate filling factor, i.e. $p^{(a)} = 0$ and $p^{(b)} = 0$, E_0 is nondegenerate. In the strongly interacting regime one can apply the non-degenerate perturbation method. Let us therefore consider the case when only one of the species is at commensurate filling, e. g. $p^{(a)} = 0, p^{(b)} \neq 0$. In this case, besides white sites, there are B red sites. The only assumption we are making on the lattice Λ is that it is connected (periodic boundary conditions do not necessarily need to be satisfied). Consider arbitrary $|\bar{\mathbf{n}}, \bar{\mathbf{m}}\rangle$ and $|\bar{\mathbf{n}}', \bar{\mathbf{m}}'\rangle$, e. g. states Fig. 3.2(a) and Fig. 3.2(i). By using induction, one can show:

Proposition 3. *When $p^{(a)} = 0, p^{(b)} \neq 0$ (or $p^{(a)} \neq 0, p^{(b)} = 0$), any $|\bar{\mathbf{n}}, \bar{\mathbf{m}}\rangle$ and $|\bar{\mathbf{n}}', \bar{\mathbf{m}}'\rangle$ are connected if and only if Λ is connected.*

Let us prove the sufficient condition by induction. Let us assume that Λ is connected. Then, it is always possible to label sites by $(i_1, i_2, \cdots, i_M)$ such that if we remove the first m sites in this sequence, the remaining $(i_{m+1}, \cdots, i_M)$ sites still form a connected lattice for all $1 \leq m < M$ [59]. Fig. 3.2(i) shows an example of labeling which satisfies this property. Constructing a state such that the color of i_1 (site 1 in our example) is the same as in $|\bar{\mathbf{n}}', \bar{\mathbf{m}}'\rangle$ can be done by first locating a site i_k (site 3 in our example) in $|\bar{\mathbf{n}}, \bar{\mathbf{m}}\rangle$ with the same color as i_1 in $|\bar{\mathbf{n}}', \bar{\mathbf{m}}'\rangle$. Next, we successively exchange the colors along a path linking i_1 to i_k (see e.g. Fig. 3.2(a)-3.2(c)). Let us assume that this can be done for an arbitrary i_m, with $1 \leq m < M$, and let us denote the constructed state by $|\chi_n, \theta_n\rangle$. Then, since $(i_{m+1}, \cdots, i_M)$ forms a connected lattice, by applying the same procedure as for i_1 we can fix the color on i_{m+1} (see e.g. Fig. 3.2(c)-3.2(f)). Therefore, by induction, we have shown that $|\bar{\mathbf{n}}, \bar{\mathbf{m}}\rangle$ and $|\bar{\mathbf{n}}', \bar{\mathbf{m}}'\rangle$ are connected.

The necessary condition is proved by a similar argument as in Proposition 2, which implies that, if Λ is not connected, then there exist $|\bar{\mathbf{n}}, \bar{\mathbf{m}}\rangle$ and $|\bar{\mathbf{n}}', \bar{\mathbf{m}}'\rangle$ which are not connected.

A direct consequence of Proposition 1 and Proposition 3 is the following:

Theorem 2. *When $p^{(a)} = 0, p^{(b)} \neq 0$ or $p^{(a)} \neq 0, p^{(b)} = 0$, E_1 is nondegenerate if Λ is connected.*

3.4.3 Useful properties of a 2-connected lattice

Let us first introduce the notion of 2-connectivity. A lattice Λ is said to be 2-connected if the removal of any site leaves the remaining sites connected. In the one-dimensional example of Fig. 3.3(a), this is equivalent to introducing periodic boundary conditions to get Fig. 3.3(c). In higher dimensions, the 2-connectivity conditions is satisfied by square, triangular, honeycomb, cubic, fcc lattices, etc. with any boundary conditions. Some useful properties of 2-connectivity are as follows:

(a) if Λ is 2-connected then it is also connected;

(b) Λ is 2-connected if and only if, for any two distinct sites, there exist two disjoint paths linking them (two paths are disjoint if they only share the two ends). This is the global version of Menger's theorem [59];

(c) for any distinct sites i_1, i_2 and i_3, there exists a path linking i_1 and i_2 which avoids i_3 (this is a direct consequence of property (b));

(d) in any state with at least one white site, one can always move the blue or red color from an arbitrary site to another arbitrary site according to the rules given in Subsection 3.4.1 (we prove this property in Section 3.8.3).

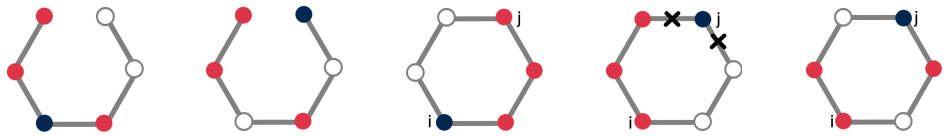

Figure 3.3: 3.3(a) and 3.3(b) are two unconnected states in $\bar{O}$ for the case of a connected one-dimensional lattice with $p^{(a)} = 1, p^{(b)} = 3$. 3.3(c) and 3.3(e) are two connected states in $\bar{O}$ for the case of a 2-connected lattice with $p^{(a)} = 1, p^{(b)} = 3$. 3.3(d) is an intermediate state in the sequence connecting 3.3(c) to 3.3(e). The two crosses in Fig. 3.3(d) indicate that the removal of site j leaves the remaining lattice still connected.

3.4.4 $p^{(a)} = 1, 0 < p^{(b)} < M-1$ and $p^{(a)} = M-1, 1 < p^{(b)} \leq M-1$

Although we will discuss our results explicitly for $p^{(a)} = 1,\ 0 < p^{(b)} < M-1$, the case of $p^{(a)} = M-1,\ 1 < p^{(b)} \leq M-1$ can be mapped onto $p^{(a)} = 1, 0 < p^{(b)} < M-1$ by replacing blue with red and vice versa, and replacing purple with white. Since purple sites can be moved in the same manner as white sites the two cases are completely equivalent.

In the case $p^{(a)} = 1,\ 0 < p^{(b)} < M-1$, i.e. one blue and B red sites are present, the requirement that Λ is connected is not sufficient for any two states to be connected. This is shown with an example in Fig. 3.3(a) and 3.3(b), where the two states represented are not connected because it is not possible to move the blue color in Fig. 3.3(a) to its position in Fig. 3.3(b) according to the rules given in Subsection 3.4.1. We need to impose that the lattice Λ is 2-connected. If this is the case, the following property holds:

Proposition 4. *Any two states* $|\bar{\mathbf{n}}, \bar{\mathbf{m}}\rangle$, $|\bar{\mathbf{n}}', \bar{\mathbf{m}}'\rangle$ *with* $p^{(a)} = 1$ *and arbitrary* $0 < p^{(b)} < M-1$ *(or* $p^{(a)} = M-1$ *and arbitrary* $1 < p^{(b)} \leq M-1$*) are connected if and only if* Λ *is 2-connected.*

Let us start by proving the sufficient condition. Consider arbitrary $|\bar{\mathbf{n}}, \bar{\mathbf{m}}\rangle$ and $|\bar{\mathbf{n}}', \bar{\mathbf{m}}'\rangle$. Without loss of generality, assume that the blue color is on site i in $|\bar{\mathbf{n}}, \bar{\mathbf{m}}\rangle$ and on site j in $|\bar{\mathbf{n}}', \bar{\mathbf{m}}'\rangle$. Due to property (d) of 2-connectivity, the blue color can be moved from i to

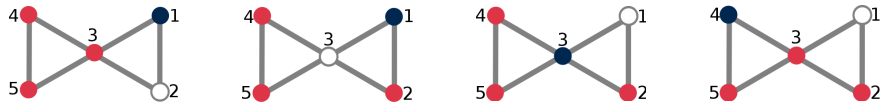

Figure 3.4: 3.4(a) through 3.4(d) represent states in $\bar{O}$ with $p^{(a)} = 1, p^{(b)} = 3$ for the case of a lattice which is *not* 2-connected. The absence of 2-connectivity implies that the removal of the site 3 leaves the remaining lattice unconnected. 3.4(a), 3.4(b) and 3.4(c) are connected with each other, but they are not connected with 3.4(d).

j. In other words, we can construct a state $|\chi_n, \theta_n\rangle$ connected with $|\bar{\mathbf{n}}, \bar{\mathbf{m}}\rangle$ in which j is blue. An example of states $|\bar{\mathbf{n}}, \bar{\mathbf{m}}\rangle$, $|\chi_n, \theta_n\rangle$ and $|\bar{\mathbf{n}}', \bar{\mathbf{m}}'\rangle$ is displayed in Fig. 3.3(c), 3.3(d) and 3.3(e) respectively. Moreover, the 2-connectivity of Λ implies that removal of site j leaves the rest of the lattice still connected (see Fig. 3.3(d)). Removing site j leaves state $|\bar{\mathbf{n}}, \bar{\mathbf{m}}\rangle$ with red and white sites only. Thus, following a similar argument as for the case $p^{(a)} = 0, p^{(b)} \neq 0$ in Proposition 3, we can show that $|\chi_n, \theta_n\rangle$ is connected to $|\bar{\mathbf{n}}', \bar{\mathbf{m}}'\rangle$. Therefore, by transitivity of connectedness, $|\bar{\mathbf{n}}, \bar{\mathbf{m}}\rangle$ is connected to $|\bar{\mathbf{n}}', \bar{\mathbf{m}}'\rangle$.

The necessary condition is proved by contradiction. For simplicity but without loss of generality we choose a counter example with a single white site. If Λ is not 2-connected (e.g. the lattice shown in Fig. 3.4(a)), then, there exists at least one site i (site 3 in our example) whose removal leaves the remaining sites partially unconnected. Let J and K denote the two unlinked sets (in our example $(1, 2)$ and $(4, 5)$ in Fig. 3.4(a)). Let us consider two states, e. g. Fig. 3.4(a) and Fig. 3.4(d), with the blue color on J and K respectively. In the attempt of transferring the blue color from J to K one can move the white color as shown in Fig. 3.4(b) and Fig. 3.4(c). At this point, though, the blue color cannot be moved to any site in K, because all sites in K are red. So it is not possible to connect state Fig. 3.4(c) to state Fig. 3.4(d)).

Finally we can conclude the following:

Theorem 3. *In the case* $p^{(a)} = 1$, $0 < p^{(b)} < M - 1$ *(or* $p^{(a)} = M - 1$, $1 < p^{(b)} \leq M - 1$*),*

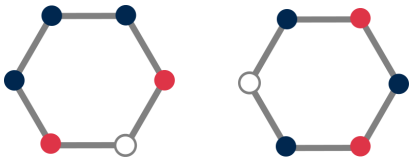

(a) (b)

Figure 3.5: 3.5(a) and 3.5(b) are two unconnected states in $\bar{O}$ for the case of a one-dimensional lattice of $M = 6$ sites with periodic boundary condition and $p^{(a)} = 3, p^{(b)} = 2$.

E_1 is nondegenerate if Λ is 2-connected.

3.5 Nondegeneracy of E_1 in the general cases $p^{(a)} + p^{(b)} < M - 1$ and $p^{(a)} + p^{(b)} > M + 1$.

We extend the results of Subsection 3.4.4 to the general case $p^{(a)}+p^{(b)} < M-1$. Replacing white with purple, the case $p^{(a)} + p^{(b)} > M + 1$ can be mapped onto $p^{(a)} + p^{(b)} < M - 1$.

In general, for $p^{(a)} + p^{(b)} < M - 1$, 2-connectivity is not a sufficient condition for any two states to be connected. This is shown by an example in Fig. 3.5(a) and 3.5(b) for a one-dimensional system with periodic boundary conditions. For later convenience we refer to this type of lattice as circle [10]. When there are at least two blue and two red sites, the order of the color on the circle becomes important. Note that the order of color only includes red and blue, since white sites can be freely moved as explained previously. It is obvious that one cannot change the order of the color in Fig. 3.5(a) to construct Fig. 3.5(b). However, it is easy to check that two states on a circle are connected if they have the same order of color. The sequence connecting them can be constructed by successively moving the white color on the circle. Using this property one can show that:

Proposition 5. *For $p^{(a)} + p^{(b)} < M - 1$ (or $p^{(a)} + p^{(b)} > M + 1$), if Λ is a circle with*

[10] A circle is a path where the two ends are the same.

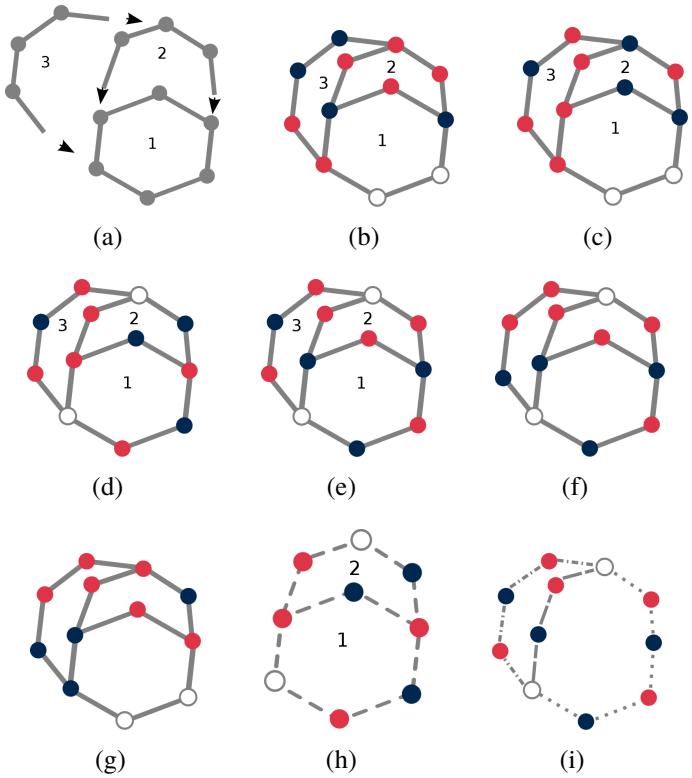

Figure 3.6: 3.6(a) displays a 2-connected lattice constructed by adding path 2 and 3 to the original circle 1. 3.6(b) and 3.6(g) represent two connected states in $\bar{O}$ for the case of the lattice represented in 3.6(a). Here $M = 12$ and $p^{(a)} = 4, p^{(b)} = 6$. 3.6(c)-3.6(f) are intermediate states in the sequence connecting 3.6(b) to 3.6(g). 3.6(h) and 3.6(i) show states 3.6(d) and 3.6(e) on sublattices. 3.6(i) also shows three different paths (dashed, dot-dashed and dotted lines) linking the end points of path 3 (see text).

one added path linking two unbonded sites on the circle, then any $|\bar{\mathbf{n}}, \bar{\mathbf{m}}\rangle$, $|\bar{\mathbf{n}}', \bar{\mathbf{m}}'\rangle$ *are connected.*

An example displaying the assumption of Proposition 5 on the lattice is shown in Fig. 3.10(i). The proof of this proposition is given in the Section 3.8.4. Note that, Λ being 2-connected is equivalent to Λ being constructed as follows: (1) start from a circle; (2) add a path which starts and ends on two distinct sites on the circle; (3) successively add paths to the already constructed lattice in the same manner as in (2) [59] (see e.g. Fig. 3.6(a)) [11].

[11]Note that in the remainder of this Subsection all added paths are non trivial in the sense that they add new sites to the already constructed lattice. Adding trivial bonds does not change our conclusions as it keeps

By using this equivalence and Proposition 5, we give a necessary and sufficient condition in order for any two states to be connected for generic cases (including all cases we discussed above) with $p^{(a)} + p^{(b)} < M - 1$ (or $p^{(a)} + p^{(b)} > M + 1$):

Proposition 6. *Any two states* $|\bar{\mathbf{n}}, \bar{\mathbf{m}}\rangle$, $|\bar{\mathbf{n}}', \bar{\mathbf{m}}'\rangle$ *with arbitrary* $p^{(a)} + p^{(b)} < M - 1$ *(or arbitrary* $p^{(a)} + p^{(b)} > M + 1$*) are connected if and only if* Λ *is 2-connected and is not a circle of* 5 *or more sites* [12].

We will show that this is true with a specific example. The argument, though, can be straightforwardly generalized to the general case. Let us start by proving the sufficient condition. Consider a 2-connected lattice (not a circle of 5 or more sites) as displayed in Fig. 3.6(a), and arbitrary $|\bar{\mathbf{n}}, \bar{\mathbf{m}}\rangle$, $|\bar{\mathbf{n}}', \bar{\mathbf{m}}'\rangle$ as displayed in Fig. 3.6(b) and 3.6(g). Note that, with $p^{(a)} + p^{(b)} < M - 1$, there exists at least two white sites. In this example we only consider two white sites [13]. Because the white color can be moved to any site in the lattice, without loss of generality, we choose the white sites to be the same for $|\bar{\mathbf{n}}, \bar{\mathbf{m}}\rangle$ and $|\bar{\mathbf{n}}', \bar{\mathbf{m}}'\rangle$ as shown Fig. 3.6(b) and 3.6(g). Starting from $|\bar{\mathbf{n}}, \bar{\mathbf{m}}\rangle$, we first construct an intermediate state $|\chi_n, \theta_n\rangle$ (Fig. 3.6(c)) connected to $|\bar{\mathbf{n}}, \bar{\mathbf{m}}\rangle$ such that the number of blue and red sites on the inner circle labelled by 1, and on the paths (in the context of this proof when we count the number of colors in the added paths we exclude the end points from the paths) labelled by 2 and 3, is the same as in $|\bar{\mathbf{n}}', \bar{\mathbf{m}}'\rangle$. This can be done according to property (d) of Section 3.4.3. Specifically, this is done by first fixing the colors on path 3, next, since the remaining lattice is still 2-connected, on path 2. Obviously, at this point, the colors on circle 1 are automatically fixed.

the 2-connectivity properties of the lattice.

[12] Two states on a circle with 4 or less sites are always connected, as shown in Lemma 4.6 of Tasaki's work [52]. In Ref. [52] the authors discuss the degeneracy problem of the ground-state energy of Fermi-Hubbard model with infinite U at fixed number of spin-up(down) fermions and in the presence of a single hole. It is interesting noting that the basis $|\bar{\mathbf{n}}, \bar{\mathbf{m}}\rangle$ that we define here is equivalent to the corresponding basis defined in Ref. [52].

[13] Nothing would change if more than two white sites are present since the white color can be freely moved on the lattice.

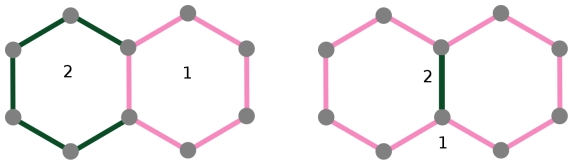

(a) (b)

Figure 3.7: 3.7(a) and 3.7(b) display two different ways of viewing the same lattice. They can both be viewed as an already constructed lattice plus an added path. In 3.7(a), two ends of the added path (dark green) form a bond on the already constructed lattice (light pink). In 3.7(b), two ends of the added path (dark green) doe not form a bond on the already constructed lattice (light pink).

Next, we construct a sequence starting forward from $|\chi_n, \theta_n\rangle$ (Fig. 3.6(c)) and backward from $|\bar{\mathbf{n}}', \bar{\mathbf{m}}'\rangle$ (Fig. 3.6(g)), by firstly moving the white color from the original circle to the two ends of path 3, only through sites on circle 1 and path 2. This step generates state Fig. 3.6(d) from Fig. 3.6(c) and state Fig. 3.6(f) from Fig. 3.6(g). In order to connect state 3.6(d) to state 3.6(f) we notice that path 2 combined with circle 1 (see Fig. 3.6(h)) satisfies the assumption of Proposition 5 [14], therefore we can construct state Fig. 3.6(e) such that colors on circle 1 and path 2 are the same as in state Fig. 3.6(f). Next, we notice that both lattices in Fig. 3.6(b) and Fig. 3.6(h) are 2-connected, therefore there exists three disjoint paths linking the two ends of path 3: path 3 itself and two paths belonging to circle 1 combined with path 2. This is shown in Fig. 3.6(i). Hence, we can apply Proposition 5 again to show that states 3.6(e) and 3.6(f) are connected. In conclusion, due to transitivity of connectedness, we have shown that $|\bar{\mathbf{n}}, \bar{\mathbf{m}}\rangle$ and $|\bar{\mathbf{n}}', \bar{\mathbf{m}}'\rangle$ are connected.

To prove the necessary condition, we simply observe that if Λ is not 2-connected or is a circle with 5 or more sites, as shown in examples Fig. 3.4(a)-3.4(d) and Fig. 4.4, there exists some cases for which not every two states are connected.

[14] If the two ends of any added path form a bond on the already constructed lattice as shown in Fig. 3.7(a), where pink indicates the already constructed lattice and green indicates the added path, then, since the path adds at least one new site, the "new" lattice we consider includes all sites as shown in Fig. 3.7(b) by pink bonds with an added green trivial path. Now, in order to apply Proposition 5, we regard the green bond in Fig. 3.7(b) as the added path.

In view of Proposition 1 and Proposition 6 we can formulate the following theorem:

Theorem 4. *In case of arbitrary* $p^{(a)} + p^{(b)} < M - 1$ *(or arbitrary* $p^{(a)} + p^{(b)} > M + 1$*),* E_1 *is nondegenerate if* Λ *is 2-connected and not a circle with* 5 *or more sites.*

In the case $p^{(a)} + p^{(b)} = M - 1$ (or $p^{(a)} + p^{(b)} = M + 1$), finding a necessary and sufficient condition on the connectivity of a lattice for any two states to be connected is still an open question. Sufficient conditions for a specific model are provided by Tasaki [56] and Katsura [60] [15]

3.6 Determination of $|\psi^0\rangle$ with N^a, N^b such that $p^{(a)} = 1, p^{(b)} = M - 1$

In the general case of $p^{(a)} + p^{(b)} = M$, there are neither white nor purple sites. Hence, according to the rules given in Subection 3.4.1, any two different states are *not* connected. This statement is valid independently on the connectivity properties of Λ. Therefore, all matrix elements in $\bar{\mathbf{W}}$ are zero, which results in $E_1 = 0$ and degenerate. We are interested in the case $p^{(a)} = 1, p^{(b)} = M - 1$ ($p^{(a)} = M - 1, p^{(b)} = 1$) which corresponds to doping species-$\mathcal{A}$ ($\mathcal{B}$) with one particle and species-$\mathcal{B}$ ($\mathcal{A}$) with one hole. In this case, $|\psi^0\rangle$ is not uniquely determined by solving Eq. 3.6. In the following we will take advantage of the symmetry properties of the lattice to uniquely determine $|\psi^0\rangle$.

Let us start by defining a symmetry operation r on the lattice and its corresponding operator S_r. We say r is a (bond-weighted) lattice automorphism of Λ if r maps $\mathcal{V}(\Lambda)$ one-to-one onto itself and satisfies (i) $\{i, j\}$ is a bond if and only if $\{r(i), r(j)\}$ is a bond, (ii) $I_{(i,j)} = I_{(r(i),r(j))}$. The inverse of r, r^{-1}, is also a lattice automorphism. Given a lattice

[15] In [60] the authors study the degeneracy of the ground-state energy of the $SU(n)$ Fermi-Hubbard model with $U = \infty$ and with exactly one hole. Another sufficient condition for the $SU(2)$ Fermi-Hubbard model requiring the lattice to be constructed by "exchange bond" was given in [56].

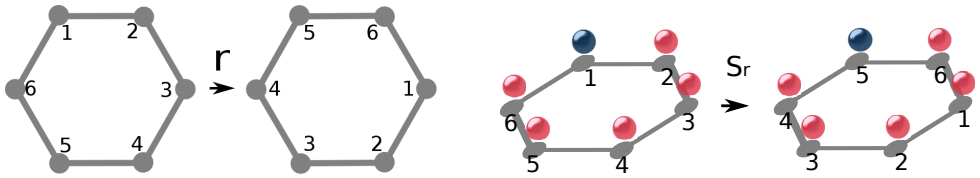

(a) (b)

Figure 3.8: 3.8(a) displays a lattice automorphism r on an hexagon. 3.8(b) displays the action on Fock states of the corresponding operator S_r: the lattice is rotated while the physical position of particles is unchanged.

automorphism r, one can define a linear operator S_r on $\mathcal{H}$ such that $S_r \left|\mathbf{n}, \mathbf{m}\right\rangle = \left|\mathbf{n}', \mathbf{m}'\right\rangle$, where $\mathbf{n}'_i = \mathbf{n}_{r(i)}$ and $\mathbf{m}'_i = \mathbf{m}_{r(i)}$. If we take the example of Fig. 3.8 with equal weight on all bonds ($I_{(i,j)} = 1$ for every $\{i, j\}$), the lattice automorphism r is a $2\pi/3$ clockwise rotation (see Fig. 3.8(a)). The action of the corresponding S_r is shown in Fig. 3.8(b), where the lattice is rotated while the physical position of particles is unchanged.

Since r is invertible, S_r also has an inverse, ${S_r}^{-1}$. It is easy to show that $S_{r^{-1}} = S_r^{-1}$. Moreover, by definition $\left|\mathbf{n}', \mathbf{m}'\right\rangle = S_r \left|\mathbf{n}, \mathbf{m}\right\rangle$ is also a normalized Fock state. Therefore S_r preserves the norm $\sqrt{\langle\psi|\psi\rangle}$ for any arbitrary state $|\psi\rangle$ in a finite-dimensional $\mathcal{H}$. Hence, S_r is a unitary operator, i.e. ${S_r}^{+} = {S_r}^{-1}$, and thus a bounded operator [16].

Note that, by definition, the state $S_r \left|\mathbf{n}, \mathbf{m}\right\rangle$ has exactly the same spatial configuration of bosons as $\left|\mathbf{n}, \mathbf{m}\right\rangle$. Then the interaction-dependent terms in H are unchanged. Hence, state $S_r \left|\mathbf{n}, \mathbf{m}\right\rangle$ has the same eigenvalue of H_0 as $\left|\mathbf{n}, \mathbf{m}\right\rangle$, and thus S_r commutes with H_0.

[16] A unitary operator is always bounded. Then, if an operator S_r is bounded, $\left(\left|\psi^0\right\rangle + \sum_{n=1}^{\infty} \epsilon^n \left|\psi^n\right\rangle\right) \to \left|\Psi\right\rangle$ implies $\left(S_r \left|\psi^0\right\rangle + \sum_{n=1}^{\infty} \epsilon^n S_r \left|\psi^n\right\rangle\right) \to S_r \left|\Psi\right\rangle$.

Moreover, according to Eq. 3.5 and the definition of r,

$$\begin{aligned}
&\langle \mathbf{n}, \mathbf{m}| S_r^{-1} W S_r |\mathbf{n}', \mathbf{m}'\rangle = \\
&-\delta_{\mathbf{m},\mathbf{m}'} t^a \sum_{(r(i),r(j))} \left[I_{r(i),r(j)} \sqrt{\mathbf{n}_{r(j)}+1}\sqrt{\mathbf{n}'_{r(i)}+1}\, \delta_{\mathbf{n}_{r(j)}+1,\mathbf{n}'_{r(j)}} \delta_{\mathbf{n}_{r(i)},\mathbf{n}'_{r(i)}+1} \prod_{l\neq r(i),r(j)}^{M} \delta_{\mathbf{n}_{r(l)}\mathbf{n}'_{r(l)}} \right] \\
&-\delta_{\mathbf{n},\mathbf{n}'} t^b \sum_{(r(i),r(j))} \left[I_{r(i),r(j)} \sqrt{\mathbf{m}_{r(j)}+1}\sqrt{\mathbf{m}'_{r(i)}+1}\, \delta_{\mathbf{m}_{r(j)}+1,\mathbf{m}'_{r(j)}} \delta_{\mathbf{m}_{r(i)},\mathbf{m}'_{r(i)}+1} \prod_{m\neq r(i),r(j)}^{M} \delta_{\mathbf{m}_m,\mathbf{m}'_m} \right] \\
&\qquad\qquad = \langle \mathbf{n}, \mathbf{m}| W |\mathbf{n}', \mathbf{m}'\rangle \,. \quad (3.7)
\end{aligned}$$

Therefore, S_r also commutes with H.

The boundedness of S_r implies:

$$S_r |\Psi\rangle = S_r |\psi^0\rangle + \sum_{n=1}^{\infty} \epsilon^n S_r |\psi^n\rangle \,. \quad (3.8)$$

Since E is nondegenerate and $H S_r |\Psi\rangle = E S_r |\Psi\rangle$, then $S_r |\Psi\rangle = e^{i\theta} |\Psi\rangle$. More specifically,

$$S_r |\psi^0\rangle + \sum_{n=1}^{\infty} \epsilon^n S_r |\psi^n\rangle = e^{i\theta} |\psi^0\rangle + \sum_{n=1}^{\infty} \epsilon^n e^{i\theta} |\psi^n\rangle \,. \quad (3.9)$$

Taking the limit $\epsilon \to 0$, we have $S_r |\psi^0\rangle = e^{i\theta} |\psi^0\rangle$. Furthermore, multiplying by $\langle \mathbf{n}, \mathbf{m}|$ Eq. 3.9, we obtain two power series of ϵ:

$$\langle \mathbf{n}, \mathbf{m}| S_r |\psi^0\rangle + \sum_{n=1}^{\infty} \epsilon^n \langle \mathbf{n}, \mathbf{m}| S_r |\psi^n\rangle = e^{i\theta} \langle \mathbf{n}, \mathbf{m}|\psi^0\rangle + \sum_{n=1}^{\infty} \epsilon^n e^{i\theta} \langle \mathbf{n}, \mathbf{m}|\psi^n\rangle \,. \quad (3.10)$$

Because the series are analytic in a small neighborhood of $\epsilon = 0$, we can equate the coefficients at each order n to get $\langle \mathbf{n}, \mathbf{m}| S_r |\psi^n\rangle = e^{i\theta} \langle \mathbf{n}, \mathbf{m}|\psi^n\rangle$. In other words, $|\psi^n\rangle$ is S_r-invariant (apart from a phase factor) for any lattice automorphism r.

In the following we will use these properties to determine the expansion coefficients

of the first order correction to the ground state Eq. 3.6. Let us consider arbitrary states $|\bar{\mathbf{n}}, \bar{\mathbf{m}}\rangle$ and $|\bar{\mathbf{n}}', \bar{\mathbf{m}}'\rangle$. We denote the unique blue site (recall $p^{(a)} = 1$ so all sites but one are red) on these states by i and j respectively. If there exists a lattice automorphism r such that $r(j) = i$, then $|\bar{\mathbf{n}}', \bar{\mathbf{m}}'\rangle = S_r |\bar{\mathbf{n}}, \bar{\mathbf{m}}\rangle$. Moreover, as shown above, $\langle \bar{\mathbf{n}}', \bar{\mathbf{m}}' | S_r | \psi^0 \rangle = \langle S_r^+ \bar{\mathbf{n}}', \bar{\mathbf{m}}' | \psi^0 \rangle = \langle S_r^{-1} \bar{\mathbf{n}}', \bar{\mathbf{m}}' | \psi^0 \rangle = \langle S_{r^{-1}} \bar{\mathbf{n}}', \bar{\mathbf{m}}' | \psi^0 \rangle = \langle \bar{\mathbf{n}}, \bar{\mathbf{m}} | \psi^0 \rangle = e^{i\theta} \langle \bar{\mathbf{n}}', \bar{\mathbf{m}}' | \psi^0 \rangle$. If we choose $|\Psi\rangle$ to be positive (see Theorem 1), in the limit of ϵ arbitrarily small, all $\langle \bar{\mathbf{n}}, \bar{\mathbf{m}} | \psi^0 \rangle$ are also positive. This implies $\langle \bar{\mathbf{n}}, \bar{\mathbf{m}} | \psi^0 \rangle = \langle \bar{\mathbf{n}}', \bar{\mathbf{m}}' | \psi^0 \rangle$. Therefore we can conclude the following:

Theorem 5. *If Λ is connected and for any two sites i and j there exists a lattice automorphism mapping j to i, then $\langle \bar{\mathbf{n}}, \bar{\mathbf{m}} | \psi^0 \rangle = 1/\sqrt{M}$.*

The assumption made on the lattice is very easily satisfied by any regular lattice with periodic boundary conditions (e.g. hypercubic, triangular, honeycomb....) as long as $I_{(i,j)} = I_{\mathbf{i}-\mathbf{j}}$, where $\mathbf{i}, \mathbf{j}$ refer to the position of sites i, j. We also note that this assumption seems to be independent from the size of the lattice.

3.7 Conclusion

We have studied the degeneracy of the ground-state energy E of the two-component Bose-Hubbard model and of the perturbative correction E_1 in terms of connectivity properties of the optical lattice. We have shown that the degeneracy properties of E and E_1 are closely related to the connectivity properties of the lattice. We can summarize our main results as follows:

- The ground-state energy E is nondegenerate if the lattice is connected.
- When $p^{(a)} = 0, p^{(b)} \neq 0$ ($p^{(b)} = 0, p^{(a)} \neq 0$), E_1 is nondegenerate if the lattice is connected.

- When $p^{(a)} = 1, 0 < p^{(b)} < M - 1$ or $p^{(a)} = M - 1$, $1 < p^{(b)} \leq M - 1$, E_1 is nondegenerate if the lattice is 2-connected.

- In generic cases with $p^{(a)} + p^{(b)} < M - 1$ or $p^{(a)} + p^{(b)} > M + 1$, E_1 is nondegenerate if the lattice is 2-connected and not a circle with 5 or more sites.

- When $p^{(a)} + p^{(b)} = M$, E_1 is degenerate independently on the connectivity of the optical lattice. In the case of $p^{(a)} = M - 1, p^{(b)} = 1$ ($p^{(a)} = 1, p^{(b)} = M - 1$), we have determined the 0th order correction of state ψ^0. We have shown that ψ^0 possesses equal expansion coefficient provided that there exists a lattice automorphism mapping a generic site of the lattice into another one.

These results are used to ensure a valid perturbative approach of the two-component Bose-Hubbard model also in the case of degenerate E_1. Details of the degenerate perturbation theory are given in Section 4.6.1. We expect that the analysis developed in this chapter and the results about the ground-state degeneracy provide an effective tool to study the asymmetric character of the Mott-insulator to superfluid transition between the particle and hole side and, more in general, the entanglement properties that appear to characterize this process.

3.8 Proofs

3.8.1 Proof of Proposition 1

We only prove the equivalence between (a) and (b). A proof based on the connectivity of the underlying graph of matrices is given in [61]. The equivalence bewteen (b) and (c) is a direct consequence of Theorem 4.3 in Ref. [52].

Let us first prove the necessary condition by contradiction. Let us assume that $|\mathbf{n}, \mathbf{m}\rangle$ and $|\mathbf{n}', \mathbf{m}'\rangle$ are not connected by X. Then $|\mathbf{n}, \mathbf{m}\rangle /\Re_X \neq |\mathbf{n}', \mathbf{m}'\rangle /\Re_X$ and they both belong to $O/\Re_X$. So $O/\Re_X$ is a nontrivial partition of O, i.e. it includes more than one subset of O, and thus $\mathbf{X}$ is reducible. We get contradiction. Therefore we proved the necessary condition.

Let us now prove the sufficient condition also by contradiction. Let us assume $\mathbf{X}$ is reducible. Then, there exists a nontrivial partition of O containing at least two disjoint nonempty subsets O_1 and O_2 of O, and the blocks $\mathbf{X}_{O_1 \times {O_1}^c}$ (${O_1}^c$ is the complement of O_1 in O), $\mathbf{X}_{{O_1}^c \times O_1}$, $\mathbf{X}_{O_2 \times {O_2}^c}$ and $\mathbf{X}_{{O_2}^c \times O_2}$ are zero. On the other hand, by hypothesis, for any $|\mathbf{n}, \mathbf{m}\rangle$ and $|\mathbf{n}', \mathbf{m}'\rangle$ which belong respectively to O_1 and O_2, there exists a finite sequence in the basis $\{|\alpha_1, \beta_1\rangle, |\alpha_2, \beta_2\rangle, \cdots, |\alpha_N, \beta_N\rangle\}$ such that $|\alpha_1, \beta_1\rangle = |\mathbf{n}, \mathbf{m}\rangle$, $|\alpha_N, \beta_N\rangle\} = |\mathbf{n}', \mathbf{m}'\rangle$ and for any $1 \leq i < N$, $\langle \alpha_i, \beta_i | X | \alpha_{i+1}, \beta_{i+1}\rangle \neq 0$. Hence, for some $1 \leq i < N$, $|\alpha_i, \beta_i\rangle \in {O_2}^c$ and $|\alpha_{i+1}, \beta_{i+1}\rangle \in O_2$ with
$\langle \alpha_i, \beta_i | X | \alpha_{i+1}, \beta_{i+1}\rangle \neq 0$ which implies $\mathbf{X}_{O_2 \times {O_2}^c} \neq 0$. We get contradiction, hence $\mathbf{X}$ is irreducible.

3.8.2 Proof of Corollary 2

Let us consider $t^{(b)} = 0$, $t^{(a)} \neq 0$ ($\leftrightarrow T^{(b)} = 0$, $T^{(a)} \neq 0$). The basic idea is to show that $\mathbf{W}$ can be block diagonalized in terms of $M^{N^{(b)}}$ identical blocks. Let us start by noticing that matrix elements of W:

$$\langle \mathbf{n}, \mathbf{m} | W | \mathbf{n}', \mathbf{m}' \rangle = -t^a \delta_{\mathbf{m},\mathbf{m}'} \sum_{\{i,j\} \in \mathcal{E}(\Lambda)} \Big[I_{(i,j)} \sqrt{\mathbf{n}_j + 1} \sqrt{\mathbf{n}'_i + 1} \delta_{\mathbf{n}_j + 1, \mathbf{n}'_j} \delta_{\mathbf{n}_i, \mathbf{n}'_i + 1} \prod_{l \neq i,j}^{M} \delta_{\mathbf{n}_l \mathbf{n}'_l} \Big]. \tag{3.11}$$

are nonzero only when $\mathbf{m} = \mathbf{m}'$. Moreover, if $\mathbf{m} = \mathbf{m}'$, the value of matrix elements is independent of $\mathbf{m}$.

Let us define a function f which provides a one-to-one mapping from the set P of all $|\mathbf{m}\rangle$s onto $O/\Re_W$, such that for any $|\mathbf{m}\rangle$, $f(|\mathbf{m}\rangle) = |\mathbf{n}, \mathbf{m}\rangle /\Re_W$. The mapping f can be easily defined and one just needs to show that f is one-to-one and onto.

Let $|\mathbf{m}\rangle$ and $|\mathbf{m}'\rangle$ be different. It's obvious that any member in $f(|\mathbf{m}\rangle)$ is not connected with any member in $f(|\mathbf{m}'\rangle)$ by W, hence $f(|\mathbf{m}\rangle) \neq f(|\mathbf{m}'\rangle)$, i.e. f is one-to-one. Next, let $x \in O/\Re_W$, i.e. $x = |\mathbf{n}'', \mathbf{m}''\rangle /\Re_W$ for some $|\mathbf{n}'', \mathbf{m}''\rangle$. Let us now consider $f(|\mathbf{m}''\rangle) = |\mathbf{n}''', \mathbf{m}''\rangle /\Re_W$ for some $|\mathbf{n}'''\rangle \neq |\mathbf{n}''\rangle$. By using connection properties of W, one can show that $|\mathbf{n}'', \mathbf{m}''\rangle \Re_W |\mathbf{n}''', \mathbf{m}''\rangle$. So $|\mathbf{n}'', \mathbf{m}''\rangle /\Re_W = |\mathbf{n}''', \mathbf{m}''\rangle /\Re_W$ and thus $x = f(|\mathbf{m}''\rangle)$, i.e. f is onto. In conclusion, f is a one-to-one mapping from P onto $O/\Re_W$.

The total number of elements in P is M^{N^b}, hence $O/\Re_W$ is a nontrivial partition of O. Then, it is obvious that for any $O_i \in O/\Re_W$, $\mathbf{W}_{O_i \times O_i{}^c}$ and $\mathbf{W}_{O_i{}^c \times O_i}$ are zero matrices. In other words, $O/\Re_W$ block-diagonalizes $\mathbf{W}$.

Next, we show that each block is an irreducible nonnegative matrix and all blocks have the same set of eigenvalues. Let $|\mathbf{m}\rangle \in P$, then $f(|\mathbf{m}\rangle) \in O/\Re_W$. We can express $f(|\mathbf{m}\rangle)$ as $f(|\mathbf{m}\rangle) = Q \otimes \{|\mathbf{m}\rangle\}$, where Q is the set of all $|\mathbf{n}\rangle$'s. From Frobenius theorem, one can conclude that $\mathbf{W}_{f(|\mathbf{m}\rangle) \times f(|\mathbf{m}\rangle)}$ has a nondegenerate ground-state energy. Since $f(|\mathbf{m}\rangle) = Q \otimes \{|\mathbf{m}\rangle\}$, one can use the identity map on Q, so that for any $|\mathbf{m}\rangle \neq |\mathbf{m}'\rangle$, a one-to-one mapping from $\mathbf{W}_{f(|\mathbf{m}\rangle) \times f(|\mathbf{m}\rangle)}$ onto $\mathbf{W}_{f(|\mathbf{m}'\rangle) \times f(|\mathbf{m}'\rangle)}$ can be constructed. By construction, this mapping keeps matrix element identical, i.e. the two matrices have the same set of eigenvalues.

In conclusion, we have shown that the ground-state energy of W is $M^{N^{(b)}}$-degenerate.

3.8.3 Proof of property (d) in Section 3.4.3

We only consider the case of blue color. The proof for the red color is trivially equal.

Consider an arbitrary state and arbitrary sites i and j, where i is blue. We want to

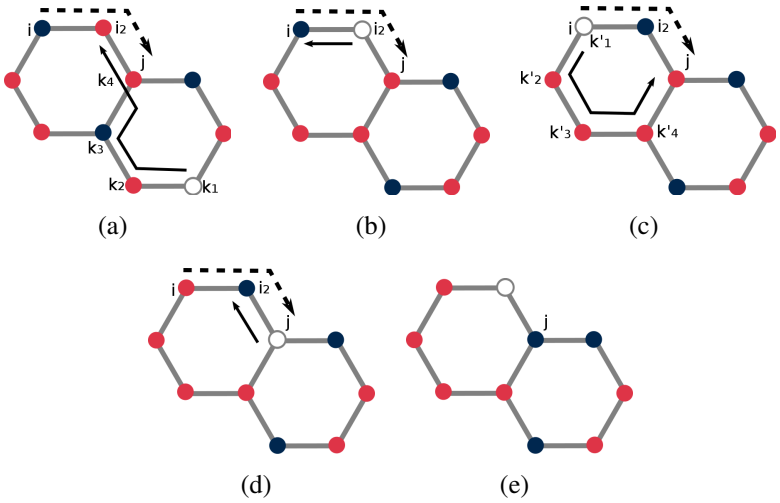

Figure 3.9: 3.9(a) through 3.9(e) are examples of states in $\bar{O}$ on a 2-connected lattice with $p^{(a)} = 3, p^{(b)} = 6$. The steps for moving the (dark) blue color from site i to j are explained in the text and displayed pictorially in the sequence 3.9(a)-3.9(e). The dashed arrow indicates a path connecting i and j. Black arrows indicate the path along which the white (circled in grey) color is moved at each step.

move the blue color from i to j according to the rules given in Subsection 3.4.1. Because Λ is connected, there exists a path $\{i, i_2, \cdots, j\}$ linking i to j. The idea of following proof is to move the blue color along this path.

To illustrate the proof, we give an example in Fig. 3.9, where 3.9(a) is the starting state, and the path $\{i, i_2, \cdots, j\}$ is indicated by a dashed arrow. To move the blue color along the path, e.g. from i_n to i_{n+1}, we need to firstly move a white color to i_{n+1} and then exchange the color on the bond $\{i_n, i_{n+1}\}$. In order to do so we observe that due to the 2-connectivity of Λ, there also exists a path $\{k_1, k_2, \cdots, i_2\}$ which avoids i but links a white site k_1 to i_2. The white color can be moved successively on $\{k_1, k_2, \cdots, i_2\}$ so that i_2 becomes white. Note that the fact that the path $\{k_1, k_2, \cdots, i_2\}$ avoids i is important, because it allows us to keep the blue color on i while moving the white color to i_2. Next step consists of exchanging the color on the bond $\{i, i_2\}$ so that i_2 becomes blue. The last two steps can be repeated successively (i.e. finding a path $\{k'_1, k'_2, \cdots, i_3\}$ linking a white site k'_1 to i_3 and

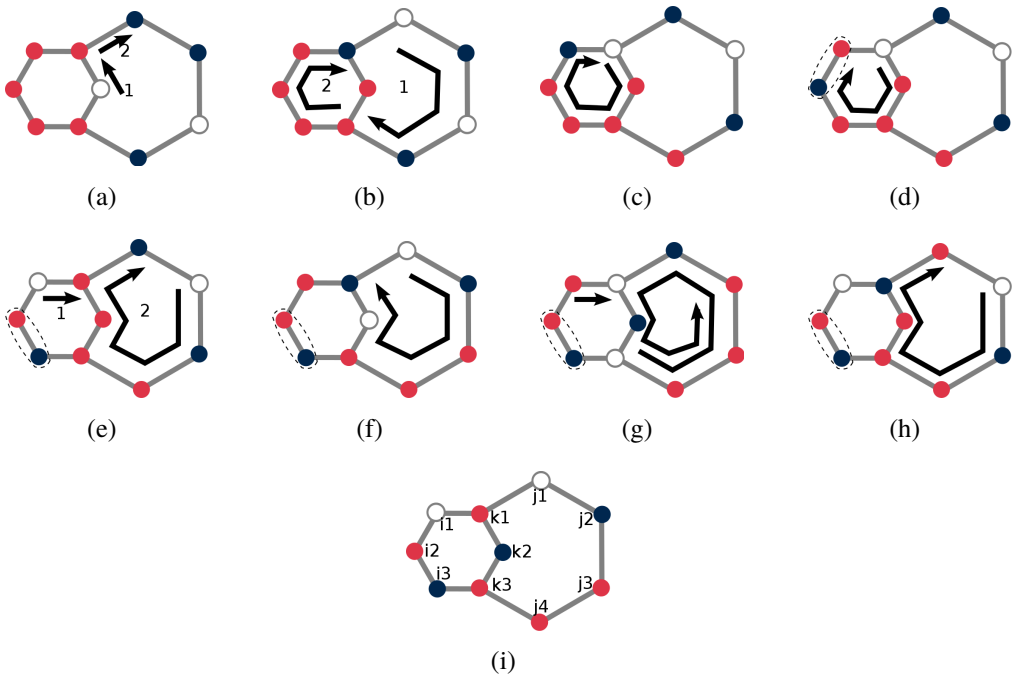

Figure 3.10: 3.10(a) through 3.10(i) represents states in $\bar{O}$ for the case of a lattice consisting of a circle with one added path linking to unbonded sites. In this example $p^{(a)} = 3, p^{(b)} = 5$. States 3.10(a) and 3.10(i) are connected through the sequence 3.10(b)-3.10(h). Black arrows indicate how the white (circled in grey) color is moved at each step. Dashed circle shows the order of the color which needs to be keep fixed (see text).

avoiding i_2, moving the white color along this path until i_3 becomes white, exchanging the color on bond $\{i_2, i_3\}$ so that i_3 becomes blue and so on) until j acquires the blue color. This process is illustrated in Fig. 3.9(a) through 3.9(e) where solid black arrows indicate the path along which the white color is moved at each step.

3.8.4 Proof of Proposition 5

For simplicity, but without loss of generality, we prove the proposition for the specific example shown in Fig. 4.6. The general case only differs in the number of sites on the circle and the extra path connecting the two sites which are unbounded in the original circle, and in the color of sites.

Let us consider the lattice shown in Fig. 3.10(i). We denote by i_l, j_l, k_1, and k_3 the sites belonging to the original circle. Sites on the extra path connecting the initially unbounded sites k_1 and k_3 are denoted by k_l (in this case we only have k_2). This path separates the original circle into the left and right circles. Let us now consider arbitrary $|\bar{\mathbf{n}}, \bar{\mathbf{m}}\rangle$ and $|\bar{\mathbf{n}}', \bar{\mathbf{m}}'\rangle$ displayed by, e.g., Fig. 3.10(a) and 3.10(i) respectively. Because the white color can be moved to any site of the lattice according to the rules given in Subsection 3.4.1, we choose $|\bar{\mathbf{n}}', \bar{\mathbf{m}}'\rangle$ such that both, left and right circles, have one white site. Note that the proof below does not depend on the number of white sites.

The proof is based on the fact that we can first construct a generic state connected with $|\bar{\mathbf{n}}, \bar{\mathbf{m}}\rangle$ and such that the order of color on i-sites is the same as in $|\bar{\mathbf{n}}', \bar{\mathbf{m}}'\rangle$. In our particular example, because one of the i sites is white, this reduces to fixing the color on the bond specified by the dashed line in Figs. 3.10(d)-3.10(h). In order to do so, we first construct a state connected to $|\bar{\mathbf{n}}, \bar{\mathbf{m}}\rangle$ where k_1 is blue, as shown in Fig. 3.10(b). This process is depicted in Fig. 3.10(a) by black arrows indicating how the white color moves. This process is always possible due to the fact that Λ is 2-connected (see a similar argument given to prove Proposition. 4). We keep moving the white color as depicted by black arrows in Fig. 3.10(b)-3.10(d), in order to construct the sequence Fig. 3.10(c)-3.10(e). We have finally constructed a state such that the order of the color on i sites is the same as $|\bar{\mathbf{n}}', \bar{\mathbf{m}}'\rangle$. Similar procedures can be followed if the color of more than two i sites need to be fixed.

Next, we need to fix the order of color on the right circle. In a general case, this is equivalent to switching the order of color on a certain number of bonds. In our case, we only need to do so for the color on bond $\{j_1, k_1\}$ of state Fig. 3.10(e). The procedure is depicted by black arrows in 3.10(e)-3.10(g), so that we end up with state Fig. 3.10(h). The idea of the procedure is to transfer the pair of colors on bond $\{j_1, k_1\}$ to bond $\{k_1, i_1\}$ (see Fig. 3.10(f)) and then move white sites in order to transfer the pair of colors back to

the original bond $\{j_1, k_1\}$ (see Fig. 3.10(h)) but with the order of the color inverted. In general, this procedure will ensure that the order of the color on $\{j_1, k_1\}$ is inverted. Now the order of color on the right circle is the same as in $|\bar{\mathbf{n}}', \bar{\mathbf{m}}'\rangle$. The last step consists of moving the white color (which does not change the order of color) on the right circle in order to reach the state $|\bar{\mathbf{n}}', \bar{\mathbf{m}}'\rangle$. This is depicted by the black arrow in Fig. 3.10(h).

In a more general case that the one described here, one simply needs to repeat similar procedures to switch the color on bonds on the right circle as needed.

Chapter 4

Inter-species entanglement of Bose-Bose mixtures trapped in optical lattices

The material presented in the chapter is based on my work published in Reference [22]. In this chapter, we discuss inter-species entanglement in Bose-Bose mixtures trapped in optical lattices. This work is motivated by the observation that, in the presence of a second component, the Mott-insulator lobe shifts *differently* on the hole- and particle-side with respect to the Mott lobe of the single species system [50, 2]. We use perturbation theory, formulated in a Hilbert space decomposed by means of lattice symmetries, in order to show that the nonuniform shift of the Mott lobe is a manifestation of inter-species entanglement which differs in the lowest excited states to remove and add a particle. Our results indicate that inter-species entanglement in mixtures can provide a new perspective in understanding quantum phase transitions. To validate our approach, we compare our results from perturbation theory with quantum Monte Carlo simulations.

4.1 Introduction

In the past decade, quantum phase transitions of Bose-Bose, Bose-Fermi and Fermi-Fermi mixtures in optical lattices have attracted considerable attention both experimentally and theoretically [40, 41, 42, 43, 44, 20, 45, 46, 47, 48, 49, 62, 63, 64, 65, 66, 67, 68, 69, 70, 71, 72]. Nonetheless, the physics of mixtures is still not completely understood. This is because the coupling between the various components introduces extra degrees of freedom which result in a wealth of exotic and novel phases. Indeed, mixtures feature quantum phase transitions otherwise absent in single species systems. Moreover, the inter-species coupling introduces non-trivial correlations between components which may result in significant inter-species entanglement. Inter-species entanglement can offer a different perspective in understanding quantum phase transitions in multicomponent systems. Hence, by applying concepts from quantum computation to many-body physics [73, 74, 75, 76, 77], one can gain further insight into the physics of mixtures.

Recent theoretical and experimental results report on the modification of the Mott lobe and, in general, of the Mott-insulator to superfluid transition [19, 18, 78] in the presence of a second component [2, 50, 79, 80, 81, 62, 63, 69]. In particular, it has been theoretically shown and experimentally observed that the influence of a second bosonic or fermionic species on the insulating phases of the other bosonic component can be controlled by the strength of the inter-species coupling and by the density of the second component. Intuitively, the strength of the inter-species coupling can be viewed as an indicator of how entangled the two species are. In particular, in the limit of negligible coupling between the two components, the same physics as for a single component system would be observed and inter-species entanglement would be absent. Thus, naturally, one can expect that the modifications on the Mott insulator lobe in the presence of a second component are a manifestation of inter-species entanglement.

In this chapter, we consider Bose-Bose mixtures trapped in optical lattices. Our main goal is to provide a *qualitative* understanding of how inter-species entanglement relates to the observations made in [2, 50] where the authors report a visible shift of the Mott lobe boundary on the hole-side (i.e. when the superfluid is reached by doping with holes) and an almost negligible shift on the particle-side of the lobe (i.e. when the superfluid is reached by doping with particles).

This chapter is organized as follows. In Section 4.2 we introduce the two-component Bose-Hubbard model. In Section 4.3 we provide intuitive understanding of how inter-species entanglement affects the Mott-insulator to superfluid phase transition in the binary mixture. In Section 4.4 we introduce the theoretical framework on which perturbation theory is based and discuss the symmetries of the system. In Section 4.5 we discuss inter-species entanglement of the two-component Bose-Hubbard model defined in a reduced and decomposed Hilbert space. In Section 4.6 we present numerical results based on perturbative calculation and we compare them with exact quantum Monte Carlo results. Finally, we conclude in Section 4.7.

4.2 The model

We consider a bosonic binary mixture trapped in an optical lattice as described by the two-component Bose-Hubbard model

$$H = \frac{U^{(a)}}{2}\sum_{i=1}^{M} n_i^{(a)}(n_i^{(a)}-1) + \frac{U^{(b)}}{2}\sum_{i=1}^{M} n_i^{(b)}(n_i^{(b)}-1) + U^{(ab)}\sum_{i=1}^{M} n_i^{(a)}n_i^{(b)} \\ -T^{(a)}\sum_{(i,j)} a_i^{+}a_j - T^{(b)}\sum_{(i,j)} b_i^{+}b_j - \mu^{(a)}N^{(a)} - \mu^{(b)}N^{(b)}, \qquad (4.1)$$

where M is the number of lattice sites, a stands for the first species (species-$\mathcal{A}$ or component-$\mathcal{A}$) while b stands for the second species (species-$\mathcal{B}$ or component-$\mathcal{B}$), a_i^{+} (b_i^{+})

and $a_i(b_i)$ are creation and annihilation operators of species-$\mathcal{A}(\mathcal{B})$ at site i, $n_i^{(a)} = a_i^+ a_i$, $n_i^{(b)} = b_i^+ b_i$, are the particle number operators at site i and $N^{(a)} = \sum_i n_i^{(a)}$, $N^{(b)} = \sum_i n_i^{(b)}$. $U^{(a)}$ and $U^{(b)}$ are the onsite intra-species interactions for component-$\mathcal{A}$ and -$\mathcal{B}$ respectively, $U^{(ab)}$ is the inter-species onsite interaction, $T^{(a)}$ and $T^{(b)}$ are the hopping amplitudes, and $\mu^{(a)}$ and $\mu^{(b)}$ are the chemical potentials which set the total number of particles. In the following we consider species-$\mathcal{A}$ to be the majority species, whose Mott lobe boundary is affected by the presence of species-$\mathcal{B}$, the minority component.

4.3 Characterization of the shift of the lobe boundary in terms of mutual information

In this Section we discuss previous observations of a shift of the Mott-insulator (MI) lobe boundary in the presence of a second bosonic minority component, and consider these observations in the context of inter-species entanglement and mutual information of states.

In References [2, 50] it was found that, in the presence of species-$\mathcal{B}$ as a minority component, the boundary of MI lobe of species-$\mathcal{A}$ is affected differently on the hole- and particle-side compared to the MI lobe in the absence of species-$\mathcal{B}$. Fig. 4.1 is borrowed from Reference [2] and shows the nonuniform boundary shift of the first Mott lobe. The diamonds correspond to the boundary of the first Mott lobe in the absence of a second component, while the circles, squares and triangles correspond to the boundary of the first Mott lobe in the presence of a second component with $U^{(ab)} = 10T^{(a)}$, $15T^{(a)}$, $20T^{(a)}$ respectively. Other parameters are set as $U^{(b)} = 10T^{(a)}$, $T^{(a)} = T^{(b)}$. The density of the second component is 0.1. Overall, the shift of the MI lobe is always more prominent on the hole-side of the boundary. The magnitude and the modality of the shift depend on the interplay between kinetic and potential energies, and the density of species-$\mathcal{B}$. For

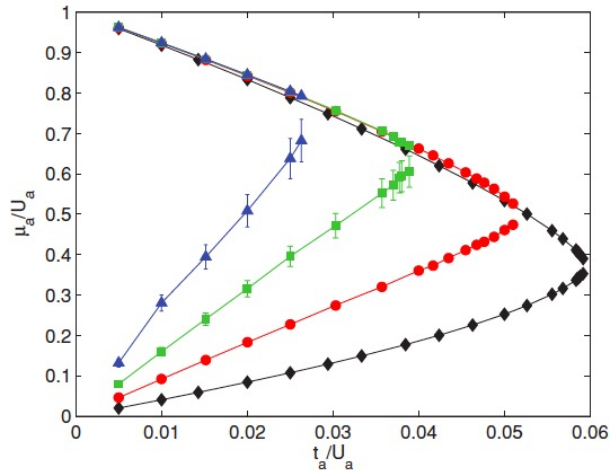

Figure 4.1: This figure, borrowed from Reference [2], shows the nonuniform boundary shift of the first Mott lobe. The diamonds correspond to the boundary of the first Mott lobe in the absence of a second component, while the circles, squares and triangles correspond to the boundary of the first Mott lobe in the presence of a second component with $U^{(ab)} = 10T^{(a)}$, $15T^{(a)}$, $20T^{(a)}$ respectively. Other parameters are set as $U^{(b)} = 10T^{(a)}$, $T^{(a)} = T^{(b)}$. The density of the second component is 0.1. Data are calculated with Monte Carlo simulations.

example, at fixed $U^{(ab)}$ and for a given density of species-$\mathcal{B}$, the first MI lobe of species-$\mathcal{A}$ always possesses a visible shift on the hole-side of the boundary with respect to the lobe in the single-species case, while the shift on the particle-side of the boundary is either absent or considerably less pronounced, depending on the density of species-$\mathcal{B}$ [2, 50]. In particular, the particle-side of the boundary shifts only for sufficiently large fillings of component-$\mathcal{B}$. It is worth noting that the lobe boundaries can either be explored by fixing $U^{(a)}$ while varying $T^{(a)}$ or vice versa. In the former case, the boundary shift on the hole-side is already observed in the limit $T^{(a)}/U^{(a)} \to 0$ and it gets progressively smaller as the hopping is increased and quantum fluctuations become more prominent. On the other hand, when the boundary is explored by fixing $T^{(a)}$ and varying $U^{(a)}$, the boundary shift is inexistent in the limit $T^{(a)}/U^{(a)} \to 0$ for which, the onsite intra-species interaction $U^{(a)}$ becomes the dominant energy scale and the interaction between the two components can be neglected. The shift becomes progressively larger upon increasing $T^{(a)}/U^{(a)}$. In

general, although the modality of the boundary shift depend on the specific choice of model parameters, overall, a larger inter-species interaction leads to a greater shift of the lobe.

In the following, we focus on exploring the lobe boundary by fixing $U^{(a)}$ while varying $T^{(a)}$. As discussed above, the shift is already visible in the limit $T^{(a)}/U^{(a)} \to 0$ which implies that one can perform a perturbative study of the phase boundary shift by treating the hopping term as perturbation, treating the onsite interactions as unperturbed Hamiltonian, and treating $T^{(a)}/U^{(a)}$ (setting $T^{(b)} = T^{(a)}$) as perturbation parameter. This perturbation method is based on a degenerate perturbation theory since the unperturbed Hamiltonian has degenerate ground states. And the corresponding perturbation theory has been systematically studied in Reference [21] where issues concerning the degeneracy in perturbation theory are analyzed and solved.

In order to gain a qualitative understanding of the role played by species-$\mathcal{B}$, let's first consider the limit $T^{(a)} \to 0$, $T^{(b)} \to 0$ and consider $N^{(b)} = 1$. It should be noted that we here study species-$\mathcal{A}$ and the single species-$\mathcal{B}$ boson within the two-component Bose-Hubbard model, though the behavior of a single boson does not display Bose-Einstein statistics. In this way, we emphasizes that $N^{(b)} = 1$ is a special case of Bose-Bose mixture and the kinetic energy together with the potential energy of the species-$\mathcal{B}$ boson in the Bose-Hubbard model (rather than the Fermi-Hubbard model [82] where a single fermion has different Hilbert space dimension and thus different hopping matrix due to half-integer spin) capture the physics consistent with cases of $N^{(b)} > 1$. Throughout this chapter, we assume all onsite interactions to be repulsive and inter-species interactions are chosen to avoid phase segregation [20]. We consider a square lattice with periodic boundary conditions.

Let us start by reviewing the determination of the boundaries of the MI lobe away from the tip. In the grand canonical ensemble, the MI lobe of species-$\mathcal{A}$ is a result of the energy

gap between the ground state and the elementary excited state which corresponds to adding a hole or a particle [19] of species-$\mathcal{A}$ to the mixture. Denoting the ground state energy by E and the lowest excited energy to add a hole (particle) by E_h (E_p), one has $E_h > E$ ($E_p > E$) inside the MI lobe, and $E_h = E$ ($E_p = E$) at the hole-side (particle-side) boundary. Hence, one can find the position of the boundary by setting the lowest excited energy equal to the ground-state energy. It is therefore easy to understand the boundary shift in terms of a change of the energy gap induced by the presence of the second component. For a given chemical potential inside the MI lobe, the hole-side (particle-side) gap is given by the distance between the chosen chemical potential and the hole (particle) boundary as shown in Fig. 4.2(a). Without the species-$\mathcal{B}$ boson and in the zero hopping limit, we have

$$E = -\mu^{(a)} M, \quad E_h = -\mu^{(a)}(M-1), \quad E_p = U^{(a)} - \mu^{(a)}(M+1)$$

and the gaps $E_h - E = \mu^{(a)}$, $E_p - E = U^{(a)} - \mu^{(a)}$. In the presence of the species-$\mathcal{B}$ boson, the repulsive inter-species interaction "helps" removing a species-$\mathcal{A}$ boson from the lattice in order to create a hole, so that the presence of species-$\mathcal{B}$ lowers the excitation energy needed to add a hole, thus shrinking the lobe on the hole-side as shown in Fig. 4.2(a). This can be easily understood in the limit of zero hopping where, in the presence of a hole of species-$\mathcal{A}$, particle-$\mathcal{B}$ occupies the same site as the hole-$\mathcal{A}$ in order to minimize the inter-species interaction (see Fig. 4.2(b)). On the other hand, the repulsive interaction between the two species has no influence on the energy needed to add a particle since, in order to minimize the inter-species interaction, the added species-$\mathcal{A}$ boson will not occupy the same site as the species-$\mathcal{B}$ boson as shown in Fig. 4.2(c). Hence, the excitation energy to add a particle remains unchanged and the lobe shift is absent. Correspondingly, in the

presence of particle-$\mathcal{B}$ we have

$$E = U^{(ab)} - \mu^{(a)} M - \mu^{(b)}, \quad E_h = -\mu^{(a)}(M-1) - \mu^{(b)}, \quad E_p = U^{(a)} + U^{(ab)} - \mu^{(a)}(M+1) - \mu^{(b)}$$

and the gaps $E_h - E = \mu^{(a)} - U^{(ab)}$, $E_p - E = U^{(a)} - \mu^{(a)}$. Obviously, the energy gap to add a hole is lowered by $U^{(ab)}$ while the energy gap to add a particle stays the same.

Let us now turn to the discussion of how inter-species entanglement is related to the non-uniform MI lobe shift we just described. Indeed, as will be shown in the following, in the intuitive picture discussed above, the species-$\mathcal{B}$ boson impacts on the excitation of species-$\mathcal{A}$ in an "entangled" way. In other words, the repulsion between the two species is reflected in the quantum correlation in excited states of the Bose-Bose mixture. In the system considered, the inter-species entanglement arises from a tensor-product form $\mathcal{H}^{(a)} \otimes \mathcal{H}^{(b)}$ of the Hilbert space of the system, where $\mathcal{H}^{(a)}$ and $\mathcal{H}^{(b)}$ are the Fock spaces corresponding to each single-species system. In the limit of zero hopping [1], the ground state of the MI and the first excited states to add a hole or a particle are expanded in terms of Fock states each with equal coefficient (weight). Moreover the Fock states entering the expansion are characterized by similar particle distribution on the lattice [21] as we explain in detail below.

In the Fock states spanning the MI ground state, species-$\mathcal{A}$ bosons are uniformly located in the lattice while the single species-$\mathcal{B}$ boson can be located anywhere (an example of this type of configurations is shown in Fig. 4.2(d)). It is clear that the location of species-$\mathcal{A}$ is *irrelevant* to the location of species-$\mathcal{B}$. In terms of *mutual information*, which, in this context, represents the ability of determining e.g. the position of particle-$\mathcal{B}$ from the

[1] Here, we consider the limit of zero hopping $T^{(a)} \to 0$, $T^{(b)} \to 0$ instead of exactly zero hopping $T^{(a)} = T^{(b)} = 0$ in order to exploit the results discussed in [21] which state that, at non-zero hopping, the ground states of the two-component Bose-Hubbard model corresponding to fixed particle numbers are always *unique*. This means that, at finite hopping, the system is described by a pure state rather than a density operator.

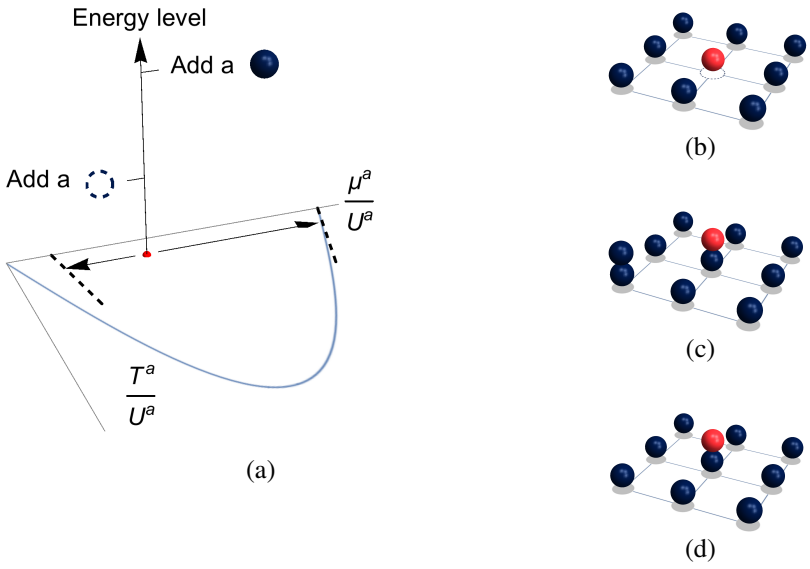

Figure 4.2: a) Sketch of the Mott insulator lobe of the single component (solid blue line). Sketch of the shifted lobe in the presence of a second component (dashed black line). The red spot inside the lobe represent at fixed value of chemical potential with arrows indicating the gap the add a hole or an extra particle. The excited energy corresponding to the addition of a hole (dotted circle) and an extra particle (solid circle) are sketched on the vertical axis. b) Representative Fock state when a hole is added to the Mott insulator. The hole of component-$\mathcal{A}$ and particle-$\mathcal{B}$ occupy the same lattice site in order to minimize the energy. c) Representative Fock state when an extra particle is added to the Mott insulator. The extra particle of component-$\mathcal{A}$ occupies a site different than the one occupied by particle-$\mathcal{B}$. d) Representative Fock state in the Mott insulator of component-$\mathcal{A}$ in the presence of particle-$\mathcal{B}$.

position of particles-$\mathcal{A}$, we can conclude that in the MI ground state there is no mutual information between the two species. For pure states, mutual information can also be seen as a measure of the entanglement [83], hence, we expect the MI ground state to be non-entangled.

In the Fock states spanning the first excited state to add a hole (in the following we refer to it by hole-side excited state), the single species-$\mathcal{B}$ boson has to be located on the same site where the hole-$\mathcal{A}$ is located in order to minimize the inter-species interaction. This is shown in Fig. 4.2(b). In this case the location of boson-$\mathcal{B}$ *uniquely* determines the location

of hole-$\mathcal{A}$. Therefore, we anticipate this state to have maximal mutual information and thus this excited state to be maximally entangled.

In the Fock states spanning the first excited state to add a particle (in the following we refer to it by particle-side excited state), the inter-species interaction is minimized with boson-$\mathcal{B}$ located everywhere in the optical lattice except for the site where the extra particle-$\mathcal{A}$ is located. An example of this type of configuration is shown in Fig. 4.2(c). In this case, the location of particles-$\mathcal{A}$ determines the location of boson-$\mathcal{B}$ only partially. More specifically, the location of particles-$\mathcal{A}$ only specifies the site where boson-$\mathcal{B}$ will *not* be located. Therefore, we anticipate a 'small' amount of mutual information between the two species and this state to be 'slightly' entangled. This statement will be quantified in the following, by calculating entanglement entropy as a measure of the entanglement in the system [83].

The above discussion can be summarized as follows: In the limit of zero hopping, the hole-side boundary has a visible shift corresponding to a maximally entangled hole-side excited state; The particle-side boundary does not shift, corresponding to a weakly-entangled particle-side excited state. Indeed, as we will show below by means of a perturbative calculation, the degree of entanglement between the two components is closely related to the extent of the shift of the lobe. Indeed, these observations suggest that the inter-species entanglement differs in the ground state, particle-side excited state and hole-side excited states. This difference leads to different shifts in the energy gaps to add a hole or a particle, hence resulting in a nonuniform shift of the lobe on the two sides. Therefore, it is expected that inter-species entanglement plays a role in quantum phases transitions of mixtures, specifically, in this case, in the Mott-insulator to superfluid transition at non-fixed number of particles.

Before introducing the framework of the perturbation theory, it is important to note that for systems described by the Bose-Hubbard model in the grand-canonical ensemble, the

first excited states corresponding to adding a hole or a particle are identical to ground states in the canonical ensemble with one less or one extra particle with respect to the ground state of the MI phase. Therefore, it is sufficient to study generic properties of the inter-species entanglement in ground states corresponding to different (fixed) particle numbers. With this in mind, in the following we introduce a framework capable of studying inter-species entanglement in ground states corresponding to fixed particle numbers. First, we reduce the Hilbert space of model 4.1 utilizing symmetries of the Hamiltonian in order to remove irrelevant degrees of freedom and facilitate numerical study. Second, we decompose the Hilbert space in terms of symmetry and degrees of freedom and give a criterion for inter-species entanglement of ground states.

In our framework, we emphasize the structure of the ground state in relation to the decomposition of Hilbert spaces. We will show that this decomposition provides simplification and convenience for the numerical implementation of the perturbation theory. Although in the following we consider a square lattice with periodic boundary conditions, our approach can be applied to any type of finite lattice. Moreover, while we focus on repulsive inter-species interaction, the method holds for attractive interaction as well.

4.4 Symmetries of the ground state

In this Section we discuss the symmetry of the ground state and utilize it in order to reduce the Hilbert space.

Consider the ground state Ψ of the Hamiltonian H given by Eq. 4.1 at fixed particle numbers $N^{(a)}$ and $N^{(b)}$. Ψ lives in the tensor product space $\mathcal{H}^{(a)} \otimes \mathcal{H}^{(b)}$ with a Fock basis $\{|\mathbf{n}\rangle \otimes |\mathbf{m}\rangle\}$. The spaces $\mathcal{H}^{a}$ and $\mathcal{H}^{(b)}$ are finite-dimensional Hilbert spaces of the single-component Bose-Hubbard model at fixed particle numbers $N^{(a)}$ and $N^{(b)}$ respectively. They are spanned by Fock bases $\{|\mathbf{n}\rangle\}$ and $\{|\mathbf{m}\rangle\}$, determined by the lowest band Wannier

functions [19, 18].

The two-component Bose-Hubbard model is defined on a lattice with a finite number of sites. To describe the nearest-neighbor tunneling, the lattice is endowed a graph structure, which is specified by bonds or edges [59], i.e. nearest-neighbor pairs of lattice sites. Lattice symmetries are described by graph automorphisms. A graph automorphism g is a one-to-one mapping on the lattice such that $\{g(i), g(j)\}$ (where i and j are sites) is a bond if and only if $\{i, j\}$ is a bond [59]. Obviously, all graph automorphisms of a finite lattice form a finite group under the function composition $(g \circ g')(i) = g(g'(i))$. We denote this group by G. In a square lattice with periodic boundary condition, G is the group generated by all translations, rotations and reflections which leave the lattice unchanged.

The group G has three unitary representations $\pi^{(ab)}$, $\pi^{(a)}$ and $\pi^{(b)}$ in the Hilbert spaces $\mathcal{H}^{(a)} \otimes \mathcal{H}^{(b)}$, $\mathcal{H}^{(a)}$ and $\mathcal{H}^{(b)}$, respectively [2]. In general, a representation π is defined by mapping any element $g \in G$ into a unitary operator $\pi(g)$ whose action is defined on the relevant Hilbert spaces. The representations are naturally defined in terms of Fock bases. Specifically, given a Fock state $|\mathbf{n}, \mathbf{m}\rangle = |\mathbf{n}\rangle \otimes |\mathbf{m}\rangle = |n_1, n_2, ...n_i, ...\rangle \otimes |m_1, m_2, ...m_i, ...\rangle$ (where n_i and m_i are occupation numbers of species-$\mathcal{A}$ and species-$\mathcal{B}$ bosons on site i) in $\mathcal{H}^{(a)} \otimes \mathcal{H}^{(b)}$, then $\pi^{(ab)}(g)(|\mathbf{n}\rangle \otimes |\mathbf{m}\rangle)$ is also a Fock state corresponding to

$$|n_{g^{-1}(1)}, n_{g^{-1}(2)}, \cdots n_{g^{-1}(i)} \cdots\rangle \otimes |m_{g^{-1}(1)}, m_{g^{-1}(2)}, \cdots m_{g^{-1}(i)} \cdots\rangle ,$$

where the action of g induces a site reshuffling. An example of $\pi^{(ab)}(g)$ on $|\mathbf{n}, \mathbf{m}\rangle$ is illustrated in Fig. 4.3. Here, g represents a 180° clockwise rotation of a 2×2 square lattice. Fig. 4.3(a) displays the initial state $|\mathbf{n}, \mathbf{m}\rangle$, while Fig. 4.3(c) displays the final state $\pi^{(ab)}(g)|\mathbf{n}, \mathbf{m}\rangle$. One can understand the action of $\pi^{(ab)}(g)$ from the intermediate step, Fig. 4.3(b), where, according to the definition of $\pi^{(ab)}(g)$, the positions of bosons are

[2] A unitary representation π of the group G in the space $\mathcal{H}$ is a group homomorphism mapping each g into a unitary operator $\pi(g)$ on $\mathcal{H}$, so that $\pi(g_1)\pi(g_2) = \pi(g_1 \circ g_2)$.

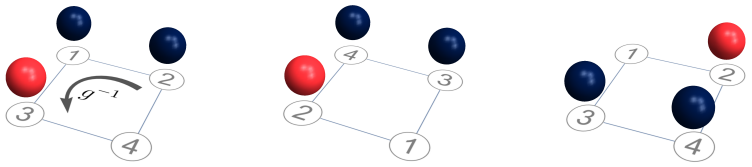

(a) (b) (c)

Figure 4.3: a) and c) Sketch of $|\mathbf{n}, \mathbf{m}\rangle$ and $\pi^{(ab)}(g)|\mathbf{n}, \mathbf{m}\rangle$ on a 2×2 square lattice. Here g represents a $180°$ clockwise rotation. b) Intermediate step where, according to the definition of $\pi^{(ab)}(g)$, the positions of bosons are fixed while g^{-1} operates on the lattice.

fixed while g^{-1} operates on the lattice. In this example g^{-1} is a $180°$ counterclockwise rotation. Hence, the action of $\pi^{(ab)}(g)$ in going directly from Fig. 4.3(a) to Fig. 4.3(c), can be viewed as the operation g on the position of bosons. Similarly, we can define $\pi^{(a)}$ and $\pi^{(b)}$, and, according to their definition, we have $\pi^{(a)}(g) \otimes \pi^{(b)}(g) = \pi^{(ab)}(g)$ for all $g \in G$.

Both, the Hamiltonian H and the ground state $|\Psi\rangle$ are invariant under the action of any graph automorphism g, i.e. they are symmetric under the group G. The invariance of H under the action of G can be easily seen by observing that $[H, \pi^{(ab)}(g)] = 0$ for any $g \in G$. On the other hand, the invariance of $|\Psi\rangle$ under G, i.e. $\pi^{(ab)}(g)|\Psi\rangle = |\Psi\rangle$ for any $g \in G$, can be seen from the following arguments. The ground state energy E is nondegenerate and the expansion coefficients of $|\Psi\rangle$ in the Fock basis are all positive, i.e. $\langle \mathbf{m}, \mathbf{n}|\Psi\rangle > 0$ for all $|\mathbf{n}, \mathbf{m}\rangle$ [21]. Thus, because any $\pi^{(ab)}(g)$ commute with H, due to the nondegeneracy of E, $\pi^{(ab)}(g)|\Psi\rangle = c|\Psi\rangle$, where c is a constant. Here, c must be positive, because the matrix elements of $\pi^{(ab)}(g)$ in the Fock basis are all real and nonnegative, and $\langle \mathbf{m}, \mathbf{n}|\Psi\rangle > 0$. Moreover, c must be 1, since the unitary operator $\pi^{(ab)}(g)$ preserves the norm. So we conclude $\pi^{(ab)}(g)|\Psi\rangle = |\Psi\rangle$.

It is also important to notice that from the definition of $\pi^{(ab)}$ which leaves unchanged the relative position of bosons, any $|\mathbf{n}, \mathbf{m}\rangle$ and $\pi^{(ab)}(g)|\mathbf{n}, \mathbf{m}\rangle$ display the same intra- and inter-species interactions, as shown in the example of Fig. 4.3(a) and 4.3(c). Hence, we say

that $|\mathbf{n},\mathbf{m}\rangle$ and $\pi^{(ab)}(g)|\mathbf{n},\mathbf{m}\rangle$ belong to the same "configuration". In what follows, when we mention "configuration" of Fock states we refer to the following formal definition.

A *configuration* of Fock states in $\mathcal{H}^{(a)}\otimes\mathcal{H}^{(b)}$ is defined as a subset in the Fock basis such that all elements in the subset are obtained by acting on some fixed $|\mathbf{n},\mathbf{m}\rangle$ with $\pi^{(ab)}(g)$, for *all* g in G. In other words, a configuration groups together all Fock states which only differ in the location of individual bosons but with the *same relative* positions of bosons. According to this definition, the Fock basis can be partitioned in terms of distinguishable configurations. These are equivalence classes [58] $[|\mathbf{n},\mathbf{m}\rangle]$ defined by the property that any Fock states $|\mathbf{n}',\mathbf{m}'\rangle$ of the class is related to the representative element $|\mathbf{n},\mathbf{m}\rangle$ by the equivalence relation $|\mathbf{n}',\mathbf{m}'\rangle = \pi^{(ab)}(g)|\mathbf{n},\mathbf{m}\rangle$ for some $g \in G$. Then, the Fock basis is the disjoint union of configurations $\bigcup_k[|\mathbf{n}_k,\mathbf{m}_k\rangle]$, where the subscript k runs through configurations. It is useful to introduce in each class $[|\mathbf{n}_k,\mathbf{m}_k\rangle] = \{|\mathbf{n}_k^\alpha,\mathbf{m}_k^\alpha\rangle, 1 \le \alpha \le n_k]\}$ the superscript α which enumerates the number n_k of Fock states belonging to the same configuration k. In terms of this partition, the Hilbert space $\mathcal{H}^{(a)}\otimes\mathcal{H}^{(b)}$ can be decomposed as a direct sum $\mathcal{H}^{(a)}\otimes\mathcal{H}^{(b)} = \oplus_k\mathcal{H}_k^{(ab)}$, where $\mathcal{H}_k^{(ab)}$ is the subspace spanned by the kth configuration.

Consider two arbitrary Fock states $|\mathbf{n}_k,\mathbf{m}_k\rangle$ and $|\mathbf{n}_k',\mathbf{m}_k'\rangle$ of the same configuration k, for which, of course, $|\mathbf{n}_k',\mathbf{m}_k'\rangle = \pi^{(ab)}(g)|\mathbf{n}_k,\mathbf{m}_k\rangle$ for some g. Based on the definition of $\pi^{(ab)}(g)$ and the symmetry of $|\Psi\rangle$ under the action of $\mathbf{g}$, we have $\langle\mathbf{n}_k',\mathbf{m}_k'|\Psi\rangle = \langle\mathbf{n}_k,\mathbf{m}_k|\pi^{(ab)}(g)^+|\Psi\rangle = \langle\mathbf{n}_k,\mathbf{m}_k|\Psi\rangle$, being $\pi^{(ab)}(g)^+ = \pi^{(ab)}(g)^{-1} = \pi^{(ab)}(g^{-1})$. It follows that the ground state $|\Psi\rangle$ has the same expansion coefficients for all Fock states belonging to the same configuration. As a consequence, the ground state is only expanded on configurations rather than states, namely

$$|\Psi\rangle = \sum_k c_k|\chi_k\rangle\,, \qquad |\chi_k\rangle \equiv \frac{1}{\sqrt{n_k}}\sum_{\alpha=1}^{n_k}|\mathbf{n}_k^\alpha,\mathbf{m}_k^\alpha\rangle\,, \tag{4.2}$$

where the class-dependent $|\chi_k\rangle$ have been defined. Here, each c_k is positive, and each $|\chi_k\rangle$ is normalized and spans an invariant subspace under the action of G, i.e. $\pi^{(ab)}(g)|\chi_k\rangle = |\chi_k\rangle$. We denote this invariant subspace by $\mathfrak{h}_k^{(ab)}$. Since $|\chi_k\rangle$ is expanded by Fock states in the kth configuration, we have $\mathfrak{h}_k^{(ab)} \subset \mathcal{H}_k^{(ab)}$. Most importantly, Eq. 4.2 implies that $|\Psi\rangle$ lives in $\oplus_k \mathfrak{h}_k^{(ab)}$. It is also important to notice that for any state $|\psi\rangle \in \mathcal{H}^{(a)} \otimes \mathcal{H}^{(b)}$, $|\psi\rangle$ is contained in $\oplus_k \mathfrak{h}_k^{(ab)}$ if and only if it is invariant under the action of G or has the G-symmetry (G-symmetry of $|\Psi\rangle$ requires it being expanded equally on Fock states in each configuration). Moreover, since the Hamiltonian H commutes with all $\pi^{(ab)}(g)$, then, for any $|\psi\rangle \in \oplus_k \mathfrak{h}_k^{(ab)}$ and $g \in G$, $\pi^{(ab)}(g)H|\psi\rangle = H\pi^{(ab)}(g)|\psi\rangle = H|\psi\rangle$, which implies that the direct sum $\oplus_k \mathfrak{h}_k^{(ab)}$ is also invariant under the action of H. Therefore, for the purpose of studying the ground state and its energy, one can reduce the two-component Bose-Hubbard model to be defined in $\oplus_k \mathfrak{h}_k^{(ab)}$.

This is one of the central results of this chapter. It demonstrates the property that quantum phase transitions of the two-component Bose-Hubbard model are only associated to the degrees of freedom describing the relative locations of bosons. Moreover, this reduction of the Hilbert space allows to greatly reduce the numerical cost of the perturbative calculation. In particular, the matrix size of the Hamiltonian can be considerably reduced. For example, for a $L \times L$ square lattice with periodic boundary condition, the number of Fock states n_k in each configuration can be as large as $8 \times L^2$. Referring to Fig. 4.4(a), all graph automorphisms can be obtained by doing the following. Consider sites, e.g., 1, 2 and 4, as specifying a coordinate system centered at position of site 1. This coordinate system can be arbitrarily mapped onto another coordinate system originating at any other site of the lattice and such that the three sites 1, 2 and 4 maintain their relative position. This gives a factor of L^2. Next, for a fixed origin of the coordinate system (position of site 1), there exist 8 choices for mapping sites 2 and 4 using rotations and reflections which leave the lattice unchanged (see Figures 4.4(b)-4.4(i)). Therefore, in this example, there

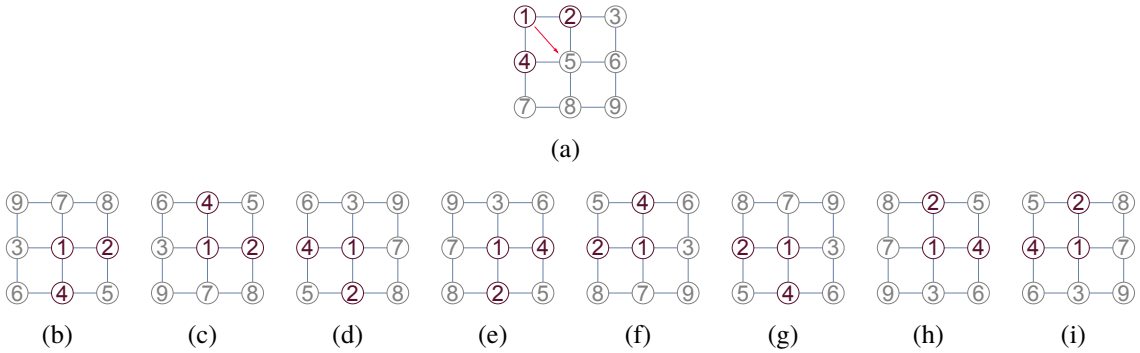

Figure 4.4: a) Sites 1,2 and 4 specify a coordinate system centered at position of site 1. b)-i) Eight graph automorphisms which specify the new positions of sites 2 and 4 while leaving the lattice unchanged (see text).

are $8\times L^2$ graph automorphisms in total. As a consequence, the matrix size can be roughly reduced by a factor $1/(8\times L^2)^2$.

4.5 The criterion of inter-species entanglement

In this Section we investigate how the inter-species entanglement arises in the ground state of a binary interacting mixture. As discussed above, we will work on a reduced Hilbert space.

The inter-species interaction characterized by a strength $U^{(ab)}$ is the source of the inter-species entanglement. This is because in the noninteracting binary mixture the Hamiltonian is simply the sum of two single-species Bose-Hubbard models, and therefore, due to the uniqueness of the ground state one has $|\Psi\rangle = |\Phi^{(a)}\rangle \otimes |\Phi^{(b)}\rangle$ and thus $|\Psi\rangle$ is non-entangled. Here $|\Phi^{(a)}\rangle$ and $|\Phi^{(b)}\rangle$ are unique ground states of the single-component systems defined in $\mathcal{H}^{(a)}$ and $\mathcal{H}^{(b)}$, respectively (the uniqueness of these ground states can be shown by similar arguments used in Reference [21]). Therefore, the inter-species interaction is a *necessary* condition for finite entanglement of binary bosonic mixtures in optical lattices.

To further understand the role played by the inter-species interaction, we start by studying the ground state of noninteracting mixtures and its symmetry properties. By applying similar arguments as in Reference [21], we can conclude that $\langle \mathbf{n}|\Phi^{(a)}\rangle > 0$ and $\langle \mathbf{m}|\Phi^{(b)}\rangle > 0$ for the Fock bases $\{|\mathbf{n}\rangle\}$ and $\{|\mathbf{m}\rangle\}$ defined in $\mathcal{H}^{(a)}$ and $\mathcal{H}^{(b)}$ respectively. Then, the above analysis on representation map $\pi^{(ab)}$ can be applied to both $\pi^{(a)}$ and $\pi^{(b)}$. For this reason, we can define subspaces $\mathfrak{h}_i^{(a)} \subset \mathcal{H}_i^{(a)}$ and $\mathfrak{h}_j^{(b)} \subset \mathcal{H}_j^{(b)}$ corresponding to the ith and the jth configurations of the single-species Fock bases $\{|\mathbf{n}\rangle\}$ and $\{|\mathbf{m}\rangle\}$, in a similar way as we defined $\mathfrak{h}_k^{(ab)} \subset \mathcal{H}_k^{(ab)}$. Likewise, we have

$$|\Phi^{(a)}\rangle \in \oplus_i \mathfrak{h}_i^{(a)} \subset \oplus_i \mathcal{H}_i^{(a)} = \mathcal{H}^{(a)}, \quad \text{and} \quad |\Phi^{(b)}\rangle \in \oplus_j \mathfrak{h}_j^{(b)} \subset \oplus_j \mathcal{H}_j^{(b)} = \mathcal{H}^{(b)} .$$

Based on the symmetries of $|\Phi^{(a)}\rangle$ and $|\Phi^{(b)}\rangle$, it follows that $\pi^{(a)}(g) \otimes \pi^{(b)}(g')|\Psi\rangle = \pi^{(a)}(g)|\Phi^{(a)}\rangle \otimes \pi^{(b)}(g')|\Phi^{(b)}\rangle = |\Phi^{(a)}\rangle \otimes |\Phi^{(b)}\rangle = |\Psi\rangle$ for any two graph automorphisms g and g'. Considering that $\pi^{(a)} \otimes \pi^{(b)} : (g, g') \mapsto \pi^{(a)}(g) \otimes \pi^{(b)}(g')$ defines a unitary representation of the direct product group $G * G$ in which the number of group elements is squared, we conclude that $|\Psi\rangle$ is invariant under the action of the direct product of the graph automorphism group. In other words, in the absence of inter-species interaction, the system is invariant when two arbitrary graph automorphisms g and g' operate on the two species independently. On the other hand, for $U^{(ab)} \neq 0$, the system is generally *not* invariant under the action of g and g' independently, unless $g = g'$. This implies that the absence of the inter-species interaction 'loosens' the restrictions on the operations which leave the ground state invariant making the system more symmetric. Indeed, the lack of $G * G$ symmetry will be shown to serve as a criterion for the appearance of entanglement in the ground state $|\Psi\rangle$ once the inter-species interaction is turned on.

We now turn on the inter-species interaction and look at the decomposition of the Hilbert spaces in order to gain further insight in the structure of $|\Psi\rangle$. First, we con-

sider the ith configuration of species-$\mathcal{A}$ and the jth configuration of species-$\mathcal{B}$, i.e. $\{|\mathbf{n}_i^1\rangle, |\mathbf{n}_i^2\rangle, ..., |\mathbf{n}_i^{r_i}\rangle\}$ and $\{|\mathbf{m}_j^1\rangle, |\mathbf{m}_j^2\rangle, ..., |\mathbf{m}_j^{s_j}\rangle\}$ with labels interpreted as for the configuration of the mixture, that is, subscripts refer to configurations while superscripts refer to Fock states within a configuration. We define the product-configuration (i, j) as

$$\{|\mathbf{n}_i^1\rangle|\mathbf{m}_j^1\rangle, |\mathbf{n}_i^1\rangle|\mathbf{m}_j^2\rangle, ..., |\mathbf{n}_i^2\rangle|\mathbf{m}_j^1\rangle, |\mathbf{n}_i^2\rangle|\mathbf{m}_j^2\rangle, ..., |\mathbf{n}_i^{r_i}\rangle|\mathbf{m}_j^{s_j}\rangle\},$$

i.e. the collection of all possible products of Fock states from the ith configuration of species-$\mathcal{A}$ and the jth configuration of species-$\mathcal{B}$. In terms of the definition of configurations for single species, one can alternatively define the product-configuration by fixing some Fock state $|\mathbf{n}, \mathbf{m}\rangle = |\mathbf{n}\rangle \otimes |\mathbf{m}\rangle$ and collecting all $\pi^{(a)}(g_1)|\mathbf{n}\rangle \otimes \pi^{(b)}(g_2)|\mathbf{m}\rangle$ running through all $g_1, g_2 \in G$.

Let us consider an arbitrary product-configuration (i, j) and fix a Fock state $|\mathbf{n}, \mathbf{m}\rangle$ in this configuration with $|\mathbf{n}\rangle$ belonging to the ith configuration of species-$\mathcal{A}$ and $|\mathbf{m}\rangle$ belonging to the jth configuration of species-$\mathcal{B}$. If we choose two arbitrary g_1 and g_2 from G, and collect all $\pi^{(a)}(g)\pi^{(a)}(g_1)|\mathbf{n}\rangle \otimes \pi^{(b)}(g)\pi^{(b)}(g_2)|\mathbf{m}\rangle = \pi^{(a)}(gg_1)|\mathbf{n}\rangle \otimes \pi^{(b)}(gg_2)|\mathbf{m}\rangle$ with g running through all $g \in G$, we obtain a configuration of the mixture which is surely included in the product-configuration (i, j). Then, we repeat this process by choosing two other g_3 and g_4 from G with $\pi^{(a)}(g_3)|\mathbf{n}\rangle \otimes \pi^{(b)}(g_4)|\mathbf{m}\rangle$ not included in the previously obtained configuration, and we obtain another configuration of the mixture which is disjoint from the former one. Thus, inductively, we can partition the product-configuration (i, j) in terms of configurations of the mixture (below we refer to configurations of the mixture simply as 'configurations', as defined in Section 4.4, as opposed to product-configurations defined above). In other words, the product-configuration (i, j) is the union of the configurations included in it. This is displayed in Fig. 4.5, where the configurations of species-$\mathcal{A}$ and species-$\mathcal{B}$, shown in 4.5(a) and 4.5(b) respectively, determine a product-configuration

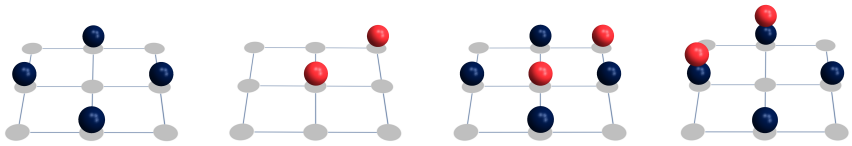

(a) (b) (c) (d)

Figure 4.5: a) and b) Example of a configuration of species-$\mathcal{A}$ and of species-$\mathcal{B}$, respectively. c) and d) Configurations of the mixture contained in the product-configuration resulting from single species configurations sketched in a) and b).

which consists of the union of the two configurations displayed in 4.5(c) and 4.5(d) (note that we only display a single Fock state per configuration).

Obviously, each configuration has to be included in some product-configuration because both configurations and product-configurations partition the same Fock basis. Let us denote the kth configuration included in the product-configuration (i, j) by $k \in (i, j)$. Then, according to the definition of $\mathcal{H}_i^{(a)}$, $\mathcal{H}_j^{(b)}$ and $\mathcal{H}_k^{(ab)}$, we have

$$\mathcal{H}_i^{(a)} \otimes \mathcal{H}_j^{(b)} = \oplus_{k\in(i,j)} \mathcal{H}_k^{(ab)} \ .$$

Furthermore, since $\mathfrak{h}_i^{(a)}$ and $\mathfrak{h}_j^{(b)}$ are spanned by $|\zeta_i\rangle = (1/\sqrt{r_i}) \sum_{\alpha=1}^{r_i} |\mathbf{n}_i^\alpha\rangle$ and $|\lambda_j\rangle = (1/\sqrt{s_j}) \sum_{\beta=1}^{s_j} |\mathbf{m}_j^\beta\rangle$, respectively, then $\mathfrak{h}_i^{(a)} \otimes \mathfrak{h}_j^{(b)}$ is spanned by

$$|\zeta_i\rangle \otimes |\lambda_j\rangle = \frac{1}{\sqrt{r_i s_j}} \sum_{\alpha=1}^{r_i} \sum_{\beta=1}^{s_j} |\mathbf{n}_i^\alpha\rangle \otimes |\mathbf{m}_j^\beta\rangle$$

i.e. the equally weighted sum of the Fock states contained in the product-configuration (i, j). Moreover, for any $k \in (i, j)$, $|\chi_k\rangle = (1/\sqrt{n_k}) \sum_{\sigma=1}^{n_k} |\mathbf{n}_k^\sigma\rangle \otimes |\mathbf{m}_k^\sigma\rangle$ is also an equally weighted sum of a subset of states in the product-configuration (i, j) which defines the kth configuration. Here, every $|\mathbf{n}_k^\sigma\rangle \otimes |\mathbf{m}_k^\sigma\rangle$ is equal to some $|\mathbf{n}_i^\alpha\rangle \otimes |\mathbf{m}_j^\beta\rangle$ in the product-configuration (to avoid confusion, we use subscript k to indicate configurations of the mixture and subscripts i and j to indicate configurations of species-$\mathcal{A}$ and species-$\mathcal{B}$

respectively). Since product-configuration (i, j) consists of all kth configurations with $k \in (i, j)$, then $|\zeta_i\rangle \otimes |\lambda_j\rangle = (1/\sqrt{r_i s_j}) \sum_{k\in(i,j)} \sqrt{n_k}|\chi_k\rangle$. The latter equality implies $\mathfrak{h}_i^{(a)} \otimes \mathfrak{h}_j^{(b)} \subset \oplus_{k\in(i,j)} \mathfrak{h}_k^{(ab)}$, and thus

$$\oplus_{i,j}(\mathfrak{h}_i^{(a)} \otimes \mathfrak{h}_j^{(b)}) \subset \oplus_k \mathfrak{h}_k^{(ab)} \ .$$

It is easy to show that a state belongs to the subspace

$$\oplus_{i,j} \left(\mathfrak{h}_i^{(a)} \otimes \mathfrak{h}_j^{(b)}\right) = \left(\oplus_i \mathfrak{h}_i^{(a)}\right) \otimes \left(\oplus_j \mathfrak{h}_j^{(b)}\right)$$

if and only if it is invariant under the action of the direct product group $G * G$ (see 4.8.1). This result is an essential property since, by applying the finiteness of the automorphism group, we can show that if the ground state $|\Psi\rangle$ is non-entangled, then $|\Psi\rangle \in \oplus_{i,j}(\mathfrak{h}_i^{(a)} \otimes \mathfrak{h}_j^{(b)})$ as proved in 4.8.2. Consequently, a non-entangled Ψ implies that it is invariant under the action of any direct product of graph automorphisms $(g, g') \in G * G$. Alternatively, breaking the $G * G$ symmetry of Ψ implies onset of entanglement of the mixture in the ground state. It is worth noting that in the case where there is only one boson of the second component, i.e. $N^{(b)} = 1$, the loss of $G * G$ symmetry of Ψ serves as a necessary and sufficient condition for the onset of entanglement. In this case, in fact, the second species has only one configuration. If $|\Psi\rangle$ is symmetric under $G * G$, then $|\Psi\rangle \in (\oplus_i \mathfrak{h}_i^{(a)}) \otimes \mathfrak{h}^{(b)}$. Since $\mathfrak{h}^{(b)}$ is one-dimensional, $|\Psi\rangle$ will always has the form $|\phi^{(a)}\rangle \otimes |\phi^{(b)}\rangle$, where $|\phi^{(b)}\rangle$ spans $\mathfrak{h}^{(b)}$, and as such $|\Psi\rangle$ will be non-entangled.

It would be interesting to investigate if, in the general case of $N^b \neq 1$, $|\Psi\rangle \in \oplus_{i,j}(\mathfrak{h}_i^{(a)} \otimes \mathfrak{h}_j^{(b)})$ also implies that $|\Psi\rangle$ is non-entangled. If this is the case, then, the fact that the ground state belongs to $\oplus_{i,j}(\mathfrak{h}_i^{(a)} \otimes \mathfrak{h}_j^{(b)})$ or, equivalently, as we have just shown, that the ground state lacks $G * G$ symmetry, is a sufficient and necessary condition for the entangling

of $|\Psi\rangle$. On the other hand, if this is *not* the case, then, the entangled ground state $|\Psi\rangle$ belongs to $\oplus_{i,j}(\mathfrak{h}_i^{(a)} \otimes \mathfrak{h}_j^{(b)})$ and possesses $G * G$ symmetry. A finite entanglement implies a non-zero inter-species interaction $U^{(ab)}$ (recall we have shown that non-zero $U^{(ab)}$ is a necessary condition for an entangled ground state $|\Psi\rangle$). As $|U^{(ab)}|$ is increased and provided all other model parameter are kept fixed, the expansion coefficients of $|\Psi\rangle$ inside each product-configuration will eventually no longer be the same since Fock states which minimize the inter-species interaction energy will be favored, i.e. will have a greater weight. Thus, $|\Psi\rangle$ will no longer belong to $\oplus_{i,j}(\mathfrak{h}_i^{(a)} \otimes \mathfrak{h}_j^{(b)})$. The implication of the above argument is that there would be a phase transition between a phase characterized by $G * G$ symmetry and non-zero $U^{(ab)}$ and a phase with *broken* $G * G$ symmetry. We are not attempting to answer this question here as this goes beyond the scope of the present work but we find this possibility intriguing and therefore worth it to mention.

4.6 Numerical results

In this Section, we discuss our results for the entanglement entropy of the ground state and the excited states corresponding to the hole- and particle-side. The entanglement entropy is the standard measure of bipartite entanglement for pure states. It is defined as the von Neumann entropy $\mathbf{S}$ of the reduced density operator $\rho^{(a)} = \mathrm{Tr}^{(b)}[\rho]$, or $\rho^{(b)} = \mathrm{Tr}^{(a)}[\rho]$ where $\rho = |\Psi\rangle\langle\Psi|$ [84]. In the following, we use the notation $\mathbf{e}(\rho) = \mathbf{S}(\rho^{(a)}) = \mathbf{S}(\rho^{(b)})$.

Our results are based on perturbation theory carried out on a 10×10 square lattice with periodic boundary conditions. We have checked finite size effects for systems of linear size $L = 6, 7, 8, 9, 10$ and found no sizable discrepancy on the lobe boundaries. The perturbative calculation treats the hopping term in Eq. 4.1 (or the W term in Eq. 3.3) as the perturbation. We calculated the second order perturbed energy and the first order perturbed ground state based on the degenerate perturbation theory developed in Chapter 3, taking

advantage of the symmetry properties of the ground state as discussed in Section 4.4. In the following, we derive the expressions of the perturbed energy and ground state which are adopted in our numerical computation.

4.6.1 Degenerate perturbation theory

We first rewrite the Hamiltonian Eq. 4.1 with fixed filling factor as

$$H = U\left[\frac{u^{(a)}}{2}\sum_{i=1}^{M} n_i^{(a)}(n_i^{(a)}-1) + \frac{u^{(b)}}{2}\sum_{i=1}^{M} n_i^{(b)}(n_i^{(b)}-1) + \frac{U^{(ab)}}{U}\sum_{i=1}^{M} n_i^{(a)} n_i^{(b)}\right] + T\left[-t^{(a)}\sum_{(i,j)} a_i^{+}\, a_j - t^{(b)}\sum_{(i,j)} b_i^{+}\, b_j\right],$$

where $Uu^{(a)} = U^{(a)}$, $Uu^{(b)} = U^{(b)}$, $Tt^{(a)} = T^{(a)}$ and $Tt^{(b)} = T^{(b)}$. The unperturbed Hamiltonian is

$$H_0 = U\left[\frac{u^{(a)}}{2}\sum_{i=1}^{M} n_i^{(a)}(n_i^{(a)}-1) + \frac{u^{(b)}}{2}\sum_{i=1}^{M} n_i^{(b)}(n_i^{(b)}-1) + \frac{U^{(ab)}}{U}\sum_{i=1}^{M} n_i^{(a)} n_i^{(b)}\right],$$

and the perturbation is

$$\frac{T}{U}W = \frac{T}{U}\left[-t^{(a)}\sum_{(i,j)} a_i^{+}\, a_j - t^{(b)}\sum_{(i,j)} b_i^{+}\, b_j\right]$$

with the perturbation parameter $\epsilon = T/U$.

Since $[H, \pi^{(ab)}(g)] = 0$, $[H_0, \pi^{(ab)}(g)] = 0$, and the ground state $|\Psi\rangle$ of H is invariant under the action of $\pi^{(ab)}(g)$ for any $g \in G$, the perturbative approximation of $|\Psi\rangle$ and of its energy E can be defined in the G-symmetry subspace $\oplus_k \mathfrak{h}_k^{(ab)}$ with the basis $\{|\chi_k\rangle\}$ (as introduced in Section 4.4). We denote the lowest energy of H_0 by E_0, and the energy of $|\chi_k\rangle$, an eigenvector of H_0 by definition, by $E_0(k)$.

According to the standard perturbation theory, the second order perturbed energy $E_0 + \epsilon E_1 + \epsilon^2 E_2$ and the first order perturbed ground state $|\psi^0\rangle + \epsilon\,|\psi^1\rangle$ are calculated from equations

$$H_0\,|\psi^0\rangle = E_0\,|\psi^0\rangle, \tag{4.3}$$

$$H_0\,|\psi^1\rangle + W\,|\psi^0\rangle = E_0\,|\psi^1\rangle + E_1\,|\psi^0\rangle \tag{4.4}$$

and

$$H_0\,|\psi^2\rangle + W\,|\psi^1\rangle = E_0\,|\psi^2\rangle + E_1\,|\psi^1\rangle + E_2\,|\psi^0\rangle\,. \tag{4.5}$$

Multiplying Eq. 4.4 and 4.5 by $\langle\psi^0|$ and $\langle\chi_k|$, we can directly derive

$$\langle\chi_k|W|\psi^0\rangle = \sum_{E_0(k')=E_0} \langle\chi_k|W|\chi_{k'}\rangle\langle\chi_{k'}|\psi^0\rangle = E_1\,\langle\chi_k|\psi^0\rangle \tag{4.6}$$

for $E_0(k) = E_0$,

$$E_1 = \langle\psi^0|W|\psi^0\rangle, \tag{4.7}$$

$$\langle\chi_k|\psi^1\rangle = \frac{\langle\chi_k|W|\psi^0\rangle}{E_0 - E_0(k)} \tag{4.8}$$

for $E_0(k) > E_0$, and

$$E_2 = \langle\psi^0|W|\psi^1\rangle\,. \tag{4.9}$$

Here Eq. 4.6 can be viewed as a matrix eigenvalue equation in which matrix $\langle\chi_k|W|\chi_{k'}\rangle$ represents the operator W projected into the subspace spanned by $|\chi_k\rangle$'s with $E_0(k) = E_0$. In the following, we denote the projected W by $\bar{W}$. Since E is always nondegenerate (see Chapter 3), according to the discussion in Section 3.6 and 4.4, in solving Eq. 4.6 with $N^{(b)} = 1$, we encounter two possibilities: (1) $N^{(a)} = M + 1$, E_0 is degenerate, and the spectra of $\bar{W}$ split all degeneracy of E_0; (2) $N^{(a)} = M - 1$, E_1 is nondegenerate. In case (1), $|\psi^0\rangle$ is the eigenvector of $\bar{W}$ corresponding to the lowest eigenvalue E_1. Hence,

$|\psi^0\rangle$ can be obtained by directly solving Eq. 4.6. In this case, we denote an arbitrary eigenvector of $\bar{W}$ with eigenvalue $E_1(l)$ by $|\phi_l\rangle$. In case (2), $|\psi^0\rangle = |\chi_k\rangle$ with $|\chi_k\rangle$ being the only eigenvector of H_0 corresponding to E_0, and we simply use the nondegenerate perturbation theory. In the following, we derive expressions of E_1, E_2 and $|\psi^1\rangle$ for case (1). Corresponding expressions for case (2) will be similar.

Taking advantage of the expression

$$|\psi^1\rangle = \sum_{E_0(k)>E_0} |\chi_k\rangle\langle\chi_k|\psi^1\rangle + \sum_{E_0(k)=E_0} |\chi_k\rangle\langle\chi_k|\psi^1\rangle,$$

we have

$$E_2 = \sum_{E_0(k)>E_0} \langle\psi^0|W|\chi_k\rangle\langle\chi_k|\psi^1\rangle + \sum_{E_0(k)=E_0} \langle\psi^0|W|\chi_k\rangle\langle\chi_k|\psi^1\rangle$$

where the second term in the right hand side is, according to Eq. 4.6, equal to $E_1\langle\psi^0|\psi^1\rangle$. Furthermore, since $|\Psi\rangle$ is normalized and has positive expansion coefficients in the basis $\{\chi_k\}$, we can derive that $\langle\psi^0|\psi^1\rangle = 0$. Hence, we have

$$E_2 = \sum_{E_0(k)>E_0} \langle\psi^0|W|\chi_k\rangle\langle\chi_k|\psi^1\rangle = \sum_{E_0(k)>E_0} \frac{\langle\psi^0|W|\chi_k\rangle\langle\chi_k|W|\psi^0\rangle}{E_0 - E_0(k)}, \tag{4.10}$$

which is the final expression used in our computation. Now, we derive $\langle\chi_k|\psi^1\rangle$ for $E_0(k) = E_0$, which, together with Eq. 4.8, gives the expression of $|\psi^1\rangle$ used in our computation.First, we multiply Eq. 4.5 by $\langle\phi_l|$, and get

$$\sum_{E_0(k)=E_0} \langle\phi_l|W|\chi_k\rangle\langle\chi_k|\psi^1\rangle + \sum_{E_0(k)>E_0} \langle\phi_l|W|\chi_k\rangle\langle\chi_k|\psi^1\rangle = E_1\langle\phi_l|\psi^1\rangle.$$

Because $|\phi_l\rangle$ is an eigenvector of $\bar{W}$ with eigenvalue $E_1(l)$, we have

$$E_1(l)\,\langle\phi_l|\psi^1\rangle + \sum_{E_0(k)>E_0} \langle\phi_l|W|\chi_k\rangle\,\langle\chi_k|\psi^1\rangle = E_1\,\langle\phi_l|\psi^1\rangle\,.$$

Then, we can derive

$$\langle\phi_l|\psi^1\rangle = \sum_{E_0(k)>E_0} \frac{\langle\phi_l|W|\chi_k\rangle\,\langle\chi_k|\psi^1\rangle}{E_1 - E_1(l)} = \sum_{E_0(k)>E_0} \frac{\langle\phi_l|W|\chi_k\rangle\,\langle\chi_k|W|\psi^0\rangle}{(E_1 - E_1(l))(E_0 - E_0(k))}.$$

Finally, we have

$$\begin{aligned}\langle\chi_k|\psi^1\rangle &= \sum_{\phi_l\neq\psi^0} \sum_{E_0(k')>E_0} \langle\chi_k|\phi_l\rangle\,\frac{\langle\phi_l|W|\chi_{k'}\rangle\,\langle\chi_{k'}|\psi^1\rangle}{E_1 - E_1(l)} \\ &= \sum_{\phi_l\neq\psi^0} \sum_{E_0(k')>E_0} \langle\chi_k|\phi_l\rangle\,\frac{\langle\phi_l|W|\chi_{k'}\rangle\,\langle\chi_{k'}|W|\psi^0\rangle}{(E_1 - E_1(l))(E_0 - E_0(k'))}. \quad (4.11)\end{aligned}$$

for $E_0(k) = E_0$.

Note that, in case (2), Eq. 4.8 and 4.10 can be directly applied while Eq. 4.11 is not needed, since E_0 is nondegenerate, $|\chi_k\rangle = |\psi^0\rangle$ and $\langle\chi_k|\psi^1\rangle = 0$ for $E_0(k) = E_0$.

4.6.2 Results

The results presented refer to $T^{(a)} = T^{(b)}$, $U^{(ab)} = 0.1U^{(a)} = 0.1U^{(b)}$, and $N^{(b)} = 1$. The validity of the perturbative calculation can be inferred by a comparison with quantum Monte Carlo (QMC) results by the two-worm algorithm [85] of the first MI lobe of component-$\mathcal{A}$. Fig. 4.6(a) shows the lobe boundaries as computed with QMC (blue squares) and by means of perturbation theory (red triangles). For comparison, we also plot the lobe boundaries of the single species Bose-Hubbard model (black circles) as computed with QMC. The QMC simulation is carried out on a 10×10 square lattice with

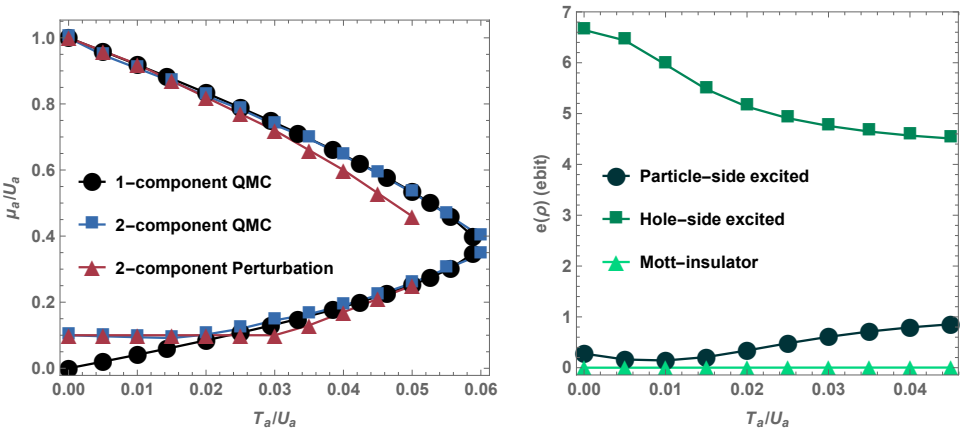

(a) (b)

Figure 4.6: a) lobe boundaries of component-$\mathcal{A}$ in the presence of a single particle-$\mathcal{B}$ as computed with quantum Monte Carlo (blue squares) and by means of perturbation theory (red triangles). For comparison, we also plot the lobe boundaries of the single species Bose-Hubbard model (black circles) as computed with quantum Monte Carlo. b) entanglement entropies of the ground state (triangle), hole-side excited state (square) and particle-side excited state (circle) calculated using perturbation theory.

periodic boundary condition. To produce the QMC results of the first MI lobe, we fix $T^{(a)}/U^{(a)}$ and scan over $\mu^{(a)}/U^{(a)}$. Then, the boundary of the first MI lobe is determined by the value of $\mu^{(a)}/U^{(a)}$ at which the integer filling factor disappears. All simulations ran till error bars were smaller than 1%.

Overall, we see that the particle-side of the lobe (upper boundary) in the presence of a single particle-$\mathcal{B}$ is basically unaffected and lies on top of the boundary for the single-species case. On the other hand, at low hopping, the hole-side of the lobe (lower boundary) is prominently different from the single-species lobe boundary. This difference is more pronounced for smaller hopping, where quantum fluctuations are less important. As the ratio $T^{(a)}/U^{(a)}$ reaches a value of 0.03, we start seeing discrepancy between the perturbative and QMC calculations.

Fig. 4.6(b) shows the entanglement entropies of the ground state (triangle), hole-side excited state (square) and particle-side excited state (circle) calculated using perturbation

theory. We find that the entanglement entropy of the hole-side excited state is much larger than the entanglement entropy of the particle-side excited state. This observation supports our intuition that the shift of the lobe boundary is closely related to the inter-species entanglement, with a larger shift on the hole-side of the boundary being accompanied by a larger inter-species entanglement compared to the particle-side of the boundary. As the hopping is increased we observe a decrease in the entanglement entropy of the hole-side excited state. This is due to the proliferation of quantum fluctuations which results in a finite contribution of Fock states with particle-hole excitations to the hole-excited state. As a consequence, a decrease in mutual information is observed as more sites corresponding to holes of component-$\mathcal{A}$ are available to be occupied by particle-$\mathcal{B}$ in each Fock state, with maximal mutual information occurring in the limit of zero hopping (and a single hole) as discussed in Section 4.3. The entanglement entropy of the particle-excited state, instead, shows a minimum as the hopping amplitude is increased. This could be explained by a two-fold effect of quantum fluctuations. On the one hand, the finite contribution of Fock states with particle-hole excitations tends to increase the mutual information due to the presence of holes, absent in the zero hopping limit. On the other hand, an initial proliferation of these states with very low weight might result in a decrease of entanglement entropy due to non-linear nature of the latter. This topic is under investigation at the moment [57]. Lastly, Fig. 4.6(b) shows that the entanglement entropy of the ground state does not change significantly as $T^{(a)}/U^{(a)}$ is increased and it remains basically the same as its value at zero hopping, i.e. $\mathbf{e}(\rho) = 0$, corresponding to absence of inter-species entanglement.

4.7 Conclusions

In summary, we have studied the inter-species entanglement of bosonic mixtures trapped in optical lattices within a perturbative approach. Motivated by the observation that, in

the presence of a second component, the Mott-insulator lobe shifts *differently* on the hole- and particle-side with respect to the Mott lobe of the single species system, we have investigated how this effect is related to the inter-species entanglement. This relationship indicates that inter-species entanglement plays an important role in the characterization of the quantum-phase transitions of mixtures, specifically in the Mott-insulator to superfluid transition.

Our perturbative calculation is formulated in a Hilbert space decomposed by means of lattice symmetries (graph automorphisms). Within this decomposition, we have shown that if the ground state is *not* invariant under the independent action of symmetry operations on the two species, then the ground state must be entangled. The decomposition of the Hilbert space also results in a drastic reduction of the dimension of the Hilbert space *relevant* to the calculations of interest and hence a drastic reduction of the numerical cost of these calculations. We have calculated the Mott-lobe boundaries in the presence of a single particle of the second component and shown that, in the limit of small hopping, the hole-side of the boundary is dramatically affected by the presence of this single particle. We have compared our results with quantum Monte Carlo simulations by the two-worm algorithm. We have then quantified the entanglement in the Mott insulator ground state and the excited states corresponding to the hole- and particle-side by calculating the entanglement entropy (von Neumann entropy) as the standard measure of bipartite entanglement. We have found that the entanglement entropy of the hole-side excited state is much larger than the entanglement entropy of the particle-side excited state. This means that the shift of the lobe boundary is closely related to the inter-species entanglement with a larger shift on the hole-side of the boundary being accompanied by a larger inter-species entanglement compared to the particle-side of the boundary.

A natural extension of the results presented in this chapter is the study of the "structural" nature of the entanglement as resulting from the ground state $|\Psi\rangle$ being written in terms of a

decomposed Hilbert space [22]. Furthermore, this study can give us a better understanding of the dependence of entanglement entropy on the model parameters and better clarify the observations of Fig. 4.6(b). Finally, we will study inter-species entanglement for Bose-Bose, Bose-Fermi, and Fermi-Fermi mixtures.

4.8 Proofs

4.8.1 A state belongs to $\oplus_{i,j}\left(\mathfrak{h}_i^{(a)} \otimes \mathfrak{h}_j^{(b)}\right)$ if and only if it is invariant under the action of $G * G$

Assume $\pi^{(a)}(g_1) \otimes \pi^{(b)}(g_2)|\psi\rangle = |\psi\rangle$ for any $g_1, g_2 \in G$. Then for two arbitrary $|\mathbf{n}, \mathbf{m}\rangle$ and $|\mathbf{n}', \mathbf{m}'\rangle$ in the product-configuration (i, j) with $|\mathbf{n}', \mathbf{m}'\rangle = \pi^{(a)}(g_1)|\mathbf{n}\rangle \otimes \pi^{(b)}(g_2)|\mathbf{m}\rangle$, one has

$$\begin{aligned}\langle \mathbf{n}', \mathbf{m}'|\psi\rangle &= \left(\langle \mathbf{n}|\pi^{(a)}(g_1)^{+} \otimes \langle \mathbf{m}|\pi^{(b)}(g_2)^{+}\right)|\psi\rangle \\ &= \langle \mathbf{n}, \mathbf{m}|(\pi^{(a)}(g_1)^{+} \otimes \pi^{(b)}(g_2)^{+})|\psi\rangle = \langle \mathbf{n}, \mathbf{m}|\psi\rangle \ .\end{aligned}$$

Therefore, $|\psi\rangle$ expands equally inside any product-configuration. By applying the trick used in Eq. 4.2, we conclude $|\psi\rangle \in \oplus_{i,j}(\mathfrak{h}_i^{(a)} \otimes \mathfrak{h}_j^{(b)})$. The reverse case is easily proved in two steps. First, we show that $\mathfrak{h}_i^{(a)}$ and $\mathfrak{h}_j^{(b)}$ are invariant under the action of G using similar arguments as in proving $\mathfrak{h}_k^{(ab)}$ is invariant under the action of G. Then, we show that $\mathfrak{h}_i^{(a)} \otimes \mathfrak{h}_j^{(b)}$ is invariant under the action of $G * G$ using the definition of the representation $\pi^{(a)} \otimes \pi^{(b)}$. Thus, $\oplus_{i,j}(\mathfrak{h}_i^{(a)} \otimes \mathfrak{h}_j^{(b)})$ is automatically invariant under the action of $G * G$.

4.8.2 Non-entangled $|\Psi\rangle$ belongs to $\oplus_{i,j}(\mathfrak{h}_i^{(a)} \otimes \mathfrak{h}_j^{(b)})$

In this section we want to show that a non-entangled $|\Psi\rangle$ belongs to $\oplus_{i,j}(\mathfrak{h}_i^{(a)} \otimes \mathfrak{h}_j^{(b)})$. For this purpose, it is sufficient to show that, given $|\mathbf{n}'', \mathbf{m}''\rangle = \pi^{(a)}(g)|\mathbf{n}\rangle \otimes \pi^{(b)}(g')|\mathbf{m}\rangle$ one has,

$$\langle \mathbf{n}'', \mathbf{m}''|\Psi\rangle = \langle \mathbf{n}| \otimes \langle \mathbf{m}|\Big(\pi^{(a)}(g)^+ \otimes \pi^{(b)}(g')^+\Big)|\Psi\rangle = \langle \mathbf{n}, \mathbf{m}|\Psi\rangle$$

for arbitrary $g, g' \in G$ and arbitrary $|\mathbf{n}, \mathbf{m}\rangle = |\mathbf{n}\rangle \otimes |\mathbf{m}\rangle$. Let $|\Psi\rangle = |\phi^{(a)}\rangle \otimes |\phi^{(b)}\rangle$. Since $|\Psi\rangle$ is invariant under the action of G, we have

$$\begin{aligned}\Big(\langle \mathbf{n}|\pi^{(a)}(g)^+ \otimes \langle \mathbf{m}|\pi^{(b)}(g')^+\Big)|\Psi\rangle \\ = \langle \mathbf{n}|\pi^{(a)}(g)^+|\phi^{(a)}\rangle \, \langle \mathbf{m}|\pi^{(b)}(g')^+|\phi^{(b)}\rangle = \langle \mathbf{n}|\phi^{(a)}\rangle \, \langle \mathbf{m}|\phi^{(b)}\rangle \, . \end{aligned} \quad (4.12)$$

Considering that $\langle \mathbf{n}|\phi^{(a)}\rangle \neq 0$ ($|\Psi\rangle$ has positive expansion coefficients), we have

$$\langle \mathbf{m}|\phi^{(b)}\rangle = \frac{\langle \mathbf{n}|\pi^{(a)}(g)^+|\phi^{(a)}\rangle}{\langle \mathbf{n}|\phi^{(a)}\rangle} \langle \mathbf{m}|\pi^{(b)}(g')^+|\phi^{(b)}\rangle \, . \quad (4.13)$$

We can now rewrite Eq. 4.12 by replacing $|\mathbf{m}\rangle$ with $\pi^{(b)}(g)|\mathbf{m}\rangle$, so that equation 4.13 becomes

$$\langle \mathbf{m}|\pi^{(b)}(g)^+|\phi^{(b)}\rangle = \frac{\langle \mathbf{n}|\pi^{(a)}(g)^+|\phi^{(a)}\rangle}{\langle \mathbf{n}|\phi^{(a)}\rangle} \langle \mathbf{m}|(\pi^{(b)}(g)^+)^2|\phi^{(b)}\rangle \, . \quad (4.14)$$

Then, inserting Eq. 4.14 in Eq. 4.13, we have

$$\langle \mathbf{m}|\phi^b\rangle = \left(\frac{\langle \mathbf{n}|\pi^{(a)}(g)^+|\phi^{(a)}\rangle}{\langle \mathbf{n}|\phi^{(a)}\rangle}\right)^2 \langle \mathbf{m}|(\pi^{(b)}(g)^+)^2|\phi^{(b)}\rangle \, . \quad (4.15)$$

We perform $n-1$ iterations of these steps, where n is chosen to be the smallest integer such that $g^n = \mathbf{1}$, and get

$$\langle \mathbf{m}|\phi^{(b)}\rangle = \left(\frac{\langle \mathbf{n}|\pi^{(a)}(g)^+|\phi^{(a)}\rangle}{\langle \mathbf{n}|\phi^{(a)}\rangle}\right)^n \langle \mathbf{m}|(\pi^{(b)}(g)^+)^n|\phi^{(b)}\rangle \tag{4.16}$$

Then, $(\pi^{(b)}(g))^n$ is the identity operator and thus

$$\langle \mathbf{m}|\phi^{(b)}\rangle = \left(\frac{\langle \mathbf{n}|\pi^{(a)}(g)^+|\phi^{(a)}\rangle}{\langle \mathbf{n}|\phi^{(a)}\rangle}\right)^n \langle \mathbf{m}|\phi^{(b)}\rangle \ . \tag{4.17}$$

Since $\langle \mathbf{m}|\phi^{(b)}\rangle \neq 0$ ($|\Psi\rangle$ has positive expansion coefficients), Eq. 4.17 implies $|\langle \mathbf{n}|\pi^{(a)}(g)^+|\phi^{(a)}\rangle| = |\langle \mathbf{n}|\phi^{(a)}\rangle|$. In a similar way, we can show $|\langle \mathbf{m}|\pi^{(b)}(g')^+|\phi^{(b)}\rangle| = |\langle \mathbf{m}|\phi^{(b)}\rangle|$.

Finally, since $\langle \mathbf{n}|\pi^{(a)}(g)^+|\phi^{(a)}\rangle\langle \mathbf{m}|\pi^{(b)}(g')^+|\phi^{(b)}\rangle > 0$ and $\langle \mathbf{n}|\phi^{(a)}\rangle\langle \mathbf{m}|\phi^{(b)}\rangle > 0$, we have
$\langle \mathbf{n}|\pi^{(a)}(g)^+|\phi^{(a)}\rangle\langle \mathbf{m}|\pi^{(b)}(g')^+|\phi^{(b)}\rangle = \langle \mathbf{n}|\phi^{(a)}\rangle\langle \mathbf{m}|\phi^{(b)}\rangle$ or

$$\langle \mathbf{n}'', \mathbf{m}''|\Psi\rangle = \langle \mathbf{n}, \mathbf{m}|\Psi\rangle \ . \tag{4.18}$$

Chapter 5

The $\mathbb{Z}_2$ toric-code and the double-semion topological order of hardcore Bose-Hubbard-type models in the strong-interaction limit

The material presented in the chapter is based on my work published in Reference [25]. In this chapter, we present a generic framework for the emergence of the $\mathbb{Z}_2$ toric-code and the double-semion topological order in a wide class of hardcore Bose-Hubbard-type models governed by density-density interaction and in the strong-interaction regime. We fix fractional filling factor and study under which conditions the density-density interaction gives rise to topological degeneracy. We further specify which dynamics determines the toric-code and the double-semion topological order. Our results indicate that the specifics of the density-density interaction determine the long-range entanglement of the model which possesses "restricted patterns" of the long-range entanglement realized in corresponding string-net models with the same topological order.

5.1 Introduction

Hardcore lattice bosons (HLB) in two spatial dimensions form a wide class of strongly correlated many-body systems which includes models realizable experimentally with cold atoms and molecules trapped in optical lattices. In the past two decades, exotic quantum phases of HLB have attracted a great deal of attention [86, 87, 88, 89, 73, 90, 91, 92]. Prominent examples include spin liquids and topologically ordered phases in the strong-interaction limit. In the strong-interaction and strongly-correlated regimes, entanglement can play a prominent role [93] making these limits particularly interesting. The quest of HLB models exhibiting certain exotic phases and which can be realized experimentally [94] is a top priority in view of their astounding potential applications in quantum information and computation[16, 17].

HLB are described by Bose-Hubbard-type models where the correlation is governed by a two-site density-density interaction which is diagonal in the Fock basis and expressed as a sum of local operators, $H_0 = \sum_{i,j} V_{ij} n_i n_j$. It has been reported that for certain lattice geometries, certain V_{ij}'s, and appropriate fixed filling factor, strongly interacting HLB harbor $\mathbb{Z}_2$ topological order and form gapped quantum spin liquid [87, 86, 73, 88, 89]. These observations prompted considerable interest in exploring strongly interacting lattice models which harbor topological order and have the potential to be experimentally realized [16, 95, 96]. This pursuit calls for a general understanding of how a certain long-range entanglement [34, 33] can be emergent in strongly-interacting lattice systems. Given that quantum phases stabilized in the strong-interaction limit are determined by H_0, it is natural to expect that the specific features of the two-site density-density interaction can give rise to patterns of long-range entanglement.

In this chapter, we unveil the connection between the specifics of the density-density interaction of hardcore lattice bosons and both the $\mathbb{Z}_2$ toric-code (TC) topological order [39],

and the double-semion (DS) topological order [97] realized in the strong-interaction limit. To the best of our knowledge, this connection is systematically investigated for the first time. We also conjecture a correspondence between hardcore Bose-Hubbard-type lattice models and string-net models by discussing the long-range-entanglement "patterns". That is, given the long-range-entanglement "pattern" in ground states of certain string-net models, we argue, under certain conditions, the existence of the *same* topological order in strong-interaction Bose-Hubbard-type lattice models through the realization of a "restricted pattern" of long-range-entanglement. Moreover, with the present work, we expect to provide an analytical guidance for future numerical studies which can pave the way for searching experimentally realizable HLB models harboring spin liquid and topological order.

5.2 Local constraints

Unlike the exactly solvable Hamiltonians of the TC topological order [39, 97, 98] and the DS topological order [97, 99] containing mutually commutative terms involving three or more sites, in a typical HLB system the interaction term and dynamics terms are non-commutative. Thus, the relationship between the interaction and the topological order harbored by certain HLB models is not as transparent as in exactly solvable models. This relationship can be unveiled by considering the nature of the interaction term. Specifically, the geometry of the lattice, the weight V_{ij}, and the filling factor specify certain "local constraints", e.g., requirements on the number of particles allowed in a plaquette and their relative position. These "local constraints" determine the Fock states spanning the ground-state subspace $\mathcal{H}_0$ of H_0. Moreover, they specify which dynamics leaves $\mathcal{H}_0$ invariant, or equivalently, stipulate how the position of bosons in a given Fock state in $\mathcal{H}_0$ can be moved generating another Fock state in $\mathcal{H}_0$. As it will become clear in the following discussion,

the "local constraints" determine the capability of strongly-interacting HLB to harbor TC topological order and DS topological order. Throughout this chapter, by topologically ordered phase in the strong-interaction limit, we mean a gapped phase (with a spectral gap and a finite ground-state degeneracy), extending upon approaching the limit of no dynamics, which has nontrivial bulk topological degeneracy and locally indistinguishable ground states.

In the following, we consider a class of HLB models and study the "local constraints" (associated with $H_0 = \sum_{i,j} V_{ij} n_i n_j$ at specific fractional filling factors) which can give rise to TC or DS topological order in the strong-interaction limit. We will first discuss the conditions on the "local constraints" which imply the 2^{2g}-fold topological degeneracy when the underlying lattice has the geometry of a closed orientable surface with genus g. Then, we show that certain dynamics determine the TC and the DS topological orders respectively. In summary, we establish a generic framework for the emergence of the TC and the DS topological order in strongly-interacting HLB models. Within the framework we have developed, the lattice can possess defects and irregularities, making the system more realistic.

5.3 Model

The general model describing HLB takes the form

$$H = -t \sum_{(i,j)} a_i^+ a_j + \sum_{[i,j]} V_{ij} n_i n_j + O(t^2/V), \tag{5.1}$$

where the creation and annihilation operators at site i a_i^+ and a_i satisfy the hard-core constraint $a_i^+ a_i^+ = 0$. The first term is the hopping between site i and site j, the second term is the diagonal density-density interaction with $n_i = a_i^+ a_i$, and the last term represents

higher order dynamics terms (V is the maximum of $\left|V_{ij}\right|$) which will be discussed below. We only consider local Hamiltonians. Notice that the hopping and the diagonal interaction can be defined on different, and not-necessarily nearest-neighboring, pairs of sites. In the following we assume fixed fractional filling factor.

For convenience in the following discussion, we can alternatively define H on a lattice Λ different from the original lattice Λ_0. The degrees of freedom, defined on vertices of Λ_0, are now defined on links of Λ as it is done in the toric code model. Note that, Λ is not the dual lattice of Λ_0. In the construction of the dual lattice of Λ_0, vertices are replaced by plaquettes. Here, vertices are replaced by links. There are multiple ways to define Λ from Λ_0. In many cases of interest, the relation between the two is best elucidated by viewing Λ_0 as defined from Λ in the following manner. The vertex (or site) of Λ_0 replaces the link (or bond) of Λ, the pair of sites (i, j) in Λ_0 form a bond if and only if (i, j) as a pair of links in Λ share a vertex, that is, i and j are adjacent links. For example, the modified kagome lattice Λ_0 (see Fig. 5.1(a) where bonds are added to the second and third nearest neighbors inside each hexagon of the kagome lattice) is defined from the triangular lattice Λ (see Fig. 5.1(c)). As shown in Fig. 5.1(b), the sites i, j and k in Fig. 5.1(a) replace the links i, j and k in Fig. 5.1(c). Since each pair of links (i, j), (i, k) and (j, k) share a vertex in Fig. 5.1(c), pairs of sites (i, j), (i, k) and (j, k) all form bonds in Fig. 5.1(a). Similarly, as shown in Fig. 5.1(e), the checkerboard lattice Λ_0 (see Fig. 5.1(d)) can be defined from the square lattice Λ (see Fig. 5.1(f)). In the following text, we only consider cases in which Λ is *non-bipartite*. This choice will be motivated below, in the discussion of topological degeneracy. It should be noted that Λ_0 being non-bipartite does not imply that Λ is non-bipartite (see Fig. 5.1(d) and 5.1(f)).

When $t \ll V$, the dynamics of H can be treated perturbatively and the low energy physics of H can be effectively described by a Hamiltonian H_{eff} solely defined within $\mathcal{H}_0$, the ground-state subspace of $H_0 = \sum_{[i,j]} V_{ij} n_i n_j$ [87, 100]. H_{eff} consists of the lowest-

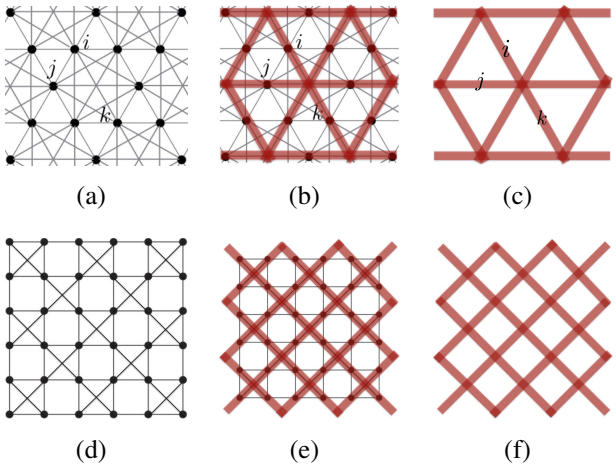

Figure 5.1: 5.1(b) shows how to define the modified kagome lattice 5.1(a) from the triangular lattice 5.1(c). A pair of links (thick red) sharing a vertex in 5.1(c) (e.g.,(i, j),(i, k) and (j, k)) is replaced by a pair of vertices forming a bond in 5.1(a). Similarly, 5.1(d) shows how to define the checkerboard lattice 5.1(d) from the square lattice 5.1(f).

order perturbative term of the hopping along with terms in $O(t^2/V)$ which leave $\mathcal{H}_0$ unchanged. The detailed form of H_{eff} depends on $\mathcal{H}_0$ and thus on the "local constraints" given by H_0. As we shall discuss in details, this effective description reveals the origin of the entanglement in the ground states of H: the dynamics, responsible for quantum fluctuation, "stacks" Fock states into a single ground state, generating entanglement while the two-site density-density interaction provides constraints on the contributing Fock states, i.e. they all belong to $\mathcal{H}_0$.

5.4 Topological degeneracy and anyonic excitation

We now discuss under which conditions H_{eff} supports topological degeneracy. In order to do so, we take the following route. In the section Topological sectors, we show that, based on certain requirements in the "local constraints", $\mathcal{H}_0$ can be decomposed into 2^{2g} topological sectors when the lattice Λ has the geometry of a closed orientable surface $\mathcal{S}$ with genus g. In the section Effective Hamiltonian, we show that these sectors are

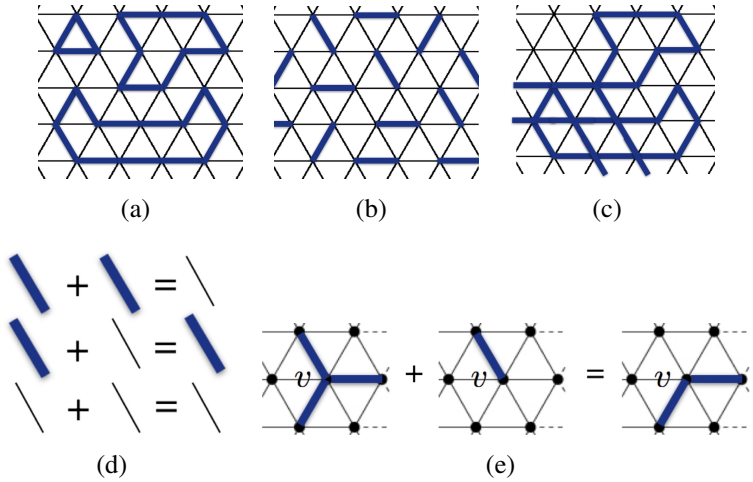

Figure 5.2: 5.2(a) represents a Fock state belonging to $\mathcal{H}_0$ and corresponding to $1/3$ filling on the triangular lattice. Dark blue links are occupied by bosons. 5.2(b) represents a Fock states corresponding to $1/6$ filling. 5.2(c) is an example of a Fock state in $\mathcal{C}$ but not in $\mathcal{C}_0$ corresponding to $1/3$ filling. 5.2(d) and 5.2(e) illustrate the formal summation defined on Fock states.

invariant under the action of H_{eff} and any local operators. In the section Ergodicity, we discuss requirements in the "local constraints" and the detailed form of H_{eff} which imply ergodicity of H_{eff} in each topological sector. Finally, in the sections Toric-code topological order and Double-semion topological order, based on the invariance property and ergodicity, we discuss the presence of topological degeneracy and anyonic excitations corresponding to the TC topological order and the DS topological order respectively.

Unless otherwise specified, in the following, we consider the model to be defined on lattice Λ where bosons are located on *links*. When necessary, we will use spin language assuming the mapping from occupation number 1 to spin down $\downarrow$, and from occupation number 0 to spin up $\uparrow$.

5.4.1 Topological sectors

Given an arbitrary Fock state, we define $s(v)$ as the number of links with occupation number 1 and adjacent to the vertex v, and $P(v)$ (with values in $\{odd, even\}$) as the parity of $s(v)$. In order to build topological sectors of $\mathcal{H}_0$, the "local constraints" associated to H_0 and the filling factor need to require that the parity $P(v)$ assigned to each vertex v is the same for all Fock states in $\mathcal{H}_0$. We call this requirement the fixed-parity condition. Fixed $P(v)$ at each vertex v for all Fock states in $\mathcal{H}_0$ means that for any two Fock states in $\mathcal{H}_0$, say $|\psi\rangle$ and $|\phi\rangle$, $P(v)_\psi = P(v)_\phi$ for all vertices v. Notice that $P(v)$ can be different from vertex to vertex, i.e. $P(v)_\psi \neq P(v')_\psi$ and $P(v)_\phi \neq P(v')_\phi$ for two vertices v and v' while $P(v)_\psi = P(v)_\phi$ and $P(v')_\psi = P(v')_\phi$. For convenience in the following discussion, we denote the set of all Fock states spanning $\mathcal{H}_0$ by $\mathcal{C}_0$.

An example of H_0 satisfying the fixed-parity condition is $H_0 = V \sum_{i,j} n_i n_j$ where each (i, j) is a pair of links on the triangular lattice Λ, which share a vertex (see (i, j) in Fig. 5.1(c)). Equivalently, each (i, j) can be viewed as a pair of sites forming a bond of the lattice Λ_0 as shown in Fig. 5.1(a). It has been shown [88] that at $1/3$ filling, $s(v) = 2$ (and $P(v) = even$) at each vertex. In other words, in each Fock state belonging to $\mathcal{C}_0$, links occupied by bosons form non-crossing closed loops on the lattice (see Fig. 5.2(a) where links in dark blue are occupied by bosons). At $1/6$ filling, $s(v) = 1$ (and $P(v) = odd$) at each vertex (see Fig. 5.2(b)), that is, occupied links in each Fock state in $\mathcal{C}_0$ form a dimer configuration. More generally, $H_0 = V \sum_{i,j} n_i n_j$ as just defined for the triangular lattice at fixed filling factor imply $s(v) = const$ also on a generic lattice. Note that fixing only the parity $P(v)$, rather than the number $s(v)$ of occupied links adjacent to a vertex, is a looser condition in the "local constraints" which guarantees the existence of topological sectors also for irregular lattices which may have defects or irregularities [101].

It should be noted that there exist Fock states satisfying the fixed-parity condition but

not consistent with the filling factor. In the case of $1/3$ filling, an example of a Fock state satisfying the fixed parity condition but which does not belong to $\mathcal{C}_0$ is illustrated in Fig. 5.2(c). In the following, in building topological sectors, we denote by $\mathcal{C}$ the set of all Fock states satisfying the fixed-parity condition but not necessarily consistent with the fixed filling factor. Then, for H_0 whose "local constraints" obey the fixed-parity condition, we have $\mathcal{C}_0 \subset \mathcal{C}$.

We now define a formal summation on Fock states. Based on this summation, topological sectors can be built from the corresponding group-theory structure. We adopt the notation $\star$ for the formal summation to distinguish it from the superposition of states. The formal summation on Fock states is based on the sum of occupation numbers modulo 2: $1 \star 1 = 0$, $1 \star 0 = 0 \star 1 = 1$, and $0 \star 0 = 0$ as illustrated in Fig. 5.2(d) and 5.2(e), which is also the group operation of the abelian group $\mathbb{Z}_2 = \{0, 1\}$. For example, we have $|1, 0, 0, 1 \cdots\rangle \star |1, 1, 0, 0 \cdots\rangle = |1 \star 1, 0 \star 1, 0 \star 0, 1 \star 0 \cdots\rangle = |0, 1, 0, 1 \cdots\rangle$. This rule generalizes the sum rule defining transition graphs in quantum dimer models [102, 103, 104]. Based on the above rule, Fock states form an abelian group. In particular, we can define a subgroup $\mathcal{Z}$ in which every Fock state satisfies the fixed-parity condition with $P(v) = even$ at all vertices (e.g., states represented by Fig. 5.2(a) and 5.2(c)). Moreover, since in any state with $P(v) = even$, links occupied by 1 boson form closed loops, also called cycles, on the surface $\mathcal{S}$ on which the lattice Λ is embedded, then, we say that $\mathcal{Z}$ consists of Fock states with loop configurations. Loop configurations can be classified according to the topology of $\mathcal{S}$. That is, for a surface $\mathcal{S}$ of genius g, $\mathcal{Z}$ can be partitioned into 2^{2g} disjoint subsets $\{\mathcal{Z}^1, \cdots, \mathcal{Z}^{2^{2g}}\}$. Loop configurations belonging to different subsets cannot be connected by local moves such as continuous deformation of loops, or by creation or deletion of loops which delimit a region on the surface $\mathcal{S}$ [105]. In order to define topological sectors in $\mathcal{C}$, we partition it in terms of $\{\mathcal{Z}^1, \cdots, \mathcal{Z}^{2^{2g}}\}$ by mapping each state in $\mathcal{C}$ to an even-parity state, i.e. a state in $\mathcal{Z}$. A simple way to do so is by fixing a

reference state belonging to $\mathcal{C}$ and using the formal summation defined above. Indeed, for an arbitrary reference state $|c_r\rangle = |c_{r1}, c_{r2}, \cdots\rangle$ in $\mathcal{C}$, we can define the map $|c\rangle \mapsto |c\rangle \star |c_r\rangle$ for every $|c\rangle = |c_1, c_2, \cdots\rangle$ in $\mathcal{C}$. Since all elements in $\mathcal{C}$ have the same parity by definition, $|c\rangle \star |c_r\rangle = |c_1 \star c_{r1}, c_2 \star c_{r2}, \cdots\rangle$ is guaranteed to have *even* parity and hence belongs to $\mathcal{Z}$ as desired. Indeed, $|c\rangle \mapsto |c\rangle \star |c_r\rangle$ maps $\mathcal{C}$ one-to-one onto $\mathcal{Z}$ and defines a partition $\{\mathcal{C}^1, \cdots, \mathcal{C}^{2^{2g}}\}$ of $\mathcal{C}$ such that $|c\rangle$ belongs to $\mathcal{C}^k$ if and only if $|c\rangle \star |c_r\rangle$ belongs to $\mathcal{Z}^k$. Note that for different reference states $|c_r\rangle$, the map $|c\rangle \mapsto |c\rangle \star |c_r\rangle$ is different, but the resultant disjoint subsets $\{\mathcal{C}^1, \cdots, \mathcal{C}^{2^{2g}}\}$ of $\mathcal{C}$ are the same. (See Methods section for a formal discussion of the map.) If we now take the intersection $\mathcal{C}_0 \cap \mathcal{C}^k$, then the set $\mathcal{C}_0$ will be partitioned into disjoint subsets $\{\mathcal{C}_0^1, \cdots, \mathcal{C}_0^{2^{2g}}\}$. These subsets span a set of orthogonal subspaces $\{\mathcal{H}_0^1, \cdots, \mathcal{H}_0^{2^{2g}}\}$ which decompose $\mathcal{H}_0$. By construction, these subspaces depend on the topology of the surface $\mathcal{S}$, and as such, they are topological sectors.

5.4.2 Effective Hamiltonian

According to the fixed-parity condition, we specify H_{eff} and show that H_{eff} does not allow transitions between states belonging to different sectors. Because of the fixed-parity condition associated with H_0, the non-vanishing perturbative hopping term of the order t^2/V in H_{eff} must have the ring-exchange form and be defined on 4-link closed loops. Likewise, other terms $O(t^2/V)$ which leave $\mathcal{H}_0$ unchanged should have the form of the ring-exchange operators, $a_i^+ a_j a_k^+ a_l \cdots + \text{H.c.}$. Hence, the effective Hamiltonian has the following generic form,

$$H_{\text{eff}} = -t^2/V \sum_{b=\{i,j,k,l,\cdots\}} q(b)(a_i^+ a_j a_k^+ a_l \cdots + \text{H.c.}), \tag{5.2}$$

where b is a closed loop of finite size in the thermodynamic limit, consisting of even number of adjacent links $\{i, j, k, l, \cdots\}$ in Λ, *contractible*, i.e. delimiting a region, on

$\mathcal{S}$. The value of the coefficient $q(b) = \pm 1$ will be specified below. For each $b = \{i, j, k, l, \cdots\}$ contributing to the sum in Eq. 5.2, we can equivalently express the operators $a_i^+ a_j a_k^+ a_l \cdots + \text{H.c.}$ as $|\bar{b}\rangle\langle\underline{b}| + |\underline{b}\rangle\langle\bar{b}|$, where $|\bar{b}\rangle$=$|1, 0, 1, 0, \cdots\rangle$ and $|\underline{b}\rangle$=$|0, 1, 0, 1, \cdots\rangle$ stand for states solely defined on links forming the loop b with bosons located alternatively on the loop b. Alternatively, we can write the ring-exchange operator for each b using Pauli operators as $\Gamma_{\mathcal{H}_0}\Gamma_b \prod_{i\in b}\sigma_i^x$ where $\Gamma_{\mathcal{H}_0}$ is the projection operator associated with $\mathcal{H}_0$ and $\Gamma_b = |\bar{b}\rangle\langle\bar{b}| + |\underline{b}\rangle\langle\underline{b}|$ is the projection operator defined on the closed loop b.

We now show that an arbitrary subspace $\mathcal{H}_0^k$ is invariant under the action of H_{eff} by using the Pauli operator expression. Let us consider a Fock state $|c\rangle = |c_1, c_2, \cdots\rangle$ in $\mathcal{C}_0^k$. Then, as discussed above, given a reference state $|c_r\rangle$ in $\mathcal{C}$, $|c\rangle \star |c_r\rangle = |z\rangle$ belongs to $\mathcal{Z}^k$. When acting with $\Gamma_{\mathcal{H}_0}\Gamma_b \prod_{i\in b}\sigma_i^x$ upon $|c\rangle$, the result is 0 if $|c\rangle$ does not have bosons occupying alternating links on the loop b, or $|c\rangle \star |b\rangle$ where $|b\rangle$ is a Fock state with occupation number $b_i = 1$ for each link i on loop b and $b_i = 0$ otherwise. Moreover, $|c\rangle \star |b\rangle \star |c_r\rangle = |c\rangle \star |c_r\rangle \star |b\rangle = |z\rangle \star |b\rangle$, where $|z\rangle \star |b\rangle$ can be obtained from $|z\rangle$ by acting upon with local moves. Hence, $|z\rangle \star |b\rangle$ belongs to $\mathcal{Z}^k$. Consequently, $|c\rangle$ and $|c\rangle \star |b\rangle$ are mapped to the same subspace $\mathcal{Z}^k$, that is, they both belong to $\mathcal{C}_0^k$. Therefore, $\Gamma_{\mathcal{H}_0}\Gamma_b \prod_{i\in b}\sigma_i^x$ maps $\mathcal{H}_0^k$ into itself, that is, $\mathcal{H}_0^k$ is invariant under the action of H_{eff}. Moreover, since an arbitrary local operator is expressed as a sum of products of Pauli operators and can be expressed in terms of local moves, it is easy to show that $\mathcal{H}_0^k$ is invariant under the action of any local operator.

5.4.3 Ergodicity

The irreducibility of $\mathcal{H}_0^k$ under the action of H_{eff} is equivalent to the ergodicity of H_{eff} in each $\mathcal{H}_0^k$. Here, ergodicity means that each $\mathcal{C}_0^k$ is nonempty and any two Fock states in $\mathcal{C}_0^k$ can be connected by sequentially applying ring-exchange operators in H_{eff}. Rigorously

proving that ergodicity holds is very challenging as efforts towards this task for the case of quantum dimer model ($s(v) = 1$) have shown [102]. This is beyond the scope of the present work. We therefore take a heuristic approach and discuss ergodicity in terms of the two requirements discussed below. The heuristic arguments used here can be viewed as a generalization of the conditions which guarantee ergodicity of quantum dimer models defined on non-bipartite lattices [104, 103]. We should notice that, in principle, ergodicity can be numerically checked by Monte Carlo simulations [86].

First, "local constraints" need to require that given a Fock state $|c\rangle$ in $\mathcal{C}_0$, for any closed loop b' consisting of even number of links –but not necessarily contributing to the sum of H_{eff}, hence not necessarily contractible– and such that bosons are located alternatively on it, positions of bosons and holes on b' can be exchanged resulting in another Fock state $|c'\rangle$ in $\mathcal{C}_0$. This is illustrated in Fig. 5.3(a) (state $|c\rangle$) and Fig. 5.3(b) (state $|c'\rangle$) where the loop b' is indicated by the red dashed line. It is important to notice that this exchange between bosons and holes does not change $s(v)$. Moreoever, if b' is contractible, states $|c\rangle$ and $|c'\rangle$ necessarily belong to the same sector since the boson-hole exchange corresponds to a local operation. On the other hand, if b' is non-contractible, $|c\rangle$ and $|c'\rangle$ belong to different sectors. The existence of non-contractible b' loops (e.g., loops in the two toroidal directions on a torus) is guaranteed by the fractional filling factor. The requirement just described associated to "local constraints" ensures that each sector is non-trivial since the existence of state $|c\rangle$ implies the existence of a state $|c'\rangle$ in each sector.

Secondly, for any state $|c\rangle$ in $\mathcal{C}_0$, the "local constraints" need to imply that the surface $\mathcal{S}$ on which the lattice is embedded can be covered by areas $\mathcal{A}$, in general partially overlapping, bounded by contractible closed loops b' on which bosons are located alternatively. Notice that the areas should be of finite-size. This requirement together with the first one ensures that no state in $\mathcal{C}_0^k$ is isolated from others upon applying ring-exchange operators. Moreover, since Eq. 5.2 can be viewed as a generalization of the dynamics in quantum

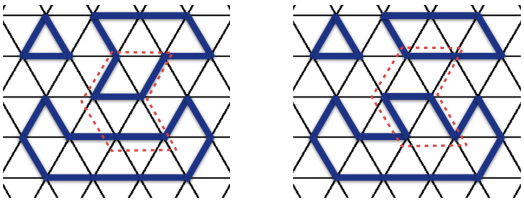

(a) (b)

Figure 5.3: 5.3(a) and 5.3(b) represent two Fock states in $\mathcal{C}_0$ corresponding to $H_0 = V \sum_{i,j} n_i n_j$, where the sum extends to all pairs of adjacent links defined on triangular lattice and at $1/3$ filling. 5.3(b) is obtained from 5.3(a) by exchanging bosons (colored links) and holes (uncolored links) on a closed loop b' indicated by the red dashed line.

dimer models, we also require Λ to be non-bipartite. If the b loops entering the sum in Eq. 5.2 satisfy the two-requirements described above and Λ is non-bipartite, then, based on this heuristic argument, we conclude that the Hamiltonian in Eq. 5.2 is ergodic in each $\mathcal{C}_0^k$.

Examples of systems whose "local constraints" are consistent with the requirements discussed above include models with $H_0 = V \sum_{i,j} n_i n_j$ where each (i, j) is a pair of links sharing a vertex on lattice Λ. See references [86, 87, 88, 89] and Equation (12) in [99]. It is an interesting and open question whether and under which conditions the topologically ordered phase corresponding to uniform weights $V_{i,j} = V$ survives when this constraint is relaxed. This question can possibly be answered using quantum Monte Carlo simulations to calculate topological entanglement entropy [106].

5.4.4 Toric-code topological order

In order to demonstrate topological degeneracy, we are left with showing that ground states $|\psi_{\text{ex}}^k\rangle$ of H_{eff} in each $\mathcal{H}_0^k$ are unique, have the same energy which is gapped above, and are locally indistinguishable.

We first study the case of the TC topological order which corresponds to

$$q(b) = 1 \tag{5.3}$$

for all b in H_{eff}. Due to the ergodicity of H_{eff} in $\mathcal{H}_0^k$, the Perron-Frobenius theorem [52] implies the uniqueness of the lowest-energy state ψ_{eff}^k in $\mathcal{H}_0^k$ in a finite-size system. We now discuss under which conditions ground-states in different sectors are degenerate and separated from other eigenstates by an energy gap independent on the system size. In some special cases, like the quantum dimer model on the Kagome lattice [103], H_{eff} itself is exactly solvable and gapped, and ground-states are equal-weight sums of Fock states in each topological sector. In this case, H_{eff} has 2^{2g}-fold topological degeneracy. More generally, for non-exactly solvable effective models, H_{eff} can be smoothly connected to an exactly solvable model H_{ex}, analogous to the Rokhsar-Kivelson (RK) quantum dimer model [102], by means of the r-parameterized Hamiltonian

$$\tilde{H}(r) = -t^2/V \sum_b (\,|\bar{b}\rangle\langle\underline{b}| + |\underline{b}\rangle\langle\bar{b}|) + r \sum_b \Gamma_b, \tag{5.4}$$

where b is a contractible loop consisting of an even number of adjacent links in Λ, $|\bar{b}\rangle$=$|1,0,1,0,\cdots\rangle$ and $|\underline{b}\rangle$=$|0,1,0,1,\cdots\rangle$ stand for states solely defined on links forming the loop b with bosons located alternatively, and $\Gamma_b = |\bar{b}\rangle\langle\bar{b}| + |\underline{b}\rangle\langle\underline{b}|$. If $r = 0$, then $\tilde{H} = H_{\text{eff}}$. If $r = t^2/V$, then one obtains an exactly solvable model $\tilde{H}(r) = H_{\text{ex}}$ with

$$H_{\text{ex}} = t^2/V \sum_b (|\bar{b}\rangle - |\underline{b}\rangle)(\langle\bar{b}| - \langle\underline{b}|). \tag{5.5}$$

The lowest-energy eigenstate $|\psi_{\text{ex}}^k\rangle$ of H_{ex} in each $\mathcal{H}_0^k$ is an equal-weight sum of all Fock states in $\mathcal{C}_0^k$ and has zero energy. For RK quantum dimer models (corresponding to Eq. 5.5 with $s(v) = 1$) on non-bipartite lattices Λ, it has been shown that there exists an energy

gap separating ground states $|\psi^k_{\rm ex}\rangle$ in each sector from other eigenstates [102]. This conclusion has also been demonstrated for models (included in our generic models) other than quantum dimer models and corresponding to $s(v) = 2, 3$ [88, 87]. In reference [102], the authors indicate that the RK quantum dimer model possesses 2^{2g}-fold topological degeneracy on a torus, and that the gap properties only depend on the graph nature of the lattice, i.e. bipartite or not, and on the ergodicity of the dynamics in $\mathcal{H}_0$. Given that our models can be viewed as generalizations of quantum dimer models, we believe these results can be extended to models considered here. Therefore, we *expect* $H_{\rm ex}$ to possess a gap and have a 2^{2g}-fold topological degeneracy.

Let us call the subspace spanned by ground-states $\{|\psi^k_{\rm ex}\rangle\}$ of $H_{\rm ex}$ as $\mathcal{E}_{\rm ex}$. If the gap remains open as the parameter r is tuned to 0, then $H_{\rm eff}$ will also be gapped and have a 2^{2g}-fold topological degeneracy. Examples of models for which the gap remains open include models corresponding to Eq. 5.4 with $s(v) = 2$ and $s(v) = 3$ on the triangular lattice [88] and $s(v) = 1$ on a kagome lattice or star lattice [103, 107]. Furthermore, as indicated in Ref. [34], local and gapped Hamiltonians smoothly connected by a family of local Hamiltonians which maintain the gap open are in the same quantum phase with their ground state subspace connected by a local unitary transformation. As a result, there exists a local unitary transformation $\mathcal{U}_{\rm ex}$ determined by $\tilde{H}(r)$, such that $\mathcal{U}_{\rm ex}(\mathcal{E}_{\rm eff}) = \mathcal{E}_{\rm ex}$, where $\mathcal{E}_{\rm eff}$ is the subspace spanned by $\{|\psi^k_{\rm eff}\rangle\}$. As a consequence, $H_{\rm eff}$ and $H_{\rm ex}$ are in the same quantum phase. Specifically, if the ground states $\{|\psi^k_{\rm ex}\rangle\}$ are *locally indistinguishable*, then both $H_{\rm ex}$ and $H_{\rm eff}$ are in the same topologically ordered phase.

We now discuss local indistinguishability of $\{|\psi^k_{\rm ex}\rangle\}$ in terms of the "local constraints". Local indistinguishability means that $\left\langle \psi^k_{\rm ex}\middle| A \middle|\psi^l_{\rm ex}\right\rangle = f(A)\delta_{k,l}$ in the thermodynamic limit for any local operator A, where $f(A)$ is independent of topological sectors. According to our discussion on topological sectors, a local operator A cannot induce any transition between different topological sectors, and thus we have $\left\langle \psi^k_{\rm ex}\middle| A \middle|\psi^l_{\rm ex}\right\rangle = 0$ for $k \neq l$.

Then, we only need to show that the value of $f(A)$ is the same in different topological sectors. Let's consider a local region including the support of A and delimited by a closed loop b, and a Fock state $|\mathbf{b}\rangle$ solely defined on this region and satisfying the "local constraints". Starting from $|\mathbf{b}\rangle$, one can imagine building Fock states in each topological sector by populating with particles links outside b according to "local constraints". Since "local constraints" stipulate how bosons are located on the lattice *locally*, the procedure of building Fock states is independent of topological sectors which differ from each other by *nonlocal* properties. As a consequence, one would expect that the number of Fock states in each sector coinciding with $|\mathbf{b}\rangle$ approaches the same value in the thermodynamic limit.

Note that this property can in principle be checked numerically. Finally, we can conclude that averages of A in each degenerate ground state $|\psi_{\text{ex}}^k\rangle$ (which is an equal-weight sum of Fock states) approach the same value in the thermodynamics limit, i.e. $f(A)$ is independent of topological sectors.

Following the discussion above, H_{eff} and H_{ex} have the same topological order and the anyons realized by excitations of H_{eff} are the same as the ones realized in H_{ex}. Excitations of H_{ex} are essentially the same as excitations of a Rokhsar-Kivelson quantum dimer model in the RVB phase [102, 108]. There are three types of anyonic excitations: (1) deconfined spin-$1/2$ fermions (analogous to spinons in quantum dimer model) appearing in pairs, corresponding to two ends of an open string in Λ, for which a typical excited state is an equal-weight sum of Fock states with two vertices with assigned parities opposite to $P(v)$; (2) spinless bosons (analogous to visons) appearing in pairs, corresponding to two ends of an open string in the dual lattice of Λ, for which the excitation can be viewed as a locally dressed operator of $\prod \sigma^z$ on an open string in the dual lattice [108]; (3) spinon-vison composition. Fusion and braiding of the three types of anyons can be studied in the same way as in the quantum dimer model of RVB phase [102, 108]. Accordingly, the anyonic excitations defines the $\mathbb{Z}_2$ toric-code topological order [39] of model 5.2 with $q(b) = 1$.

5.4.5 Double-semion topological order

In order to study the case of DS topological order, we can similarly define

$$H_{\text{ex}}^{\text{DS}} = t^2/V \sum_b (|\bar{b}\rangle - q(b)\,|\underline{b}\rangle)(\langle\bar{b}| - q(b)\,\langle\underline{b}|) \tag{5.6}$$

connected to $H_{\text{eff}}^{\text{DS}}$ via the r-parametrized Hamiltonian

$$\tilde{H}^{\text{DS}}(r) = -t^2/V \sum_b q(b)(\,|\bar{b}\rangle\langle\underline{b}| + \,|\underline{b}\rangle\langle\bar{b}|) + r\sum_b \Gamma_b \tag{5.7}$$

where b, $|\bar{b}\rangle$, $|\underline{b}\rangle$, and Γ_b are defined as in Eq. 5.4. First, we specify the phase factor $q(b)$ according to considerations below. Then, we show that the DS topological order is implied by the specified phase factor.

As shown in the exactly solvable model of the DS topological order [97, 33], the anyonic excitations are determined by the fact that the ground state is a sum of *non-crossing-closed-loop* configurations on a trivalent lattice with expansion coefficients $(-1)^{N(z)}$ where $N(z)$ is the number of loops in $|z\rangle$ [33]. (Notice that non-crossing-closed-loop configurations belong to $\mathcal{Z}$ by definition). In order to study the DS topological order of $H_{\text{ex}}^{\text{DS}}$ defined on an arbitrary non-bipartite lattice Λ, we will "equivalently" represent the ground state of $H_{\text{ex}}^{\text{DS}}$ by a sum of non-crossing-closed-loop configurations with expansion coefficients determined by the number of loops. Note that the number of loops can be uniquely defined only for non-crossing-closed-loop configurations. One obvious way to realize non-crossing-closed-loop configurations corresponds to $s(v) = 0$ or 2 for all vertices so that, in each $|c\rangle$ belonging to $\mathcal{C}_0$, links with occupation number 1 directly form non-crossing closed loops, see e.g. fig 5.3(a). However, in this case, to realize the expansion coefficients $(-1)^{N(c)}$, the phase factor $q(b)$ must be replaced by an operator, similar to the operator-valued phase factor in the exactly solvable model [97, 99]. Adopting the operator-

valued phase factor will deviate from our goal of making Eq. 5.1 as realistic as possible. Hence, we consider another way to realize non-crossing-closed-loop configurations by considering $s(v) = 1$ for all vertices. In this case, in order to represent the ground state of $H_{\rm ex}^{\rm DS}$ as a sum of non-crossing-closed-loop configurations, we make use of a local unitary transformation, as explained below.

By fixing a reference Fock state $|c_r\rangle$ in $\mathcal{C}_0$, we can define a quantum circuit operator $\mathcal{U}' = \prod_{c_{ri}=1} \sigma_i^x$ which is local unitary [34]. Then, we construct the locally and unitarily transformed Hamiltonian $\mathcal{U}' H_{\rm ex}^{\rm DS} \mathcal{U}'^{+}$ which possesses the same quantum phase as $H_{\rm ex}^{\rm DS}$. Let us assume that the ground state $|\psi_{\rm ex}^k\rangle$ of $H_{\rm ex}^{\rm DS}$ is a sum of $|c\rangle$ belonging to $\mathcal{C}_0^k$ (we will later show that this is indeed the case), then, the ground state of $\mathcal{U}' H_{\rm ex}^{\rm DS} \mathcal{U}'^{+}$, $\mathcal{U}' |\psi_{\rm ex}^k\rangle$, is a sum of $\mathcal{U}' |c\rangle = |c\rangle \star |c_r\rangle$. Due to the fixed parity condition, $|c\rangle \star |c_r\rangle$ belongs to $\mathcal{Z}$ with $s(v) = 0, 2$ at each vertex and, as a cosequence, has a non-crossing-closed-loop configuration. Thus, $\mathcal{U}' |\psi_{\rm ex}^k\rangle$ is the desired "equivalent" representation of $|\psi_{\rm ex}^k\rangle$.

Now, in terms of the fixed reference state $|c_r\rangle$ in $\mathcal{C}_0$, we specify $q(b)$ in $H_{\rm eff}^{\rm DS}$ defined on an arbitrary non-bipartite lattice Λ. In terms of the specified $q(b)$, we will show that the ground state of $H_{\rm ex}^{\rm DS}$ is a superposition of $|c\rangle$ belonging to $\mathcal{C}_0^k$ with expansion coefficients depending on the number of loops in $|c\rangle \star |c_r\rangle$.

Let us consider an arbitrary loop b contributing to the sum of $H_{\rm eff}^{\rm DS}$. Fig. 5.4(a) shows the loop b and links emanating from it, where blue color represents occupied links in the reference state $|c_r\rangle$ and black links are unoccupied. We omit the lattice structure complementary to the loop b and the links emanating from it. Here, loop b in Fig. 5.4(a) is made long enough to illustrate general arguments below while in well known quantum dimer models [104, 107] loops contributing to Eq. 5.2 are shorter. Consider an arbitrary $|c\rangle$ in $\mathcal{C}_0$ in which bosons are located alternatively on b. Note that the existence of such a $|c\rangle$ is guaranteed by the way we specify the dynamics in Eq. 5.1 as discussed in the Ergodicity section. We want to specify $q(b)$ only in terms of b and $|c_r\rangle$ and such that, given the

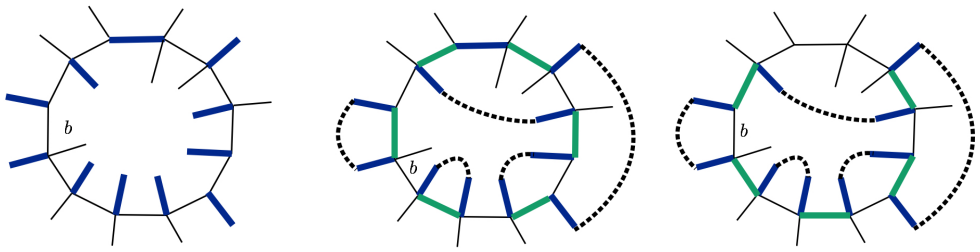

(a) (b) (c)

Figure 5.4: 5.4(a) represent an arbitrary loop b contributing to the sum of $H_{\text{eff}}^{\text{DS}}$ and links emanating from it, where blue color represents occupied links in the reference state $|c_r\rangle$, black links are unoccupied. We omit the lattice structure complementary to the loop b and links emanating from b. 5.4(b) represents $|c\rangle \star |c_r\rangle$ and 5.4(c) represents $|c'\rangle \star |c_r\rangle$. Green color represents occupied links in state $|c\rangle$ and $|c'\rangle$, black dashed lines complete the loops outside and inside b.

state $|c'\rangle = (\,|\bar{b}\rangle\langle\underline{b}| + |\underline{b}\rangle\langle\bar{b}|)\,|c\rangle$, when $q(b) = 1$ the number of loops in $|c'\rangle \star |c_r\rangle$ has the same parity as in $|c\rangle \star |c_r\rangle$; when $q(b) = -1$ the parity is changed. Since $|\bar{b}\rangle\langle\underline{b}| + |\underline{b}\rangle\langle\bar{b}|$ only acts on the loop b, the change in the number of loops only depends on how the loops are reconnected on b. As an example, Fig. 5.4(b) represents $|c\rangle \star |c_r\rangle$ and Fig. 5.4(c) represents $|c'\rangle \star |c_r\rangle$, where blue links correspond to occupied links in $|c_r\rangle$ while green links correspond to occupied links in $|c\rangle$ or $|c'\rangle$ respectively, black links are unoccupied, and black dashed lines complete the loops outside and inside b. Note that, if a green and a blue link overlap, the link will appear black in the representation of $|c\rangle \star |c_r\rangle$ or $|c'\rangle \star |c_r\rangle$ due to the sum rule $1 \star 1 = 0$. The action of $|\bar{b}\rangle\langle\underline{b}| + |\underline{b}\rangle\langle\bar{b}|$ corresponds to shifting the green links clockwise (or counterclockwise) on b. As we show in the Methods section, $q(b)$ is defined in terms of the number of outer and inner links occupied by bosons in state $|c_r\rangle$ and emanating from vertices on b. We will define two even numbers, $M_1(b, c_r)$ and $M_2(b, c_r)$, by reducing the number of outer and inner links emanating from b and occupied by bosons in $|c_r\rangle$, so that the parity change in the number of loops from $|c\rangle \star |c_r\rangle$ to $|c'\rangle \star |c_r\rangle$ can be characterized by the number of removable links $M_1(b, c_r)$ and the

number of non-removable links $M_2(b, c_r)$. Accordingly, we set

$$q(b) = i^{M_1(b,c_r)+M_2(b,c_r)+2}. \tag{5.8}$$

As shown in the Methods section such defined $q(b)$ satisfies the desired properties.

We now define state $|\psi^k_{\rm ex}\rangle = \sum_{c\in\mathcal{C}^k_0} -1^{N(|c\rangle\star|c_r\rangle)} |c\rangle$ where $N(|c\rangle\star|c_r\rangle)$ is the number of loops in the state $|c\rangle\star|c_r\rangle$ and show that it is a unique ground state in the topological sector $\mathcal{H}^k_0$. Indeed, according to above discussion on the properties of $q(b)$, when $q(b) = 1$, $(|\bar{b}\rangle - |\underline{b}\rangle)(\langle\bar{b}| - \langle\underline{b}|)\,|\psi^k_{\rm ex}\rangle = 0$; when $q(b) = -1$, $(|\bar{b}\rangle + |\underline{b}\rangle)(\langle\bar{b}| + \langle\underline{b}|)\,|\psi^k_{\rm ex}\rangle = 0$. Therefore, $|\psi^k_{\rm ex}\rangle$ is obviously a ground state of $H^{\rm DS}_{\rm ex}$ with the lowest energy 0. Next, we show that $H^{\rm DS}_{\rm ex}$ is gapped and $|\psi^k_{\rm ex}\rangle$ is unique in each topological sector. To this end, we define a *non-local* unitary operator $\mathcal{V}$ such that $\mathcal{V}\,|c\rangle = -1^{N(|c\rangle\star|c_r\rangle)}\,|c\rangle$ for all $|c\rangle \in \mathcal{C}_0$. By calculating matrix elements of $\mathcal{V}H^{\rm DS}_{\rm ex}\mathcal{V}^+$, it is easy to show that $\mathcal{V}H^{\rm DS}_{\rm ex}\mathcal{V}^+ = t^2/V\sum_b(|\bar{b}\rangle - |\underline{b}\rangle)(\langle\bar{b}| - \langle\underline{b}|)$ which is the Hamiltonian $H_{\rm ex}$ for the TC topological order. Moreover, $\mathcal{V}\,|\psi^k_{\rm ex}\rangle = \sum_{c\in\mathcal{C}^k_0}|c\rangle$ is the ground state of $\mathcal{V}H^{\rm DS}_{\rm ex}\mathcal{V}^+$ which has been shown to possess TC topological order. Therefore, according to the previous discussion, $|\psi^k_{\rm ex}\rangle$ is the unique ground state of $H^{\rm DS}_{\rm ex}$ in the sector $\mathcal{H}^k_0$ with an energy gap in the thermodynamic limit. In addition, using similar arguments as for the case of TC topological order, we can show that the ground states of $H^{\rm DS}_{\rm ex}$ are locally indistinguishable. Therefore, we conclude that $H^{\rm DS}_{\rm ex}$ is topologically ordered. By construction, $\mathcal{U}'H^{\rm DS}_{\rm ex}\mathcal{U}'^+$ possess the same topological order as $H^{\rm DS}_{\rm ex}$. Finally, if the gap remains open when tuning r to 0, $H^{\rm DS}_{\rm eff}$ is also gapped and has the same ground-state degeneracy as $H^{\rm DS}_{\rm ex}$. As a result $H^{\rm DS}_{\rm eff}$ possesses the same topological order as $H^{\rm DS}_{\rm ex}$

In order to discuss anyonic excitations of $H^{\rm DS}_{\rm ex}$, we work with $|\phi^k\rangle = \mathcal{U}'\,|\psi^k_{\rm ex}\rangle = \sum_{c\in\mathcal{C}^k_0} -1^{N(|c\rangle\star|c_r\rangle)}\,|c\rangle\star|c_r\rangle$ which is a sum of non-crossing-closed-loop configurations (see also Ref. [107]). We can define the monomer, antimonomer, and vison excitations

of $|\psi^k_{\rm ex}\rangle$ by directly generalizing the case where Λ is the triangular lattice [107]. Using the same arguments as in Ref. [107] made for the case of triangular lattice, we can show that the three types of excitation define anyons of the DS topological order: semion, antisemion, and bosonic bound state.

5.5 Discussion

The most important conclusion that one can draw from the above discussion is that it is possible to realize the toric-code (TC) and the double-semion (DS) topological order in simpler, more realistic hamiltonians, specifically Bose-Hubbard-type models with two-site interaction terms. This becomes clear from the fact that ground states for the TC or DS topological order of Bose-Hubbard-type models discussed here can be locally unitarily transformed (and hence they possess the same topological order) into ground states which resemble ground-states of string-net models with the TC or DS topological order. Indeed, the long-range entangled ground states for the TC or DS topological order of the models studied in this work can be locally unitarily transformed into a state $|\psi\rangle$. $|\psi\rangle$ is a sum of all Fock states in $\mathcal{C}_0$ which enter with equal-weight for the case of TC topological order or with a phase-factor for the case of DS topological order. By comparing $|\psi\rangle$ with the ground state of the exactly solvable models for the TC or DS topological order, one can see that their long-range-entanglement "patterns" are different. As discussed in Reference [33], "pattern" of long-range entanglement refers to (1) common features describing Fock states (or spin product states) participating in the expansion of an entangled state, e.g., all Fock states in the expansion are closed-loop configuration; (2) how these Fock states participate in the expansion, i.e. their coefficients. Here, we discuss the TC topological order as an example. The DS topological order can be considered similarly.

We define a generalized toric code on Λ, $H^{TC} = -\sum_v (-1)^{P(v)} A_v - \sum_p B_p$, where

$A_v = \prod_{v\in\partial i} \sigma_i^z$ is defined on each vertex v, $B_p = \prod_{i\in\partial p} \sigma_i^x$ is defined on each plaquette p. Here, ∂i denotes the two vertices delimiting link i, ∂p is the set of links belonging to the boundary of plaquette p. $P(v)$ is the parity associated to vertices, as defined in the Topological sectors section. (Recall that spin $\downarrow$ and $\uparrow$ are identified with occupation numbers 1 and 0.) By a local unitary transformation [1], the model can be mapped to the original toric code [39], so that H^{TC} possesses the toric-code topological order. Moreover, the ground state $|\Psi\rangle$ of H^{TC} is an equal-weight sum of *all* Fock states in $\mathcal{C}$ (that is, all states which satisfy the fixed-parity condition given by $P(v)$). Due to the nature of the two-site density-density interaction and the fixed filling factor, $\mathcal{C}_0$ is a subset of $\mathcal{C}$. In other words, the sum defining $|\psi\rangle$ runs through only a part of states contributing to the sum defining $|\Psi\rangle$. By interpreting the equal-weight sum as long-range-entanglement "pattern", we conclude that $|\psi\rangle$ has a more restricted "pattern" than $|\Psi\rangle$, though both $|\psi\rangle$ and $|\Psi\rangle$ correspond to the same topological order.

This difference in the long-range-entanglement "pattern" corresponds to different ways of realizing topological order. In a string-net model, the topological order is determined by local rules which determine spin product states expanding $|\Psi\rangle$ and the dynamics [97]. In a strong-interaction hardcore Bose-Hubbard-type lattice model, the topological order is determined by the "local constraints" (associated to density-density interaction and filling factor) which characterize Fock states expanding $|\psi\rangle$ and specify the dynamics. In light of the above discussion, we conjecture that there exists a correspondence between topological order realized in Bose-Hubbard-type lattice models and in string-net models. That is, given the long-range-entanglement "pattern" in ground states of certain string-net models, we can argue the existence of the same topological order in strong-interaction Bose-Hubbard-type

[1] We fix a reference Fock state $|c_r\rangle$ in $\mathcal{C}$ and define $\mathcal{U}' = \prod_{c_r i=1} \sigma_i^x$. Obviously $\mathcal{U}'$ is a quantum circuit and thus local unitary. It is easy to check that $\mathcal{U}' H^{TC} \mathcal{U}'^{+} = -\sum_v A_v - \sum_p B_p$ which is the original toric-code. Due to the unitarity, $\mathcal{U}' H^{TC} \mathcal{U}'^{+}$ and H^{TC} have the same spectrum. The ground state of H^{TC} is $\sum_{|z\rangle\in\mathcal{Z}} \mathcal{U}'^{+} |z\rangle = \sum_{|z\rangle} (|z\rangle \star |c_r\rangle) = \sum_{|c\rangle\in\mathcal{C}} |c\rangle$

lattice models by realizing a "restricted pattern" of long-range-entanglement in ground states.

5.6 Conclusions

We have studied the emergence of the $\mathbb{Z}_2$ toric-code topological order and the double-semion topological order in a wide class of strongly-interacting hardcore lattice bosons described by Bose-Hubbard-type models Eq. 5.1 with density-density interaction. The model is defined on a non-bipartite lattice Λ where degrees of freedom are located on links rather than sites. We have shown that model Eq. 5.1 harbors toric-code or double-semion topological order, with phase factor in the dynamics specified by Eq. 5.3 or 5.8 respectively, if the following two conditions are satisfied.

The first condition concerns "local constraints" determined by the interaction H_0 together with the fractional filling. "Local constraints", which characterize the Fock states spanning the lowest-energy subspace $\mathcal{H}_0$ of the interaction H_0, need to include the following two requirements. (i) The parity $P(v)$ assigned to each vertex v is the same for all Fock states in $\mathcal{H}_0$. Here, $P(v)$ refers to the parity of $s(v)$, the number of links with occupation number 1 adjacent to the vertex v. (ii) Positions of bosons in a given Fock state in $\mathcal{H}_0$ can be moved thus generating another Fock state in $\mathcal{H}_0$ in a way which generalizes how dimer configurations can be connected by resonances in quantum dimer models, as described in the Ergodicity section.

The second condition concerns the existence of an energy gap at $r = t^2/V$ of the r-parametrized hamiltonian $\tilde{H}(r)$ (given by Eq. 5.4 and 5.7 for the toric-code and the double-semion topological order, respectively) which connects an exactly solvable model to the effective hamiltonian. The gap needs to remain open when the parameter r is tuned to 0.

An example of lattice system satisfying these two conditions and harboring the toric-code topological order is given by the hardcore Bose-Hubbard model defined on sites of a Kagome lattice (or equivalently on links of a triangular lattice) with filling factor equal to $1/3$ [88]. On the other hand, at filling factor $1/6$, there is no topological order (as numerically demonstrated [88]) since the second condition of energy gap fails to be satisfied.

We have shown that the above two conditions are both determined by H_0 along with the fixed filling factor. Hence, these two conditions establish a connection between the density-density interaction and the emergence of the toric-code and the double-semion topological order of the hardcore lattice bosons in the strong-interaction limit.

We also conjectured that there exists a correspondence between hardcore Bose-Hubbard-type lattice models and string-net models by discussing the long-range-entanglement "patterns". That is, given the long-range-entanglement "pattern" in ground states of certain string-net models, we argued the existence of the *same* topological order in strong-interaction Bose-Hubbard-type lattice models through the realization of a "restricted pattern" of long-range-entanglement.

We expect that the work developed here will provide guidance to numerical studies which can pave the way for searching experimentally realizable lattice systems harboring topological order.

5.7 Proofs

5.7.1 Specifying $q(b)$ for the case of DS topological order

In this section, we specify the phase factor $q(b)$ in Eq. 5.6 for the DS topological order. Let's consider a contractible closed loop b on Λ which contributes to the sum in Eq. 5.6,

a reference state $|c_r\rangle$ in $\mathcal{C}_0$, and an arbitrary state $|c\rangle$ in $\mathcal{C}_0$ such that bosons are located alternatively on b. In the following, we will define $q(b)$ in terms of b and $|c_r\rangle$ and show that, given the state $|c'\rangle = (|\bar{b}\rangle\langle\underline{b}| + |\underline{b}\rangle\langle\bar{b}|)\,|c\rangle$, if $q(b) = 1$ then the number of loops in $|c'\rangle \star |c_r\rangle$ has the same parity as in $|c\rangle \star |c_r\rangle$; if, instead, $q(b) = -1$ the parity is changed. Below, we illustrate arguments using figures, though we have formalized them into rigorous proof in the context of topological graph theory [109] (not presented here for the sake of readability).

We start by discussing the relationship between the parity change under the action of $|\bar{b}\rangle\langle\underline{b}| + |\underline{b}\rangle\langle\bar{b}|$ on $|c\rangle$ and the links emanating from b which, in the reference state $|c_r\rangle$, are occupied by bosons. Fig. 5.5(a) shows state $|c_r\rangle$ on loop b, where thick blue links are occupied by bosons and black links are unoccupied (we omit the lattice structure complementary to b). We denote by l^o the outer links emanating from b with occupation number $c_r(l^o) = 1$, l^i the inner links emanating from b with occupation number $c_r(l^i) = 1$, and l^b the links forming the loop b with occupation number $c_r(l^b) = 1$ (see Fig. 5.5(a)). Due to the fixed-parity condition, i.e. $P(v) = odd$ and $s(v) = 1$ for all vertices, the number of l^o links and the number of l^i links are even. In order to show this, let's consider the non-crossing-closed-loop configurations of $|c\rangle \star |c_r\rangle$ or $|c'\rangle \star |c_r\rangle$ shown in Fig. 5.5(b) and 5.5(c) respectively, where blue links correspond to occupied links in $|c_r\rangle$, green links correspond to occupied links in $|c\rangle$ or $|c'\rangle$ respectively, black links are unoccupied links, and black dashed lines complete the loops outside and inside b. Note that, if a green and a blue link overlap, the link will appear black in the representation of $|c\rangle \star |c_r\rangle$ or $|c'\rangle \star |c_r\rangle$ due to the sum rule $1 \star 1 = 0$. Any string inside b must start and end with l^i links since no inner link emanating from b has occupation number 1 in $|c\rangle$ or $|c'\rangle$ (otherwise bosons cannot be located alternatively on b in state $|c\rangle$ or $|c'\rangle$). Therefore, the total number of l^i links is even. Similarly, the number of l^o links is also even. Notice that in the illustrations Fig. 5.5(b) and 5.5(c), under the action of $|\bar{b}\rangle\langle\underline{b}| + |\underline{b}\rangle\langle\bar{b}|$ on $|c\rangle$, non-crossing closed loops

are reconnected on loop b. In particular, as will be shown below, the reconnection is determined by how many inner links l^i are in between two successive outer links l^o.

We now show that the parity change under the action of $|\bar{b}\rangle\langle\underline{b}| + |\underline{b}\rangle\langle\bar{b}|$ is independent of $|c\rangle$. For this purpose, let us consider another state $|c_1\rangle$ in $\mathcal{C}_0$, in which bosons are located alternatively on b. Let $|c_1'\rangle = (|\bar{b}\rangle\langle\underline{b}| + |\underline{b}\rangle\langle\bar{b}|)\,|c_1\rangle$. We set $|c_1\rangle$ to coincide with $|c\rangle$ on b and $|c_1'\rangle$ to coincide with $|c'\rangle$ on b. The configurations of $|c_1\rangle \star |c_r\rangle$ and $|c_1'\rangle \star |c_r\rangle$ are represented by Fig. 5.5(d) and 5.5(e) respectively. Notice that loops in $|c_1\rangle \star |c_r\rangle$ and $|c_1'\rangle \star |c_r\rangle$ are connected in a different way from those in $|c\rangle \star |c_r\rangle$ and $|c'\rangle \star |c_r\rangle$. We can show that, if, upon reconnecting loops going from Fig. 5.5(b) to 5.5(d), the parity of the number of loops is unchanged (changed), then, upon reconnecting loops going from Fig. 5.5(c) to 5.5(e), the parity of the number of loops is also unchanged (changed). This can be shown from an elementary loop reconnection illustrated in Fig. 5.6, where the colored links are interpreted in the same way as in previous figures. Note that Fig. 5.6(a) coincides with 5.6(c) on b though loops are reconnected in such a way that 5.6(c) possesses one extra loop. Likewise, 5.6(b) coincides with 5.6(d) on b but 5.6(d) possesses one less loop than 5.6(b). Therefore, upon shifting the green links clockwise (or counterclockwise), which is equivalent to acting with $(|\bar{b}\rangle\langle\underline{b}| + |\underline{b}\rangle\langle\bar{b}|)$ on $|c\rangle$, the parity change from Fig. 5.6(a) to 5.6(b) is the same as from Fig. 5.6(c) to 5.6(d). As a result, since the action of $|\bar{b}\rangle\langle\underline{b}| + |\underline{b}\rangle\langle\bar{b}|$ only reconnects loops on b, the parity change in the number of loops in going from $|c\rangle \star |c_r\rangle$ to $|c'\rangle \star |c_r\rangle$ is the same as the parity change in the number of loops in going from $|c_1\rangle \star |c_r\rangle$ to $|c_1'\rangle \star |c_r\rangle$, as was shown in Fig. 5.5. In other words, the parity change is not affected by how links are connected outside or inside the loop b. Simply put it, dashed lines in Fig. 5.5 do not matter.

For simplicity, in the following, we equivalently work on the surface $\mathcal{S}$ on which the lattice Λ is embedded and interpret Fig. 5.5(b), 5.5(c), 5.5(d) and 5.5(e) as the images of links and loops on $\mathcal{S}$. With this interpretation, we are allowed to modify loop b by

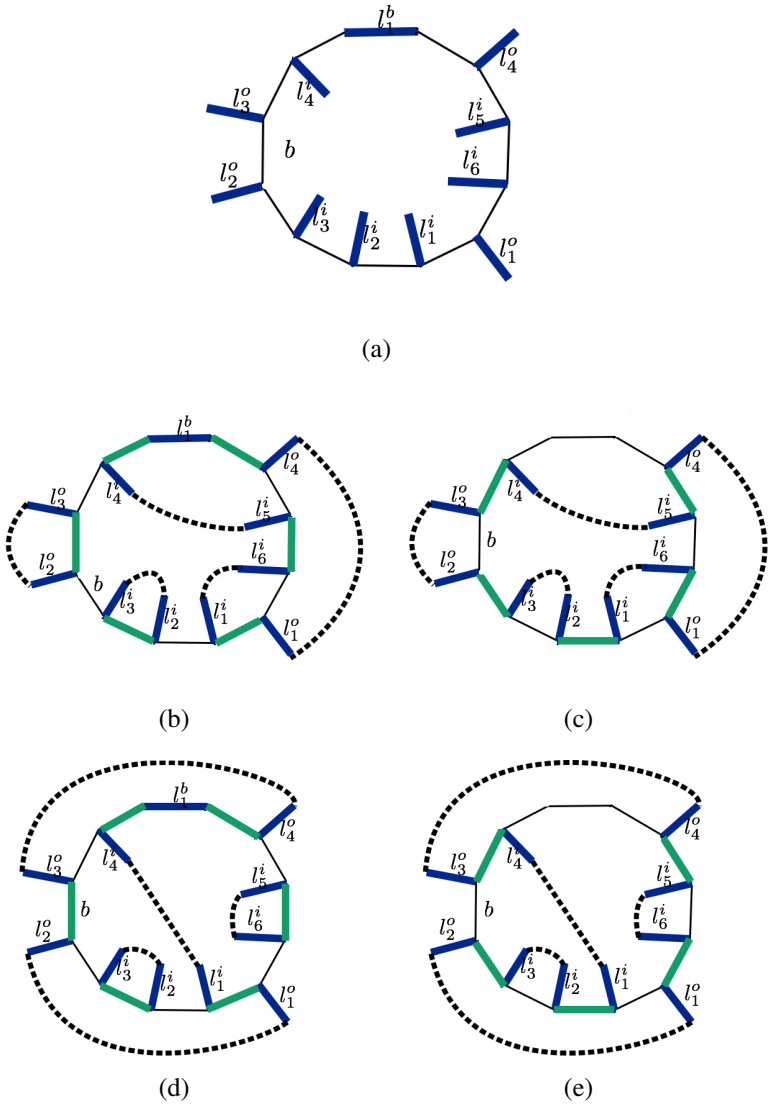

Figure 5.5: 5.5(a) represent an arbitrary loop b contributing to the sum of $H_{\text{eff}}^{\text{DS}}$, where blue links emanating from b and indexed clockwise by l^o, l^i and l^b represent occupied links in the reference state $|c_r\rangle$ while black links are unoccupied. We omit the lattice structure complementary to the loop b and the links emanating from it. Fig. 5.5(b) and 5.5(c) represent the configuration of $|c\rangle \star |c_r\rangle$ and $|c'\rangle \star |c_r\rangle$, respectively. Blue links represent occupied links in $|c_r\rangle$, green links represent occupied links in $|c\rangle$ or $|c'\rangle$, black links are unoccupied, and black dashed lines complete loops outside and inside b. Fig. 5.5(d) and 5.5(e) represent the configuration of $|c_1\rangle \star |c_r\rangle$ and $|c_1'\rangle \star |c_r\rangle$, respectively. The significance of the colors is the same as above. Notice that loops outside and inside b are connected differently than in 5.5(b) and 5.5(c).

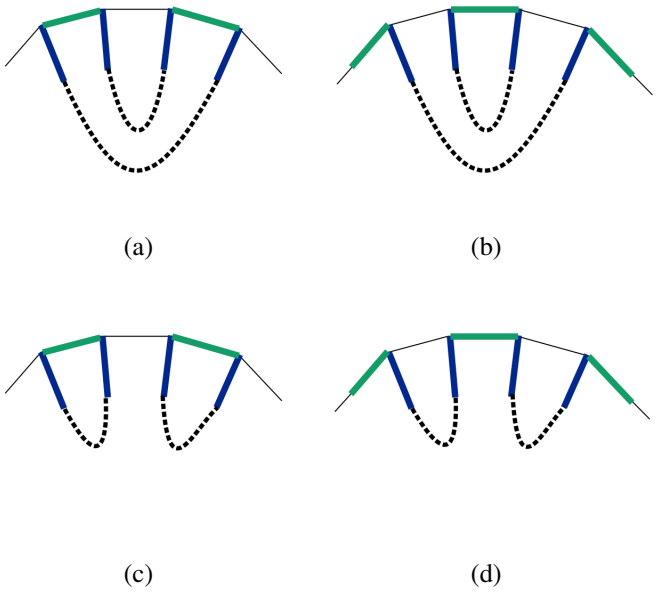

Figure 5.6: 5.6(a) and 5.6(c) illustrate an elementary loop reconnection operation which is also illustrated in 5.6(b) and 5.6(d). The lop reconnection does not affect the parity change upon shifting green links clockwise (or counterclockwise) on b. Colored links have the same meaning as in previous figures.

removing links without worrying about the lattice structure as long as green links are alternating on loop b and each site on b possesses exactly one blue link. As we explain below in details, this procedure allows us to determine the parity change in question. To this end, we define two even numbers $M_1(b, c_r)$ and $M_2(b, c_r)$ as follows.

We start by removing l^b links. As shown in Fig. 5.5(b) and 5.5(c), link l^b_1 either forms a segment of a closed loop together with green links, or overlaps with a green link and does not contribute to any loop. As a consequence, removing l^b links has no effect on the number of loops and hence on the parity change. Fig. 5.7(a) and 5.7(b) show the new configurations obtained after removing l^b links from Fig. 5.5(b) and 5.5(c). Notice that, in order for the number of links on b to stay even, links must be removed in pairs.

We now fix any two successive l^o links and remove an even number of l^i links existing in between until there is at most one such l^i link. As an example of such removal, we remove links l^i_2, l^i_3 between links l^o_1 and l^o_2, and l^i_5, l^i_6 between links l^o_1 and l^o_4 from Fig. 5.7(a) and 5.7(b). Note that, for each l^i removed, an adjacent link on b needs to be removed in order to have exactly one blue link attached to each vertex. After the removal, we obtain configurations Fig. 5.7(c) and 5.7(d). The parity change in the configurations obtained after this removal is the same as before if we remove an even total number of pairs while the parity change is opposite if the total number of removed pairs is odd. To see this, consider such a pair of l^i links, say l^i_2 and l^i_3 in Fig. 5.7(a) and 5.7(b), which are connected by a black dashed line. Note that, if such a pair is not connected by a black dashed line, we can always reconnect loops so that the pair is connected by a black dashed line inside b without affecting the parity change. l^i_2 and l^i_3 form a loop together with a green link and a black dashed line in Fig. 5.7(a). After shifting green links clockwise on b, this loop no longer exists in Fig. 5.7(b). As a result, the removal of an odd number of pairs of l^i links results in the opposite parity change compared to the parity change of the initial configurations.

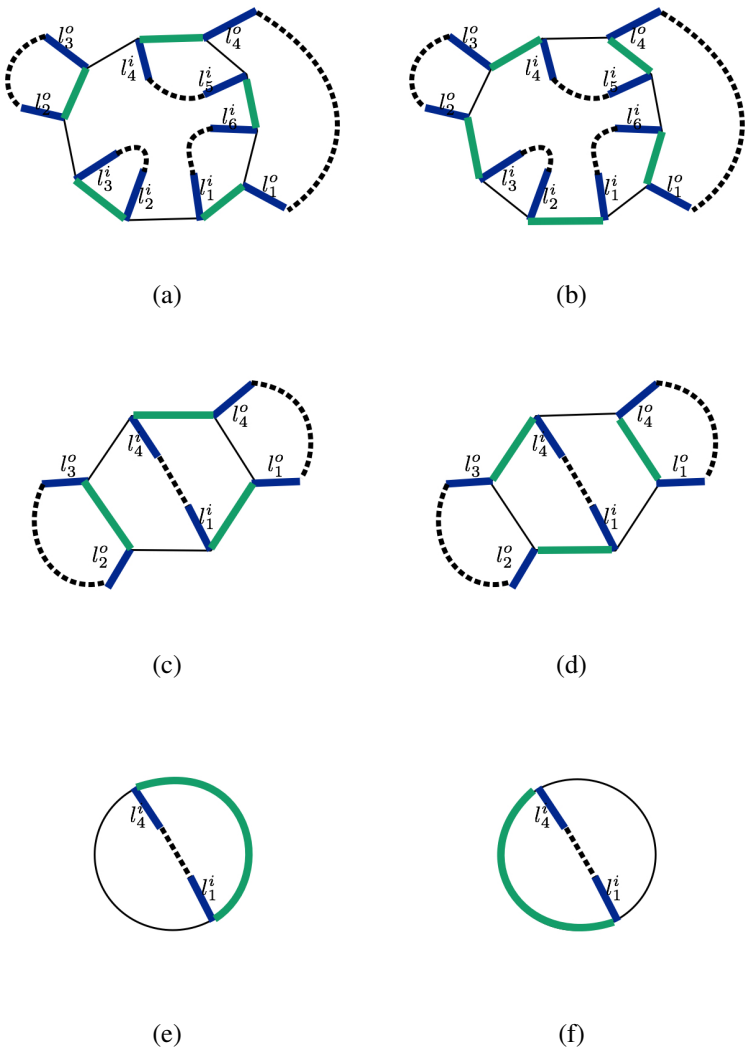

Figure 5.7: 5.7(a) and 5.7(b) show configurations obtained after removing l^b links from Fig. 5.5(b) and 5.5(c). Note that the parity change is the same as before removing l^b links. 5.7(c) and 5.7(d) show configurations obtained after removing links l^i_2, l^i_3, l^i_5 and l^i_6 from Fig. 5.7(a) and 5.7(b). Note that, since an even number of pairs of links has been removed, the parity change stays the same. 5.7(e) and 5.7(f) show configurations obtained after removing links l^o_1, l^o_2, l^o_3 and l^o_4 from Fig. 5.7(c) and 5.7(d). Again, since an even number of pairs of links has been removed, the parity change stays the same. Colored links and dashed links have the same meaning as in previous figures.

Subsequently, in the same manner, we remove an even number of l^o links which are located in between two consecutive l^i links. Once again, the removal alters the parity change in the same way as explained above for removal of l^i links.

Finally, we repeat these two removal processes until meeting one of these three situations: (1) there are only l^o links; (2) there are only l^i links; (3) l^o links and l^i links are located alternatively along the loop b. As an example, we further remove links l^o_1, l^o_2, l^o_3 and l^o_4 from Fig. 5.7(c) and 5.7(d) to obtain the final configurations Fig. 5.7(e) to 5.7(f).

We are now ready to define $M_1(b, c_r)$ and $M_2(b, c_r)$ as follows. $M_1(b, c_r)$ is the total number of l^o and l^i links removed. $M_2(b, c_r)$ is the number of l^o links if we end up in situation (1), the number of l^i links if we end up in situation (2), or the number of l^o (or l^i) links if we end up in situation (3). Note that $M_1(b, c_r)$ is even by definition and $M_2(b, c_r)$ is even since the number of l^o links and the number of l^i links are both even.

Let us consider the example shown in Fig. 5.8, where 5.8(a) and 5.8(b) show the parity change in situation (1); 5.8(c) and 5.8(d) show the parity change in situation (2); and 5.8(e) and 5.8(f) show the parity changein situation (3). One can easily check that $M_2(b, c_r)$ as defined above characterizes the parity change as follows. If $i^{M_2(b,c_r)+2} = 1$, then the parity change stays the same under the action of shifting green links clockwise, while if $i^{M_2(b,c_r)+2} = -1$, then the parity change is opposite.

Furthermore, recall that $M_1(b, c_r)$, by definition, records the total number of l^o and l^i links removed and, as a consequence, keeps track of whether the parity change between initial configurations is the same or not as in the final configurations. Recall, an even number of removed pairs implies the same parity change, while an odd number of removed pairs implies the opposite parity change. Then, combining $M_1(b, c_r)$ and $M_2(b, c_r)$, we can conclude that $i^{M_1(b,c_r)+M_2(b,c_r)+2}$ gives the parity change between the initial configurations.

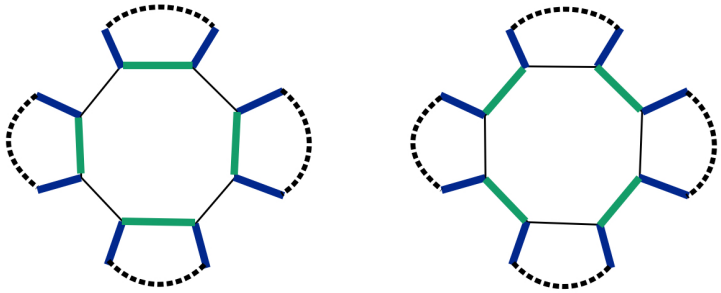

(a)

(b)

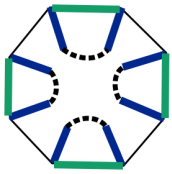

(c)

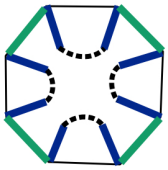

(d)

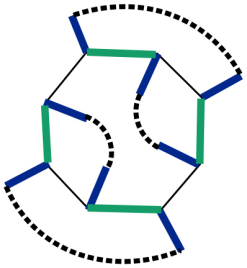

(e)

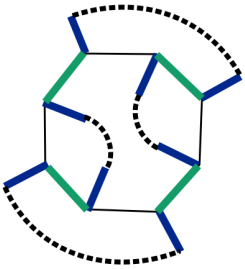

(f)

Figure 5.8: 5.8(a) and 5.8(b) show parity change in situation when there are only l^o links; 5.8(c) and 5.8(d) show parity change in situation when there are only l^i links; 5.8(e) and 5.8(f) show parity change in situation when l^o and l^i links are located alternatively along loop b. Colored links and dashed lines have the same meaning as in previous figures.

Chapter 6

Conclusive remarks and outlook

In this dissertation, I have adopted analytic techniques from condensed matter physics, entanglement theory and mathematical physics to study the entanglement structure in ground states and its relation to quantum phases of Bose-Hubbard-type models.

In particular, my work on the two-component Bose-Hubbard model has revealed a close relationship between the interspecies entanglement and the Mott-insulator-to-superfluid quantum phase transition of one component in the presence of a second component. This work provides a new perspective for the study of quantum phases in mixtures. Interestingly, this new perspective has recently been adopted in experimental studies [110].

My work on the emergence of certain topological order in a wide class of strongly interacting Bose-Hubbard-type models has unveiled the relationship between certain type of long-range entanglement in ground states and the interaction term in Bose-Hubbard-type models. This work provides a guidance for numerical studies of non-abelian topological order in Bose-Hubbard-type models, with the ultimate goal of finding Hamiltonians harboring non-trivial topological order which can be engineered with cold-atom systems trapped in optical lattices. Promising experimental systems which may realize nontrivially entangled state include polar molecules and charged ions trapped in optical

lattices [111, 112]. These systems can realize off-site interaction. This type of interaction, together with appropriate filling factor, may give rise to nontrivially entangled ground state according to what discussed in Chapter 5.

My study on ground state entanglement has demonstrated that in the strongly interacting regime, the interaction, in the form of interspecies interaction in binary mixtures or in the form of site-site interaction in the single-component case, plays a decisive role in determining the *macroscopic* properties of the system, e.g., topological order. Indeed, the interaction term determines ground-state entanglement properties which are the *microscopic* counterparts of quantum phases. This insight motivates future studies on the ground state entanglement of lattice systems with potential to realize exotic phenomena of interest in areas of quantum optics, soft matter physics, quantum information and quantum computation science.

The major challenge for these studies is to bridge a *microscopic* property, such as entanglement, studied in terms of certain tensor product structure at fixed finite system size, to the *macroscopic* collective behavior which becomes evident as system size increases. In other words, techniques like quantum field theory and renormalization group, which capture the collective behavior, can hardly probe the structure of entanglement, especially multipartite spatial entanglement. Meanwhile, techniques from quantum information, like entanglement theory, which are specialized in studying entanglement structure, can not efficiently describe macroscopic properties. The gap between the two perspectives calls for new approaches in the study of strongly correlated systems. My current and future research is motivated by two technical developments which compensate the viewpoint of each other: (1) study of the scaling behavior of the *Rényi entanglement entropy* and of the *entanglement negativity* in ground states to characterize quantum phases; (2) application of tensor network methods to probe the entanglement structure. I will briefly introduce them below.

The Rényi entanglement entropy [113] measures the bipartite ground-state entanglement between a sublattice and its complement. In a gapped system described by a local Hamiltonian, it is believed to satisfy the *area law* [113], that is, the leading term in the scaling of the Rényi entanglement entropy is αL where α is a constant and L is the lattice size [1]. Moreover, when a 2D system is in a topologically ordered phase, the Rényi entanglement entropy has been shown to scale as $\alpha L - \gamma$ where γ, the *topological entanglement entropy* [114, 115], is a universal constant representing nonlocal properties of the ground states. During the last year, I have introduced the replica trick [116] to the worm-algorithm quantum Monte Carlo code to perform large-scale numerical simulations of Bose-Hubbard-type models in order to compute the Rényi entanglement entropy. Currently, I am studying the topological entanglement entropy for hardcore Bose-Hubbard models defined on a Kagome lattice where the site-site interaction term includes the nearest, the second nearest and the third nearest neighbors inside each hexagon. The goal of this project is to determine if the $\mathbb{Z}_2$-topologically ordered phase, which has been shown to exist for uniform interaction strength [88, 89], is stable when decreasing the interaction weights on the the second and the third nearest neighbors, as a more realistic Hamiltonian would requires. The code will also be used to study the scaling behavior of the Rényi entanglement entropy in gapless lattice systems with *local* Hamiltonian and gapped systems with *nonlocal* Hamiltonians in which the area law can fail and new properties of the scaling behavior are expected. At the moment, I am also working on introducing a modified replica trick in the quantum Monte Carlo code in order to calculate ground-state entanglement negativity [117]. The entanglement negativity is a more comprehensive measure of entanglement. It can measure the bipartite entanglement between two arbitrarily separated *non-complementary* sublattices, and thus directly probe long-range properties in

[1] For 1D gapped lattice systems described by a local Hamiltonian, the area law is rigorously proved. For 2D systems, it remains an open question.

ground states. It can also be used to study the entanglement between two complementary sublattices at finite temperature when the system is in a mixed state.

I am also planning to use tensor network methods [118, 119] to study the entanglement structure of ground states in Bose-Hubbard-type models. In particular, tensor network methods can be utilized to study the capability of Bose-Hubbard-type models of realizing non-abelian topological order harbored by string-net models (see Section 5.5). For a given lattice system, tensor network methods propose a class of states which encode the entanglement structure of the ground state. Then, these proposed states can be used in a variational manner, e.g., density matrix renormalization, to efficiently obtain a ground state. Tensor network methods not only introduce new algorithm to efficiently simulate lattice systems with large size, but also provide new perspectives to understand the structure of ground state entanglement.

Bibliography

[1] H. Bombin, "An Introduction to Topological Quantum Codes," *arXiv:1311.0277*, 2013.

[2] M. Guglielmino, V. Penna, and B. Capogrosso-Sansone, "Mott-insulator-to-superfluid transition in Bose-Bose mixtures in a two-dimensional lattice," *Phys. Rev. A*, vol. 82, p. 021601, 2010.

[3] E. Morosan, D. Natelson, A. H. Nevidomskyy, and Q. Si, "Strongly correlated materials," *Adv. Mater.*, vol. 24, p. 4896, 2012.

[4] A. J. Leggett, "What DO we know about high Tc?," *Nat. Phys.*, vol. 2, p. 134, 2006.

[5] C. Nayak, S. H. Simon, A. Stern, M. Freedman, and S. Das Sarma, "Non-Abelian anyons and topological quantum computation," *Rev. Mod. Phys.*, vol. 80, p. 1083, 2008.

[6] A. Bolotin, "Limits of reductionism and the measurement problem," *Phys. Essays*, vol. 26, p. 350, 2013.

[7] J. Doyle, "Bose-Einstein condensation.," *Proc. Natl. Acad. Sci. U. S. A.*, vol. 94, p. 2774, 1997.

[8] R. Rojas, *Neural Networks: A Systematic Introduction*. Springer-Verlag, 1996.

[9] I. Bloch, "Ultracold quantum gases in optical lattices," *Nat. Phys.*, vol. 1, p. 23, 2005.

[10] K. Sengupta and N. Dupuis, "Mott-insulator-to-superfluid transition in the Bose-Hubbard model: A strong-coupling approach," *Phys. Rev. A*, vol. 71, p. 033629, 2005.

[11] P. Buonsante and A. Vezzani, "Ground-state fidelity and bipartite entanglement in the bose-hubbard model," *Phys. Rev. Lett.*, vol. 98, p. 110601, 2007.

[12] N. Elstner and H. Monien, "Dynamics and thermodynamics of the Bose-Hubbard model," *Phys. Rev. B*, vol. 59, p. 12184, 1999.

[13] B. Capogrosso-Sansone, N. V. Prokof'ev, and B. V. Svistunov, "Phase diagram and thermodynamics of the three-dimensional Bose-Hubbard model," *Phys. Rev. B*, vol. 75, p. 134302, 2007.

[14] B. Capogrosso-Sansone, Å. G. Söyler, N. Prokof'ev, and B. Svistunov, "Monte Carlo study of the two-dimensional Bose-Hubbard model," *Phys. Rev. A*, vol. 77, p. 015602, 2008.

[15] J. K. Freericks and H. Monien, "Phase diagram of the Bose-Hubbard Model," *Europhys. Lett.*, vol. 26, p. 545, 1994.

[16] M. Freedman, C. Nayak, and K. Shtengel, "Extended Hubbard model with ring exchange: A route to a non-Abelian topological phase," *Phys. Rev. Lett.*, vol. 94, p. 066401, 2005.

[17] S. J. Large, M. S. Underwood, and D. L. Feder, "Perfect quantum state transfer of hard-core bosons on weighted path graphs," *Phys. Rev. A*, vol. 91, p. 032319, 2015.

[18] D. Jaksch, C. Bruder, J. I. Cirac, C. W. Gardiner, and P. Zoller, "Cold Bosonic Atoms in Optical Lattices," *Phys. Rev. Lett.*, vol. 81, p. 3108, 1998.

[19] M. P. Fisher, P. B. Weichman, G. Grinstein, and D. S. Fisher, "Boson localization and the superfluid-insulator transition," *Phys. Rev. B*, vol. 40, p. 546, 1989.

[20] A. B. Kuklov and B. V. Svistunov, "Counterflow Superfluidity of Two-Species Ultracold Atoms in a Commensurate Optical Lattice," *Phys. Rev. Lett.*, vol. 90, p. 100401, 2003.

[21] W. Wang, V. Penna, and B. Capogrosso-Sansone, "Analysis and resolution of the ground-state degeneracy of the two-component Bose-Hubbard model," *Phys. Rev. E*, vol. 90, p. 022116, 2014.

[22] W. Wang, V. Penna, and B. Capogrosso-Sansone, "Inter-species entanglement of Bose-Bose mixtures trapped in optical lattices," *New J. Phys.*, vol. 18, p. 063002, 2016.

[23] V. W. Scarola and S. Das Sarma, "Quantum phases of the extended bose-hubbard hamiltonian: Possibility of a supersolid state of cold atoms in optical lattices," *Phys. Rev. Lett.*, vol. 95, p. 033003, 2005.

[24] C. Trefzger, C. Menotti, B. Capogrosso-Sansone, and M. Lewenstein, "Ultracold dipolar gases in optical lattices," *J. Phys. B At. Mol. Opt. Phys.*, vol. 44, p. 193001, 2011.

[25] W. Wang and B. Capogrosso-Sansone, "The Z2 toric-code and the double-semion topological order of strongly interacting hardcore lattice bosons governed by density-density interaction," *arXiv:1612.08514*, 2016.

[26] I. Hen, M. Iskin, and M. Rigol, "Phase diagram of the hard-core Bose-Hubbard model on a checkerboard superlattice," *Phys. Rev. B*, vol. 81, p. 064503, 2010.

[27] G. G. Batrouni, R. T. Scalettar, G. T. Zimanyi, and A. P. Kampf, "Supersolids in the Bose-Hubbard Hamiltonian," *Phys. Rev. Lett.*, vol. 74, p. 2527, 1995.

[28] C. Zhang, A. Safavi-Naini, A. M. Rey, and B. Capogrosso-Sansone, "Equilibrium phases of tilted dipolar lattice bosons," *New J. Phys.*, vol. 17, p. 123014, 2015.

[29] M. Lewenstein, A. Sanpera, and V. Ahufinger, *Ultracold Atoms in Optical Lattices: Simulating quantum many-body systems*. Oxford University Press, 2012.

[30] G. Moore and N. Read, "Nonabelions in the fractional quantum Hall effect," *Nucl. Phys. B*, vol. 360, p. 362, 1991.

[31] P. Bonderson and C. Nayak, "Quasi-topological phases of matter and topological protection," *Phys. Rev. B*, vol. 87, p. 195451, 2013.

[32] M. H. Freedman, A. Kitaev, M. J. Larsen, and Z. H. Wang, "Topological quantum computation," *Bull. Am. Math. Soc.*, vol. 40, p. 31, 2003.

[33] B. Zeng, X. Chen, D.-L. Zhou, and X.-G. Wen, "Quantum Information Meets Quantum Matter – From Quantum Entanglement to Topological Phase in Many-Body Systems," *arXiv:1508.02595v2*, 2015.

[34] X. Chen, Z. C. Gu, and X. G. Wen, "Local unitary transformation, long-range quantum entanglement, wave function renormalization, and topological order," *Phys. Rev. B*, vol. 82, p. 155138, 2010.

[35] L. Amico, R. Fazio, A. Osterloh, and V. Vedral, "Entanglement in many-body systems," *Rev. Mod. Phys.*, vol. 80, p. 517, 2008.

[36] T. Sowiński, O. Dutta, P. Hauke, L. Tagliacozzo, and M. Lewenstein, "Dipolar molecules in optical lattices," *Phys. Rev. Lett.*, vol. 108, p. 115301, 2012.

[37] M. Nielsen and I. Chuang, *Quantum Computation and Quantum Information*. Cambridge University Press, 2000.

[38] S. Bravyi, M. B. Hastings, and S. Michalakis, "Topological quantum order: Stability under local perturbations," *J. Math. Phys.*, vol. 51, p. 93512, 2010.

[39] A. Y. Kitaev, "Fault-tolerant quantum computation by anyons," *Ann. Phys. (N. Y.)*, vol. 303, p. 2, 2003.

[40] E. Altman, W. Hofstetter, E. Demler, and M. D. Lukin, "Phase diagram of two-component bosons on an optical lattice," *New J. Phys.*, vol. 5, p. 113, 2003.

[41] J. Catani, L. De Sarlo, G. Barontini, F. Minardi, and M. Inguscio, "Degenerate Bose-Bose mixture in a three-dimensional optical lattice," *Phys. Rev. A*, vol. 77, p. 011603, 2008.

[42] G. Thalhammer, G. Barontini, L. De Sarlo, J. Catani, F. Minardi, and M. Inguscio, "Double species Bose-Einstein condensate with tunable interspecies interactions," *Phys. Rev. Lett.*, vol. 100, p. 210402, 2008.

[43] B. Gadway, D. Pertot, R. Reimann, and D. Schneble, "Superfluidity of Interacting Bosonic Mixtures in Optical Lattices," *Phys. Rev. Lett.*, vol. 105, p. 045303, 2010.

[44] M. Iskin, "Strong-coupling expansion for the two-species Bose-Hubbard model," *Phys. Rev. A*, vol. 82, p. 033630, 2010.

[45] A. Kuklov, N. Prokof'ev, and B. Svistunov, "Commensurate two-component bosons in an optical lattice: Ground state phase diagram," *Phys. Rev. Lett.*, vol. 92, p. 050402, 2004.

[46] A. Isacsson, M. C. Cha, K. Sengupta, and S. M. Girvin, "Superfluid-insulator transitions of two-species bosons in an optical lattice," *Phys. Rev. B*, vol. 72, p. 184507, 2005.

[47] R. V. Pai, J. M. Kurdestany, K. Sheshadri, and R. Pandit, "Bose-Hubbard models in confining potentials: Inhomogeneous mean-field theory," *Phys. Rev. B*, vol. 85, p. 214524, 2012.

[48] T. Ozaki, I. Danshita, and T. Nikuni, "Bose-Bose mixtures in an optical lattice: First-order superfluid-insulator transition and elementary excitations," *arXiv:1210.1370*, 2012.

[49] Y. Nakano, T. Ishima, N. Kobayashi, T. Yamamoto, I. Ichinose, and T. Matsui, "Finite-temperature phase diagram of two-component bosons in a cubic optical lattice: Three-dimensional t-J model of hard-core bosons," *Phys. Rev. A*, vol. 85, p. 023617, 2012.

[50] B. Capogrosso-Sansone, M. Guglielmino, and V. Penna, "Mott-insulator-SF transition lobe in the presence of a second superfluid component," *Laser Phys.*, vol. 21, p. 1443, 2011.

[51] W. Wang, V. Penna, and B. Capogrosso-Sansone, "in progress,"

[52] H. Tasaki, "From Nagaoka's Ferromagnetism to Flat-Band Ferromagnetism and Beyond: An Introduction to Ferromagnetism in the Hubbard Model," *Prog. Theor. Phys.*, vol. 99, p. 489, 1998.

[53] H. Katsura and H. Tasaki, "Ground States of the Spin-1 Bose-Hubbard Model," *Phys. Rev. Lett.*, vol. 110, p. 130405, 2013.

[54] Y. Nagaoka, "Ferromagnetism in a Narrow Almost Half-Filled S Band," *Phys. Rev.*, vol. 147, p. 392, 1966.

[55] D. J. Thouless, "Exchange in Solid 3he and Heisenberg Hamiltonian," *Proc. Phys. Soc. London*, vol. 86, p. 893, 1965.

[56] H. Tasaki, "Extension of Nagaoka Theorem on the Large-U Hubbard-Model," *Phys. Rev. B*, vol. 40, p. 9192, 1989.

[57] W. Wang and B. Capogrosso-Sansone, "in progress,"

[58] P. R. Halmos, *Naive Set Theory*. Undergraduate Texts in Mathematics, Springer, 1960.

[59] R. Diestel, *Graph Theory*. Graduate Texts in Mathematics, Springer, 2010.

[60] H. Katsura and A. Tanaka, "Nagaoka states in the SU(n) Hubbard model," *Phys. Rev. A*, vol. 87, p. 013617, 2013.

[61] C. Godsil and G. F. Royle, *Algebraic Graph Theory*. Graduate Texts in Mathematics, Springer New York, 2001.

[62] F. Hebert, F. Haudin, L. Pollet, and G. G. Batrouni, "Mott insulators and correlated superfluids in ultracold Bose-Fermi mixtures," *Phys. Rev. A*, vol. 76, p. 043619, 2007.

[63] G. Refael and E. Demler, "Superfluid-insulator transition in Fermi-Bose mixtures and the orthogonality catastrophe," *Phys. Rev. B*, vol. 77, p. 144511, 2008.

[64] A. Zujev, A. Baldwin, R. T. Scalettar, V. G. Rousseau, P. J. H. Denteneer, and M. Rigol, "Superfluid and Mott-insulator phases of one-dimensional Bose-Fermi mixtures," *Phys. Rev. A*, vol. 78, p. 033619, 2008.

[65] B. Ramachandhran, S. G. Bhongale, and H. Pu, "Finite-temperature study of Bose-Fermi superfluid mixtures," *Phys. Rev. A*, vol. 83, p. 033607, 2011.

[66] M. Lewenstein, L. Santos, M. A. Baranov, and H. Fehrmann, "Atomic Bose-Fermi mixtures in an optical lattice," *Phys. Rev. Lett.*, vol. 92, p. 050401, 2004.

[67] K. Sengupta, N. Dupuis, and P. Majumdar, "Bose-Fermi mixtures in an optical lattice," *Phys. Rev. A*, vol. 75, p. 063625, 2007.

[68] F. Ferlaino, E. De Mirandes, R. Heidemann, G. Roati, G. Modugno, and M. Inguscio, "Quasi-2D Bose-Fermi mixtures in an optical lattice," *J. Phys. Iv*, vol. 116, p. 253, 2004.

[69] K. Gunter, T. Stoferle, H. Moritz, M. Kohl, and T. Esslinger, "Bose-Fermi mixtures in a three-dimensional optical lattice," *Phys. Rev. Lett.*, vol. 96, p. 180402, 2006.

[70] M. Iskin and C. A. R. S. de Melo, "Quantum phases of Fermi-Fermi mixtures in optical lattices," *Phys. Rev. A*, vol. 78, p. 013607, 2008.

[71] C. Y. Lai, C. T. Shi, and S. W. Tsai, "Correlated phases of population imbalanced Fermi-Fermi mixtures on an optical lattice," *Phys. Rev. B*, vol. 87, p. 075134, 2013.

[72] S. Pahl and Z. Koinov, "Phase Diagram of a Li-6-K-40 Mixture in a Square Lattice," *J. Low Temp. Phys.*, vol. 176, p. 113, 2014.

[73] S. V. Isakov, M. B. Hastings, and R. G. Melko, "Topological entanglement entropy of a Bose-Hubbard spin liquid," *Nat. Phys.*, vol. 7, p. 772, 2011.

[74] M. Cramer, A. Bernard, N. Fabbri, L. Fallani, C. Fort, S. Rosi, F. Caruso, M. Inguscio, and M. B. Plenio, "Spatial entanglement of bosons in optical lattices," *Nat. Commun.*, vol. 4, p. 2161, 2013.

[75] V. Alba, M. Haque, and A. M. Lauchli, "Entanglement Spectrum of the Two-Dimensional Bose-Hubbard Model," *Phys. Rev. Lett.*, vol. 110, p. 260403, 2013.

[76] P. Buonsante and A. Vezzani, "Ground-state fidelity and bipartite entanglement in the Bose-Hubbard model," *Phys. Rev. Lett.*, vol. 98, p. 110601, 2007.

[77] I. Frérot and T. Roscilde, "Entanglement entropy across the superfluid-insulator transition : a signature of bosonic criticality," *arXiv:1512.00805*, 2015.

[78] M. Greiner, O. Mandel, T. Esslinger, T. W. Hansch, and I. Bloch, "Quantum phase transition from a superfluid to a Mott insulator in a gas of ultracold atoms," *Nat.*, vol. 415, p. 39, 2001.

[79] A. Albus, F. Illuminati, and J. Eisert, "Mixtures of bosonic and fermionic atoms in optical lattices," *Phys. Rev. A*, vol. 68, p. 023606, 2003.

[80] F. Illuminati and A. Albus, "High-temperature atomic superfluidity in lattice Bose-Fermi mixtures," *Phys. Rev. Lett.*, vol. 93, p. 090406, 2004.

[81] P. Buonsante, S. M. Giampaolo, F. Illuminati, V. Penna, and A. Vezzani, "Mixtures of strongly interacting bosons in optical lattices," *Phys. Rev. Lett.*, vol. 100, p. 240402, 2008.

[82] J. Hubbard, "Electron Correlations in Narrow Energy Bands," *Proc. R. Soc. Lond. A*, vol. 276, p. 238, 1963.

[83] J. Audretsch, *Entangled systems : new directions in quantum physics*. Physics textbook, Wiley-VCH, 2007.

[84] V. Vedral, *Introduction to quantum information science*. Oxford graduate texts, Oxford University Press, 2006.

[85] S. G. Soyler, B. Capogrosso-Sansone, N. V. Prokof'ev, and B. V. Svistunov, "Sign-alternating interaction mediated by strongly correlated lattice bosons," *New J. Phys.*, vol. 11, p. 073036, 2009.

[86] S. V. Isakov, Y. B. Kim, and A. Paramekanti, "Spin-liquid phase in a spin-1/2 quantum magnet on the kagome lattice," *Phys. Rev. Lett.*, vol. 97, p. 207204, 2006.

[87] L. Balents, M. P. A. Fisher, and S. M. Girvin, "Fractionalization in an easy-axis Kagome antiferromagnet," *Phys. Rev. B*, vol. 65, p. 224412, 2002.

[88] K. Roychowdhury, S. Bhattacharjee, and F. Pollmann, "Z(2) topological liquid of hard-core bosons on a kagome lattice at 1/3 filling," *Phys. Rev. B*, vol. 92, p. 075141, 2015.

[89] X. Plat, F. Alet, S. Capponi, and K. Totsuka, "Magnetization plateaus of an easy-axis kagome antiferromagnet with extended interactions," *Phys. Rev. B*, vol. 92, p. 174402, 2015.

[90] R. G. Melko, A. Del Maestro, and A. A. Burkov, "Striped supersolid phase and the search for deconfined quantum criticality in hard-core bosons on the triangular lattice," *Phys. Rev. B*, vol. 74, p. 214517, 2006.

[91] A. Safavi-Naini, B. Capogrosso-Sansone, and A. Kuklov, "Quantum phases of hard-core dipolar bosons in coupled one-dimensional optical lattices," *Phys. Rev. A*, vol. 90, p. 043604, 2014.

[92] Y. Zhou, "Hardcore bosons on checkerboard lattices near half filling: Geometric frustration, vanishing charge order, and a fractional phase," *Phys. Rev. B*, vol. 72, p. 205116, 2005.

[93] L. Amico, R. Fazio, A. Osterloh, and V. Vedral, "Entanglement in many-body systems," *Rev. Mod. Phys.*, vol. 80, p. 517, 2008.

[94] S. Baier, M. J. Mark, D. Petter, K. Aikawa, L. Chomaz, Z. Cai, M. Baranov, P. Zoller, and F. Ferlaino, "Extended Bose-Hubbard models with ultracold magnetic atoms," *Science (80-.).*, vol. 352, p. 201, 2016.

[95] X. H. Peng, Z. H. Luo, W. Q. Zheng, S. P. Kou, D. Suter, and J. F. Du, "Experimental Implementation of Adiabatic Passage between Different Topological Orders," *Phys. Rev. Lett.*, vol. 113, p. 080404, 2014.

[96] N. Goldman, J. C. Budich, and P. Zoller, "Topological quantum matter with ultracold gases in optical lattices," *Nat. Phys.*, vol. 12, p. 639, 2016.

[97] M. A. Levin and X. G. Wen, "String-net condensation: A physical mechanism for topological phases," *Phys. Rev. B*, vol. 71, p. 045110, 2005.

[98] E. Dennis, A. Kitaev, A. Landahl, and J. Preskill, "Topological quantum memory," *J. Math. Phys.*, vol. 43, p. 4452, 2002.

[99] O. Buerschaper, S. C. Morampudi, and F. Pollmann, "Double semion phase in an exactly solvable quantum dimer model on the kagome lattice," *Phys. Rev. B*, vol. 90, p. 195148, 2014.

[100] A. Kitaev, "Anyons in an exactly solved model and beyond," *Ann. Phys. (N. Y.)*, vol. 321, p. 2, 2006.

[101] P. Buonsante, V. Penna, and A. Vezzani, "Strong-coupling expansions for the topologically inhomogeneous Bose-Hubbard model," *Phys. Rev. B*, vol. 70, p. 184520, 2004.

[102] R. Moessner and K. S. Raman, "Quantum dimer models," *arXiv:0809.3051*, 2008.

[103] G. Misguich, D. Serban, and V. Pasquier, "Quantum dimer model on the kagome lattice: Solvable dimer-liquid and Ising gauge theory," *Phys. Rev. Lett.*, vol. 89, p. 137202, 2002.

[104] R. Moessner and S. L. Sondhi, "Resonating valence bond phase in the triangular lattice quantum dimer model," *Phys. Rev. Lett.*, vol. 86, p. 1881, 2001.

[105] D. A. Lidar and T. A. Brun, *Quantum Error Correction*. Cambridge University Press, 2013.

[106] W. Wang, F. Lingua, V. Penna, and B. Capogrosso-Sansone, "in progress,"

[107] Y. Qi, Z. C. Gu, and H. Yao, "Double-semion topological order from exactly solvable quantum dimer models," *Phys. Rev. B*, vol. 92, p. 155105, 2015.

[108] D. A. Ivanov, "Vortexlike elementary excitations in the Rokhsar-Kivelson dimer model on the triangular lattice," *Phys. Rev. B*, vol. 70, p. 094430, 2004.

[109] J. L. Gross and T. W. Tucker, *Topological Graph Theory*. Courier Corporation, 1987.

[110] Y. Zeng, P. Xu, X. D. He, Y. Y. Liu, M. Liu, J. Wang, D. J. Papoular, G. V. Shlyapnikov, and M. S. Zhan, "Entangling two atoms of different isotopes via Rydberg blockade," *arXiv:1702.00349*, 2017.

[111] B. Yan, S. A. Moses, B. Gadway, J. P. Covey, K. R. A. Hazzard, A. M. Rey, D. S. Jin, and J. Ye, "Observation of dipolar spin-exchange interactions with lattice-confined polar molecules.," *Nature*, vol. 501, p. 521, 2013.

[112] T. Schaetz, "Trapping ions and atoms optically," *J. Phys. B At. Mol. Opt. Phys.*, vol. 50, p. 102001, 2017.

[113] J. Eisert, M. Cramer, and M. B. Plenio, "Colloquium: Area laws for the entanglement entropy," *Rev. Mod. Phys.*, vol. 82, p. 277, 2010.

[114] A. Kitaev and J. Preskill, "Topological entanglement entropy," *Phys. Rev. Lett.*, vol. 96, p. 110404, 2006.

[115] M. Levin and X. G. Wen, "Detecting topological order in a ground state wave function," *Phys. Rev. Lett.*, vol. 96, p. 110405, 2006.

[116] D. J. Luitz, X. Plat, N. Laflorencie, and F. Alet, "Improving entanglement and thermodynamic Renyi entropy measurements in quantum Monte Carlo," *Phys. Rev. B*, vol. 90, p. 125105, 2014.

[117] Y. A. Lee and G. Vidal, "Entanglement negativity and topological order," *Phys. Rev. A*, vol. 88, p. 042318, 2013.

[118] J. I. Cirac and F. Verstraete, "Renormalization and tensor product states in spin chains and lattices," *J. Phys. A Math. Theor.*, vol. 42, p. 504004, 2009.

[119] R. Orús, "A practical introduction to tensor networks: Matrix product states and projected entangled pair states," *Ann. Phys. (N. Y).*, vol. 349, p. 117, 2014.